MECHANISMS GOVERNING EPITHELIAL MESENCHYMAL TRANSITION IN BLADDER CARCINOMA

<u>SIM</u> WEN JING

(B.Sc. (Hons.), NTU)

A THESIS SUBMITTED FOR
THE DEGREE OF DOCTOR OF PHILOSOPHY

DEPARTMENT OF BIOLOGICAL SCIENCES

NATIONAL UNIVERSITY OF SINGAPORE

2013

DECLARATION

I hereby declare that the thesis is my original work and it has been written by me in its entirety. I have duly acknowledged all the sources of information which have been used in the thesis.

This thesis has also not been submitted for any degree in any university previously.

Sim Wen Jing

19 December 2013

Acknowledgements

I would like to acknowledge my supervisor, Jean Paul Thiery, for his continued guidance and support throughout the course of my PhD. My supervisor had been a great mentor, pointing out critical issues and providing valuable opinions. I would also like to thank my thesis advisory committee members, Leung Thomas King Chor, Sohail Ahmed and Yasuhiro Sawada, for their guidance.

I would like to show my appreciation to all members of Jean Paul Thiery Laboratory in Institute of Molecular and Cell Biology (IMCB). Special thanks go to Yap Lai Lai, Victor Racine and Aloysius Ng for their help in some of the techniques used in the work presented in this thesis.

I would also like to thank my collaborators for their help in this project. Kelvin Chua Kian Ngiap (CSI) for the cell-based screening of Epithelial Mesenchymal Transition inhibitors. Eytan Domany (Weizmann Institute) and Lior Haviv Gelibter (Weizmann Institute) for the microarray analysis. Jean Pierre Abastado (SIgN) and Benjamin Toh (SIgN) for providing the RETAAD immune infiltrates.

Lastly, I would like to thank my family and friends for their support, especially my fiancé, who painstakingly helped with the editing of this thesis.

Table of Contents

Summary

Bladder cancer is the fourth most common malignant tumour after prostate, lung, and colorectal cancer in men and the fifth most common cancer in women in the United States. Bladder cancer patients who exhibit high expression of autocrine growth factor receptors have significantly lower survival rates. Among all bladder cancer patients, those with metastatic bladder cancer had the highest levels of HGF in serum and tissue. It has also been suggested that the serum level of HGF could be used as a predictor of bladder cancer progression and patient survival. Therefore, we are interested to investigate the impact of HGF/c-MET in bladder cancer progression. Bladder carcinoma progressed by invading the different layers of the bladder wall and one of the causal factors for cell migration and invasion is Epithelial Mesenchymal Transition (EMT). Using HGF as an inducer to study bladder cancer progression via EMT *in vitro* could aid the understanding of the molecular mechanism behind tumour progression. This study should contribute to unravel the stepwise activation and possible cross-talks between signalling pathways critical for acquiring the mesenchymal phenotype which provide cells the ability to migrate and invade into the bladder wall as well as to metastasize.

In this study, we have focused on a bladder carcinoma cell line model system to unravel mechanisms driving invasive migration. Firstly, we analysed the expression profiling at different times during the execution of the EMT programme stimulated by hepatocyte growth factor (HGF). We identified the significantly differential expressed genes at the different time-points post HGF stimulation and performed a pathway analysis. Distinct pathways activated at

different time-points include MAPK, ERBB, TGF-β and focal adhesion pathways. Secondly, we utilised small molecular weight kinase inhibitors to interfere with downstream signalling systems to c-Met (HGFR) and identified inhibitors that target c-Met, MEK, PI3K and TGFRβ. The shortlisted inhibitors were able to block EMT and transwell migration. Next, we tested the potential of a TGFβRI inhibitor on an orthotopic bladder mouse model and shown that carcinoma bladder wall invasion was delayed in inhibitor-treated mice. Our studies provide further support to the concept that EMT plays a critical role in the progression of carcinoma.

List of Tables

List of Figures

List of Appendices

List of Videos

List of Publications

An EMT spectrum defines an anoikis-resistant and spheroidogenic intermediate mesenchymal state that is sensitive to e-cadherin restoration by a src-kinase inhibitor, saracatinib (AZD0530).
R Y-J Huang, M K Wong, T Z Tan, K T Kuay, A H C Ng, V Y Chung, Y-S Chu, N Matsumura, H-C Lai, Y F Lee, **W-J Sim**, C Chai, E Pietschmann, S Mori, J J H Low, M Choolani and J P Thiery
Cell Death Dis 4: e915; doi:10.1038/cddis.2013.442

Screening therapeutic EMT blocking agents in a three-dimensional microenvironment.
Aref AR, Huang RY, Yu W, Chua KN, Sun W, Tu TY, Bai J, **Sim WJ**, Zervantonakis IK, Thiery JP, Kamm RD.
Integr Biol (Camb). 2013 Feb;5(2):381-9. doi: 10.1039/c2ib20209c.

A cell-based small molecule screening method for identifying inhibitors of epithelial-mesenchymal transition in carcinoma.
Chua KN, **Sim WJ**, Racine V, Lee SY, Goh BC, Thiery JP.
PLoS One. 2012;7(3):e33183. doi: 10.1371/journal.pone.0033183. Epub 2012 Mar 14.

Mesenchymal transition and dissemination of cancer cells is driven by myeloid-derived suppressor cells infiltrating the primary tumor.
Toh B, Wang X, Keeble J, **Sim WJ**, Khoo K, Wong WC, Kato M, Prevost-Blondel A, Thiery JP, Abastado JP.
PLoS Biol. 2011 Sep;9(9):e1001162. doi: 10.1371/journal.pbio.1001162. Epub 2011 Sep 27.

Target cell movement in tumor and cardiovascular diseases based on the epithelial-mesenchymal transition concept.
Chua KN, Poon KL, Lim J, **Sim WJ**, Huang RY, Thiery JP.
Adv Drug Deliv Rev. 2011 Jul 18;63(8):558-67. doi: 10.1016/j.addr.2011.02.003. Epub 2011 Feb 16. Review.

Epithelial mesenchymal transition during development in fibrosis and in the progression of carcinoma.
Thiery JP, Chua K, **Sim WJ**, Huang R.
Bull Cancer. 2010 Nov;97(11):1285-95. doi: 10.1684/bdc.2010.1206. Review. French.

List of Abbreviations

5FU   Fluorouracil

Actn1   Actinin, alpha 1

Actg1   Actin, gamma 1

Akt   v-akt murine thymoma viral oncogene

APC   Adenomatous polyposis coli

Areg   Amphiregulin

BCG   Bacillus Calmette-Guerin

Bli   Bioluminescent intensity

BMP 2-7   Bone morphogenetic proteins 2-7

BTA   bladder tumour-associated antigen

Calcein AM   Acetomethoxy derivate of calcein

Cav 1   Caveolin 1

Ccnd1   Cyclin D1

CDKN1a   Cyclin-dependent kinase inhibitor 1

CIS   carcinoma in situ

Cis –Pt   Cis-platinum

CISCA   Cisplatin, Doxorubicin and Cyclophosphamide

Cldn4   Claudin 4

CMV   Cisplatin, Methotrexate and Vinblastine

CRB3   Crumbs protein homolog 3

Crk   v-crk sarcoma virus CT10 oncogene homolog

CSL   C-protein binding factor1

CT   Computed tomography

CTCs	Circulating tumour cells
Cxcl1	Chemokine (C-X-C motif) ligand 1
DMSO	Dimethyl sulfoxide
DNA	Deoxyribonucleic acid
DNMT1	DNA methyl-transferase 1
Dsp	Desmoplakin
Dusp 6	Dual specificity phosphatase 6
E2F1	E2F transcription factor 1
ECM	extracellular matrix
EGF	Epidermal growth factor
Egr-1	Early growth response 1
ELK3	ETS-domain protein
EMT	Epithelial Mesenchymal Transition
ERK	Extracellular signal-regulated kinase
FC	Fold change
FDR	False discovery rate
FGF	Fibroblast growth factor
FGFR3	Fibroblast growth factor receptor 3
Fn III	Fibronectin Type III
Fosl1	FOS-like antigen 1
Gab1	Grb-2 associated binding protein 1
GAG	Glycosaminoglycan
GFF 1-15	Growth differentiation factors 1-15
GO	Gene ontology
Grb-2	Growth factor receptor bound protein 2

GSK3B	Glycogen synthase kinase 3B
HGF	hepatocyte growth factor
HIF-1α	Hypoxia inducible factor 1alpha
Hmga1	High mobility group AT-hook 1
HPLC	High-performance liquid chromatography
H-Ras	v-Ha-ras Harvey rat sarcoma viral oncogene homolog
HSPGs	Heparan sulphate proteoglycans
ICN	Intracellular Notch domain
IFN-γ	Cytokine interferon, gamma
IGF	Insulin-like growth factor
IL-1β	Interleukin 1 beta
IL-6/23	Interleukin 6/23
Inha	Inhibin, alpha
Inhba	Inhibin, beta A
Inhbb	Inhibin, beta B
Inhbc	Inhibin, beta C
Inhbe	Inhibin, beta E
IRS-1	Insulin receptor substrate 1
Itga3	Integrin, alpha3
IVP	intravenous pyelogram
JNK	Jun-amino-terminal kinase
Jund	Jun D proto-oncogene
K-Ras	v-Ki-ras2 Kirsten rat sarcoma viral oncogene homolog
Krt19	Keratin 19
Lama3	Laminin, alpha 3

Lamc2	Laminin, gamma2
LGL2	Lethal giant larvae 2
LOX	Lysyl oxidase
Lrp5/6	Low density lipoprotein receptor related protein 5/6
MAGI3 containing 3	Membrane associated guanylate kinase, WW and PDZ domain
MAPK	Mitogen activated protein kinase
MDSCs	Myeloid-derived suppressor cells
MET	Mesenchymal-Epithelial Transition
miRNA	micro ribonucleic acid
MMP3/13	Matrix metalloproteinase 3/13
MMPs	Matrix metalloproteinases
MRI	Magnetic resonance imaging
mTOR	Mammalian target of rapamycin
MVAC	Methotrexate, Vinblastine, Doxorubicin and Cisplatin
NBT-II	Nara Bladder Tumour-II
N-CAM	Cell adhesion molecule
NMP-22	Nuclear Matrix Protein No.22
NOX4	NADPH oxidase 4
N-Ras	neuroblastom RAS viral (v-ras) oncogene homolog
Ocln	Occludin
p53	tumour protein p53
Pak4	Recruits p21 protein (Cdc42/Rac)-associated kinase 4
PAR-3/6	Partitioning-defective protein-3/6
PDGF	Platelet-derived growth factor

PET	Positron Emission Tomography
PI3K	Phosphoinositide 3-kinase
PIK3CA polypeptide	Phosphatidylinositol-4,5-biphosphate 3-kinase, catalytic, alpha
PIP	Phosphatidylinositol 4,5-biphosphate
PLC-γ	Phosphoinositide phospholipase C
PMN-MDSCs	Polymorphonuclear myeloid-derived suppressor cells
PTEN	Phosphatase and tensin homolog (PTEN)
Ptgs2	Prostaglandin-endoperoxide synthase2
PVRL4	Poliovirus receptor-related 4
qRT-PCR	Quantitative reverse transcription polymerase chain reaction
Rac	ras-related C3 botulinum toxin substrate
Raf	v-raf murine sarcoma viral oncogene homolog
SAPK	Stress-activated protein kinase
SDF	Stromal cell-derived factor
SEM	Standard error of mean
Serpine1	Serpine peptidase inhibitor, clade e, member1
Shc	Src homology 2 domain containing transforming protein
siRNA	Small interfering ribonucleic acid
Smad2/3	Mothers against decapentaplegic homolog 2/3
Smad2dnC	Non-phosphorylating Smad2 C-terminus
Smad2dnL	Non-phosphorylating Smad2 linker
Snai1/2	Snail 1/2
ST14	suppressor of tumourigenicity 14
Stat3	Signal transducer and activator of transcription 3

TAMs	Tumour-associated macrophages
TASc	Tumour-associated stromal cells
TCC	transitional cell carcinoma
Tcf/Lef	T cell factor/lymphoid enhancer-binding factor
TGF-β	Transforming growth factor-β
Thbs2	Thrombospondin2
Tjp2	Tight junction protein 2
TKI	Tyrosine kinase inhibitors
TMA	Total Migration Area
TNF	Tumor necrosis factor (TNF)
TNM	tumour, node, metastasis
TRAF-6	Tumor necrosis factor receptor-associated factor 6
TRegs	Regulatory T cells
Twist	Twist basic helix-loop-helix transcription factor
Vav1/2	Vav 1/2 guanine nucleotide exchange factor
VEGF	Vascular endothelial growth factor
Zeb1/2	Zinc finger E-box binding homolog 1/2
ZO-1	Zonula occludens-1

Chapter1: Introduction

Epithelial Mesenchymal Transition

Epithelial Mesenchymal Transition (EMT) is a fundamental mechanism that drives the transdifferentiation of epithelial cells into mesenchymal cells, accompanied by the loss of apico-basal polarity of epithelial cells and the acquisition of fibroblastic-like morphology. EMT is an essential process for the body plan formation and the associated morphological and biochemical changes of most metazoans during gastrulation. The primitive ectoderm undergoes a major reorganisation in order to establish the formation of two layers in the diploblasts and three layers in triploblasts, which is achieved via the plasticity of epithelial cells. The neural crest, a transient structure of the vertebrate embryo delaminates from the neural fold through EMT before engaging into extensive migration and to subsequently differentiate into the peripheral nervous system, melanocytes and in the head craniofacial structures. EMT has also been clearly implicated in heart morphogenesis which requires four consecutive cycles of EMT and its reverse process Mesenchymal-Epithelial Transition (MET). EMT also plays a major role in somite morphogenesis and differentiation to form the striated muscle and the vertebra (Reese, Mikawa et al. 2002; Lee, Dedhar et al. 2006; Lim and Thiery 2012).

Epithelial and mesenchymal cells were first described in the 19th century based on their morphology and topological organization in embryos. Epithelial cells are characterized by an apico-basal polarity and by the formation of junctional complexes called tight junctions next to the apex and adherens junctions and desmosomes more basally. The basal domain of epithelial cells is lined by a basement membrane separating the epithelium from the mesenchyme. Mesenchymal cells are organized as a loose assembly of cells intermingled within an extracellular matrix. During the early stages of development, mesenchymal cells can exhibit a front-to-end polarity, a morphology that favours migration.

During EMT, epithelial cells alter their junctional complexes and consequently or independently lose their apico-basal polarity. The tight junctional components zonula occludens-1 (ZO-1) as well as occludins, claudins and E-cadherin are among the first proteins to be targeted during the EMT process. In addition, the deregulation or redistribution of major polarity complex components, such as Crumbs protein homolog 3 CRB3, lethal giant larvae 2 (LGL2) and partitioning-defective protein-3/6 (Par-3/6), causes cells to lose their polarity and progressively assume a fibroblastic-like morphology to engage in locomotion (Thiery 2002). Cytokeratin intermediate filaments connected to desmosomes are disrupted and replaced by vimentin intermediate filaments. The actin cytoskeleton becomes rapidly altered to ensure the transition in morphology and to initiate acto-myosin contractility for lamellipodial dynamics and migration.

EMT inducers and effector

Numerous cytokines and growth factors have been shown to induce EMT during embryonic development as well as in *in vitro* carcinoma cell lines. These factors trigger signalling pathways that regulate EMT effectors such as the transcriptional repressors of the Snail and Zinc finger E-box binding homolog (Zeb) families and Twist basic helix-loop-helix transcription factor (Twist). These transcriptional repressors in turn target E-cadherin by binding to the E-box elements proximal to E-cadherin promoter; this loss of E-cadherin expression is one of the many hallmarks of EMT. Some of these cytokines and growth factors and their role in mediating EMT will be discussed in detail in the following sections.

TGF-β

The transforming growth factor-β superfamily comprises TGFβ isoforms (TGFB1-3), activin (Inha) and inhibins (Inhba, Inhbb, Inhbc, Inhbe), bone morphogenetic proteins (BMP2-7), growth differentiation factors (GDF1-15), cytokines and their associated receptors. TGFβ signalling is achieved via the formation of a heterotetrameric complex of type I and type II serine/threonine kinase receptors. The downstream signalling axis can either be receptor regulated mothers against decapentaplegic homolog 2/3 (Smad2/3)-dependent or -independent via the activity of extracellular signal-regulated kinase (Erk), Transforming growth factor beta activated kinase 1 (Tak1), c-Jun/p38 mitogen activated protein kinase (MAPK) or tumor necrosis factor (TNF) receptor-associated factor (TRAF)-6. Both signalling axes contribute to EMT via

repression of microRNA-200 gene family and the induction of Snail-1, Snail-2, Twist and Zeb 1 expression. It is also controlled by repression of miR-491-5, a negative regulator of the Par-3 polarity gene. Smad-dependent signalling is involved in epigenetic control of EMT through induction of the DNA methyl-transferase, DNMT1. The TGFβ-Smad3 signalling cascade also cooperates with HDAC6 to induce expression of TGFβ1-induced EMT genes. This duo regulates cell motility by favouring the acetylation of alpha-tubulin in microtubules. (Heldin, Vanlandewijck et al. 2012)

Wnt

The Wnt proteins comprise a highly conserved family of secreted signalling molecules that play a key role in regulating cell-to-cell interactions during embryogenesis. The name derives from the *Drosophila* Wingless polarity gene. The receptors for Wnt consist of members of the Frizzled family and low density lipoprotein receptor related protein (Lrp5/6), which are activated upon ligand binding. Upon initiation of canonical Wnt signalling, β-catenin escapes degradation in the proteasome by dissociating from a complex comprising Axin, tumour suppressor, adenomatous polyposis coli and glycogen synthase kinase 3B (Axin-APC-GSK3β). The unbound β-catenin then translocates to the nucleus and binds T cell factor/lymphoid enhancer-binding factor Tcf/Lef transcription factors to activate target genes. Canonical Wnt signalling induces EMT by stabilising intracellular levels of Snail-1 and β-catenin. In the absence of Wnt signalling, Snail-1 is targeted for proteasomal degradation by β-TrCP-containing E3-

ubiquitin ligases when phosphorylated by GSK3β. The activation of Wnt signalling thus triggers Axin2-dependent nuclear export of GSK3β and increases the half-life of nuclear Snail-1. Snail-1 can then regulate the transcription of genes that contribute to the EMT programme (Reya and Clevers 2005).

Notch

The Notch family consists of four transmembrane receptors (Notch1-4) and five ligands (Dll-1, Dll-3, Dll4, Jagged-1 and Jagged-2). These ligands bind to Notch residing on adjacent cells for pathway activation. Notch undergoes proteolytic cleavage by a complex comprising a TNF-α-converting enzyme and γ-secretase, which releases the intracellular Notch domain (ICN). The ICN translocates to the nucleus where it binds to C-protein binding factor1 (CSL) to activate the transcription of downstream targets. Notch signalling contributes to EMT via the interaction between the ICN/CSL complex with Snail-1 and Snail-2 promoters. Notch also induces hypoxia inducible factor (HIF)-1α expression, which binds to and activates the lysyl oxidase (LOX) promoter, leading to Snail family protein stabilization (Wang, Li et al. 2010). Notch ligands also up-regulate the expression of GATA-binding factors and elevates the expression of EMT effectors by suppressing the miRNAs of the miR-200 family (Yang, Ahn et al. 2011).

EGF

Epidermal growth factor signalling is initiated when EGF ligands, EGF-like proteins and neuregulins bind to their cognate receptors. This results in receptor dimerization and autophosphorylation and recruitment of various adaptor proteins to elicit downstream signalling. EGF signalling primarily acts through the MAPKs, v-akt murine thymoma viral oncogene (Akt) and Jun-amino-terminal kinase (JNK) to regulate survival, cell adhesion and cell migration. EGF induces EMT by targeting the adherens junction protein, E-cadherin, by various mechanisms: EGF signalling stimulates Snail-2 expression to represses E-cadherin transcription, promotes caveolin-mediated endocytosis of E-cadherin (Lu, Ghosh et al. 2003) and stimulates metalloproteinase-dependent cleavage of the E-cadherin extracellular domain (Chavez, Buhr et al. 2012). These mechanisms provoke the E-cadherin disappearance from cell-cell contacts and causes destabilization of the epithelial cell architecture.

HGF

Binding of hepatocyte growth factor (HGF)/scatter factor to its receptor (c-Met) induces the autophosphorylation of two tyrosine residues, Y1234/1235, in the activation loop of the c-Met kinase domain. The subsequent tyrosine phosphorylation at Y1349, Y1356 and Y1365 in the c-Met C-terminus creates a docking site for adaptor proteins such as growth factor receptor bound protein 2 associated binding protein 1 (Gab1), growth factor receptor bound protein 2 (Grb2) and Src homology 2 domain containing transforming protein (Shc)

(Schaeper, Gehring et al. 2000). Grb2 and Shc directly bind Ras and activate the Ras/Raf/MAPK pathway for morphogenesis, growth and differentiation (Fixman, Fournier et al. 1996). Gab1 recruits p85, a subunit of phosphoinositide 3-kinase (PI3K) to promote cancer cell survival, among other cellular activities. In addition, Gab1 recruits v-crk sarcoma virus CT10 oncogene homolog (Crk), which activates the small GTPases ras-related C3 botulinum toxin substrate (Rac) and Rap1 for actin cytoskeleton reorganization and cell migration (Lai, Abella et al. 2009). Gab1 also recruits p21 protein (Cdc42/Rac)-associated kinase 4 (Pak4), a serine threonine kinase, which is essential for cell invasion (Lai, Abella et al. 2009). In the context of EMT, HGF is involved in up-regulating Snail-1 expression through the mitogen activated protein kinase/early growth response 1 (MAPK/Egr-1) signalling axis and Zeb1 expression via repression of miR200c. Snail-1, in turn, represses E-cadherin and Claudin-3 gene expression to destabilize cell-cell contact, thus favouring cellular scatter. HGF activation also represses miR27b, which results in the up-regulation of suppressor of tumourigenicity 14 ST14/matriptase, an enzyme for extracellular matrix (ECM) degradation, to aid in cell migration and invasion during EMT (Susuki, Kimura et al. 2011).

IGF

The insulin-like growth factor family consists of two ligands (IGF-1 and IGF-2) and three receptors (IGF1R, IGF2R and insulin receptor). Ligands bind to receptor 1 to initiate downstream signalling, while receptor 2 acts as a clearance receptor for IGF-2. IGF signals through PI3K, which activates the v-Akt murine

thymoma viral oncogene homolog1/mammalian target of rapamycin (Akt/mTOR) and c-Jun N-terminal kinases/stress-activated protein kinase (JNK/SAPK) pathways for downstream signalling. IGF signalling induces EMT through several mechanisms. In the absence of signalling, IGF receptor 1 forms a membrane complex with E-cadherin and β-catenin. Ligand binding results in the translocation of β-catenin to the nucleus and internalization of E-cadherin at the plasma membrane, which then becomes targeted for proteasomal degradation (Morali, Delmas et al. 2001). IGF signalling also elevates Snail-1 expression via Akt/NFκB (nuclear factor kappa-light-chain-enhancer of activated B cells) axis to further downregulate E-cadherin expression (Kim, Litzenburger et al. 2007; Graham, Zhau et al. 2008; Thiery, Acloque et al. 2009).

PDGF

The platelet-derived growth factor ligands (PDGF-A, PDGF-B, PDGF-C and PDGF-D) form disulphide linked dimers and bind to PDGF receptors, PDGFRα and PDGFRβ, to initiate PDGF signalling. This binding results in receptor dimerization and auto-phosphorylation of tyrosine residues that are important for downstream signalling. PDGF receptors signal through Ras/MAPK, PI3K and phosphoinositide phospholipase C (PLC)-γ signalling axis to modulate cell growth and motility (Andrae, Gallini et al. 2008). PDGF signalling induces EMT by promoting p68 RNA helicase-mediated nuclear translocation of β-catenin. Upon activation, p68 is phosphorylated and displaces Axin from β-catenin, which in turn prevents GSK3β-mediated phosphorylation of β-catenin and causes β-

catenin to translocate into the nucleus to activate the transcription of target genes (Yang, Lin et al. 2006).

VEGF

The vascular endothelial growth factor (VEGF) family comprises five ligands (VEGFA-D, PLGF) and three tyrosine kinase receptors (VEGFR1-3). As with other growth factor families, such as the fibroblast growth factor (FGF) family, ligand binding results in receptor dimerization and the concomitant interaction with specific co-receptors, such as heparan sulphate proteoglycans (HSPGs) and neuropilins to activate different signalling modules. VEGF receptors also signal through the Ras/MAPK, PI3K and PLC-γ pathways to regulate cell growth and migration (Olsson, Dimberg et al. 2006). In the context of EMT, VEGF signalling is found to up-regulate a number of mesenchymal markers, such as N-cadherin, Snail gene family and vimentin (Gonzalez-Moreno, Lecanda et al. 2010). For example, VEGF signalling induces Snail-1 expression by suppressing GSK-3β (Wanami, Chen et al. 2008), where Snail-1 in turn represses E-cadherin expression to facilitate the acquisition of EMT.

EMT in cancer

Metastasis requires that a group of cells or single cells reach and intravasate into lymph and blood vessels for dissemination to distant organs. There are currently two mechanisms for the spread of cancer to distant sites – collective cell migration and single cell migration. Increasing evidence suggests that EMT, a mechanism governing morphogenesis and histogenesis, may have been co-opted

by cancer cells to facilitate tumour formation and dissemination. A large body of data is now supporting this hypothesis for the transition of carcinoma in situ to invasive and metastatic stages. However, there are also data showing that collective cell migration may contribute significantly to tumour progression. Current studies aimed at characterizing circulating tumour cells (CTCs) have provided strong evidence for the presence of single cells and cell clusters or microemboli. Microemboli may form through the detachment of a group of cells in the primary tumour by mechanisms such as engulfment by angiogenic endothelial cells or following necrosis in neighbouring cells. Microemboli can also form in blood vessels through proliferation in the capillary bed or through binding to platelets (Thiery, Acloque et al. 2009; Friedl, Locker et al. 2012; Thiery and Lim 2013; Yu, Bardia et al. 2013).

Microemboli are thought to utilise mechanisms that are distinct from single cell invasion mechanisms; however, there exists a possibility that carcinoma cells inside or at the leading edge of the invasion zones may undergo partial or transient EMT, guiding the invasion of the group of carcinoma cells. Single cell invasion, by comparison, requires carcinoma cells at the tumour periphery to engage into the EMT programme and delaminate from the primary tumour and enter into the blood stream (Thiery 2009). Single cell invasion may enhance metastatic efficiency and there is increasing evidence implicating EMT in cancer cell dissemination. The EMT process occurs at the invasive front in tumours of colon, breast and papillary thyroid carcinoma and produces single migratory cells that display the transitioned ('EMTed') expression profile. Cancer cells also

alternate between EMT and MET states to increase tumour spread along the walls

of the colon, stomach and peritoneal cavity.
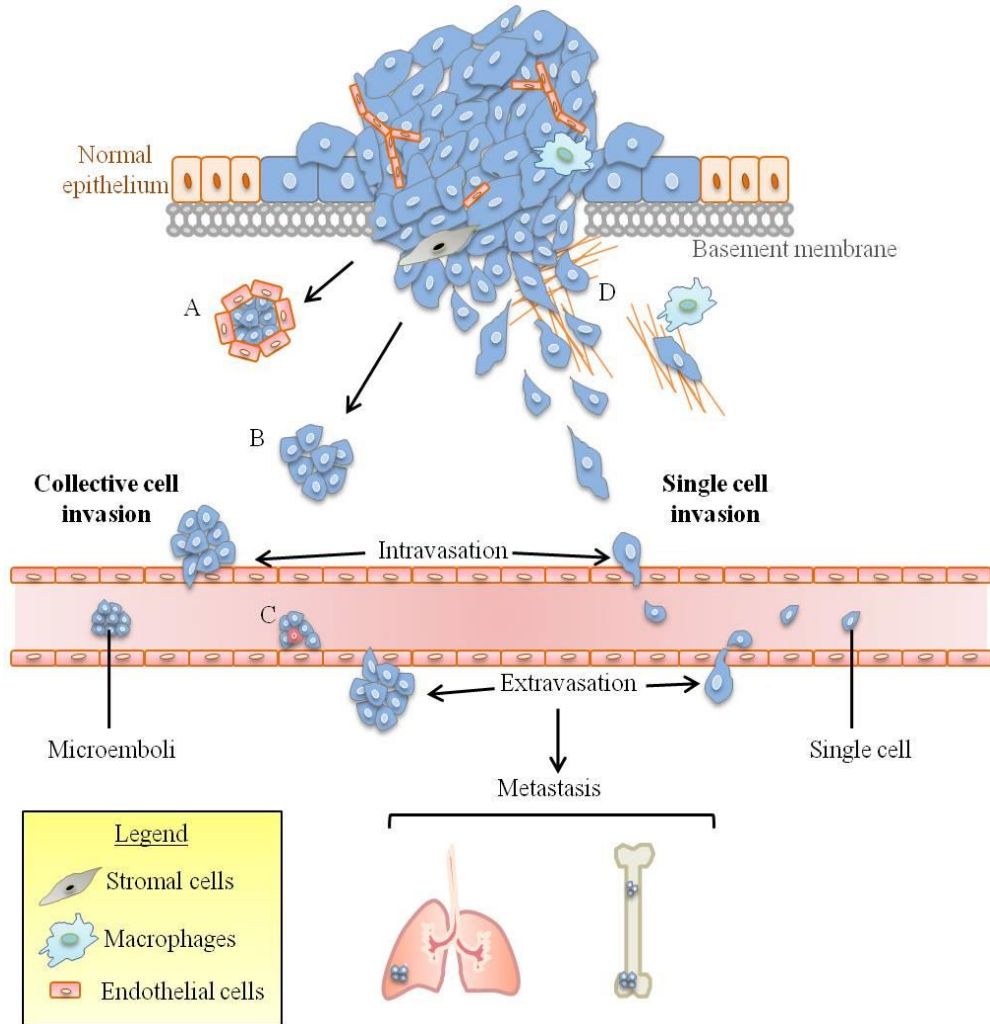
Figure 1: Illustration of the 2 mechanisms of cell invasion during metastasis. Collective cell migration describes the presence of a group of cells, termed microemboli that form by A) engulfment of carcinoma cells by angiogenic endothelial cells; B) detachment of a group of cells from the primary tumour; C) proliferation in the capillary bed or through binding to platelets. Single cell migration describes the presence of single cells in the blood stream caused by D) epithelial-mesenchymal transition, a process in which cells assume a mesenchymal morphology and detach from the primary tumour intravasate as single cells in the blood/lymph vessels. Microemboli and single cells extravasate and form micrometastases at secondary metastatic niches (lung/ bone).

The acquisition of EMT may confer chemoresistance in carcinoma cells and thus result in failure of chemotherapy treatment (Marchini, Fruscio et al. 2013). Carcinoma cells which escape treatment by chemotherapy often exhibit the mesenchymal phenotype. Furthermore, studies show that miRNAs that are responsible for negatively regulating EMT effectors are repressed in chemoresistant carcinoma cells as well as in patients with poor survival (Hu, Macdonald et al. 2009; Cochrane, Howe et al. 2010; Feng, Wang et al. 2012). Indeed, forced expression of the repressed miRNA can restore chemotherapeutic sensitivity in chemoresistant cells (Cittelly, Dimitrova et al. 2012). Thus, therapies directed toward abrogating the onset of EMT in cells or reversing its process may contribute to improved prognosis in susceptible, chemoresistant cancer patients.

Tumour microenvironment and growth factors

As a first step in metastatic processes, cells of the primary tumour may undergo EMT, directed by interaction with the tumour microenvironment. The tumour microenvironment consists of endothelial cells, tumour-associated stromal cells (TASc), infiltrating immune cells and ECM proteins. TASc are fibroblastic cells that surround or are present in the tumour and release inducers of EMT such as EGF, HGF and TGFβ. These factors bind to their cognate receptors present on cancer cells and elicit a change within signalling pathways to induce EMT. TASc also release VEGF and stromal cell-derived factor (SDF) to support the growth of

endothelial cells and pericytes, both of which are essential for the formation and maintenance of angiogenesis within the tumour. These blood vessels provide a route for EMTed cancer cells to escape the primary tumour and to disseminate to secondary sites.

The infiltrating immune cells consist of T cells, cells of the B cell lineage, macrophages and myeloid-derived cells. CD8$^+$ cytotoxic T cells and CD4$^+$ Th1 T cells, as well as the production of cytokine interferon (IFN)-γ, function as the major anti-tumoural immune effectors. However, a specialized subset of CD4+ T cells, known as CD4$^+$CD25$^+$ regulatory T cells (TRegs), can hamper the anti-tumoural immune response and contribute to tumour evasion. Tumour-associated macrophages (TAMs) or myeloid-derived suppressor cells (MDSCs) and their derived cytokines (TNF and interleukins IL-6, IL-1β and IL-23) are recognized as drivers of tumour promotion. These TAMs and MDSCs also release soluble ligands, including TGFβ and HGF, which bind to their respective receptors to elicit the EMT programme, further aiding in tumour dissemination.

The ECM serves as a reservoir for growth factors and various ECM proteins are thought to play different roles in modulating growth factor signalling. ECM proteins for example, heparin sulphate proteoglycans (HSPGs), fibronectin, tenascin-C and neural cell adhesion molecule (N-CAM) can increase the local concentration of the growth factors by ensuring their bioavailability. One important type of ECM proteins is the HSPGs. In addition to their role in facilitating signalling, HSPGs also act as 'fly-traps' for free growth factors in the

ECM, such as FGF and VEGF. These ligands can be released following the activity of the HSPG-specific enzyme heparanase, which cleaves glycosaminoglycan components of HSPGs and releases them and any bound molecules into the ECM. There are various other ECM proteins that interact with free growth factors via specific domains within their amino acid sequence. For example, fibronectin and tenascin-C contain FnIII domains to which VEGF can bind and potentiate signalling through VEGFR2 (Wijelath, Rahman et al. 2006). Fibronectin and vitronectin also bind HGF and form complexes with c-MET to activate c-MET signalling (Kim, Turnbull et al. 2011). Other protein domains within ECM proteins can act as non-canonical ligands for growth factor receptors; for example, the FnIII domain of neural cell adhesion molecule (NCAM) binds to FGFR1 to elicit ligand-independent receptor phosphorylation (Kiselyov, Skladchikova et al. 2003). Similarly, EGF-like domains in laminin and thrombospondin bind directly to EGF receptors as soluble ligands to modulate EGF signalling (Schenk, Hintermann et al. 2003).

In situ tumours are surrounded by a basement membrane consisting mainly of numerous structural ECM components, including proteoglycans, type IV collagen, and laminins, which function to physically segregate the pre-invasive tumour epithelia from the vascular structures within the stroma. However, studies have shown that signalling by various growth factors and cytokines can in fact enhance the expression and activity of matrix metalloproteinases (MMPs) and enzymes to disrupt the tumour capsule and facilitate metastasis. MMPs are zinc-dependent endopeptidases present within the ECM that are normally expressed

only during stages of tissue repair and remodelling. However, recent studies have implicated the expression of MMPs during the various stages of cancer progression. Indeed, upon basement membrane disintegration, the tumour mass penetrates the surrounding stroma, leading to local invasion and an increase in the blood supply for the tumour.

It is largely unknown which factors are involved in guiding tumour cells to a specific tissue. However, recent studies demonstrate the role of a pre-metastatic niche, where bone marrow-derived hematopoietic progenitor cells act to initiate early changes within the ECM and create a favourable microenvironment for tumor growth at distant tissue sites (Psaila, Kaplan et al. 2006). Extracellular proteins also play key roles as metastasis niche components for tumour-initiating cells during tissue invasion. The pre-metastatic niche provides an array of cytokines, growth factors, and adhesion molecules to support the arrival of metastatic cells. Before tumour cells colonize distant organs, the primary tumour releases VEGFA, which directs VEGFR1+ myeloid cells to mobilize to distant pre-metastatic sites (Kaplan, Riba et al. 2005). Other soluble factors, such as TGF-β and TNF-α, together with VEGFA, are released by the primary tumour to induce the expression of the inflammatory chemoattractants S100A8 and S100A9 (Hiratsuka, Watanabe et al. 2006) and signal transducer and activator of transcription 3 (Stat3), which activates fibroblasts at the pre-metastatic site, leading to an increase in the production of fibronectin. The upregulation of S100A8 and S100A9 attracts mac1+ bone marrow-derived cells to the pre-metastatic site (Rafii and Lyden 2006) and together attract tumour cells to

metastasize (Cheng, Corzo et al. 2008). It is the combination of this specific up-regulation of fibronectin and clustering of bone marrow-derived cellular infiltrates at distant sites that creates the pre-metastatic niche (Peinado, Aleckovic et al. 2012).

This concept has been well demonstrated in the lungs. The matricellular protein periostin has been shown to concentrate Wnt ligands within the metastastic niche to stimulate metastasis-initiating cells and enhance tumour colonization in the lungs. Tenascin-C, an ECM glycoprotein, also functions to sensitize cancer cells to Wnt and Notch signalling, thereby supporting the survival and fitness of the metastasis-initiating cells (Oskarsson and Massague 2012).

The bladder

The urinary bladder is a hollow, muscular organ situated at the front of the pelvic floor, behind the symphysis pubis and below the peritoneum. It is connected to the two kidneys via the ureters, and functions as a reservoir to collect and expel the urine excreted by the kidneys via the urethra. The bladder muscles then help to eliminate urine by expanding and contracting the organ. The ureters and urethral openings outline a triangular region, the trigonum vesicae, at the interior base of the bladder. The neck of the bladder is the lowest part of the organ immediately surrounding the urethral opening. The top surface of the bladder is triangular and is covered with peritoneum. The bladder is supported on the levator

ani muscles, which constitute the major part of the floor of the pelvic to keep the bladder and other pelvic organs in position.
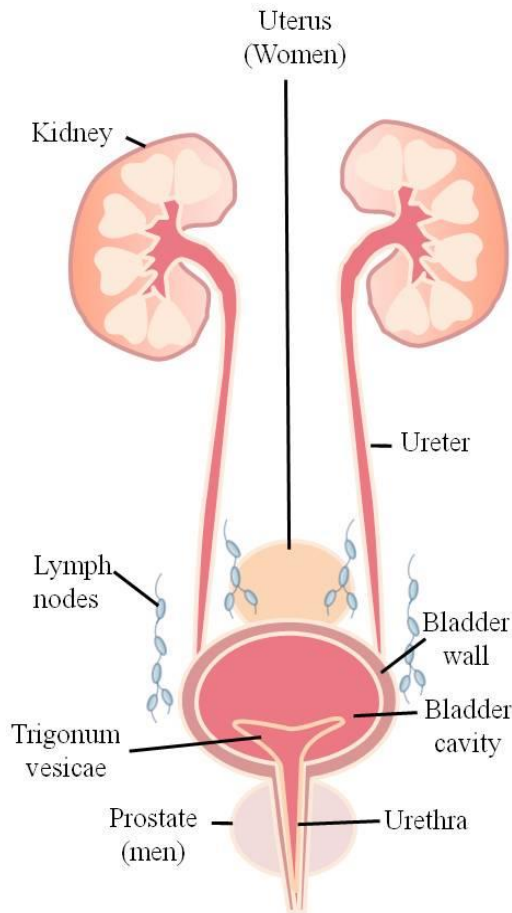
Figure 2: Illustration of the urinary system.

The urinary system is made up of two kidneys linked to the urinary bladder via two ureters and an outlet known as the urethra, which is used to expel urine out of the body. The urinary bladder is a hollow, muscular organ that lies at the front of the pelvic floor. The bladder comprises the bladder wall, bladder cavity and the trigonum vesicae, situated at the interior base of the bladder. The bladder functions to act as a reservoir for storage of urine prior to its elimination from the body.

The bladder is supplied by the superior, middle and inferior vesical arteries. The superior vesical artery delivers blood to the dome of the bladder, while the middle vesical artery supplies blood to the base of the bladder. The inferior vesical artery provides blood supply to the inferolateral surfaces of the bladder and also the base of the bladder and the lower end of the ureter.

The bladder is innervated by sympathetic and parasympathetic ganglia of the autonomic nervous system. The sympathetic nerves carry the sensations associated with distension of the bladder to the nervous system and may also participate in relaxation of the muscular layer and contraction of the sphincter that closes the urethral opening. Parasympathetic nerves are involved in contraction of the muscular layer and relaxation of the sphincter. Both nerves are required for urination.

Structure of the bladder wall

The bladder is composed of four layers: mucosa, submucosa, muscular and serosa.
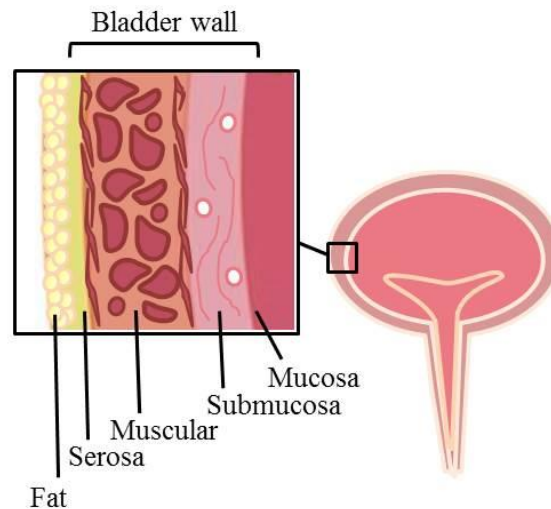
Figure 3: Illustration of the bladder wall.
The bladder wall consists of 4 layers: mucosa, submucosa, muscular and serosa. Mucosa consists of the transitional epithelium and houses the transitional cells and a single layer of umbrella cells that make the bladder wall impermeable to water and ions. Submucosa serves to maintain the structural shape of the bladder. Muscular layer helps to contract the bladder while voiding. Serosa is the outer most layer of the bladder wall and helps to hold the bladder in position and serosa is surrounded by perivesical fat.

The mucosa, or the urothelium, is a transitional epithelium consisting of superficial, intermediate and basal cell zones, which lines the bladder and is impervious to urine. The superficial cell layer contains a single layer of umbrella cells, which are large often binucleated. Umbrella cells are histologically distinct, characterised by a specialized apical plasma membrane in which the outer leaflet appears twice as thick as the inner one. The surface plasma membrane consists of thickened inflexible plaques, often termed the asymmetrical unit membrane, which is interspersed with narrow zones of normal membrane. This structure allows the umbrella cells to expand greatly and quickly when the bladder is distended. The umbrella cells are characterized by well-developed tight junctions that serve to resist paracellular ion flux (Lewis, Eaton et al. 1976; Truschel, Ruiz et al. 1999). The apical membrane is highly impermeable to water and solutes, and contains an array of glycosaminoglycans which may prevent bacterial adhesion (Parsons, Boychuk et al. 1990; Chang, Hammond et al. 1994). The intermediate cell zone consists of several layers of cuboidal-to-low columnar cells with regularly arranged nuclei, well defined borders and amphiphilic cytoplasm that is rich in glycogen. The basal layer consists of a single layer of cells in contact with the basement membrane, a sheet of extracellular material that provides structural support for the mucosal layer. Basal cells are more cylindrical and perpendicularly oriented to the plane of the basement membrane.

The submucosa, also known as the lamina propria, is situated between the mucosal basement membrane and the muscular coat. The lamina propria consists of loose-to-dense connective tissue with blood vessels, nerves, and glands in some regions. The superficial lamina propria contains the capillary network of the bladder, surrounded by a dense layer of collagen fibers, whereas the deeper lamina propria contains a thick layer of collagen type I fibers. The lamina propria creates a connective tissue matrix that functions to maintain the structural shape of the bladder wall.

The detrusor muscular coat, commonly termed the muscularis propria, houses muscle fiber bundles that provide contraction capabilities to aid in voiding. The muscularis propria consists of smooth muscle cells surrounded by an ECM comprising collagen and elastic fibrils that form muscle fiber bundles. It is subdivided into inner longitudinal, middle circular and outer longitudinal layers of thick muscle bundles. The muscle layers are distinct only near the bladder neck; the three layers are difficult to distinguish in the remaining areas, as the longitudinal and circular layers mix freely without definite orientation.

The serosa is the outermost layer of the bladder wall and is derived from the peritoneum, covering only the upper and lateral surfaces of the bladder. Fibrous adventitia, a layer of areolar connective tissue, covers the posterior and anterior surfaces of the bladder wall. These two layers help to hold the bladder in position and reduce friction with neighbouring organs. There is also a layer of fat, known as perivesical fat, which surrounds the bladder outside the serosa/adventitia.

Bladder cancer

Bladder cancer is the most common cancer in the Middle East and Africa, the fifth most common in the Western world and the tenth most common amongst males in Singapore. The age standardized rate of bladder cancer is four times higher in men compared with women. Bladder cancer is the second most frequently diagnosed of the genitourinary cancers.

Bladder cancer describes the malignancy of cells residing in the bladder wall. The type of bladder cancer is characterized by the type of cells affected amongst the various several layers of the bladder wall. Transitional cell carcinoma arises from the clonal expansion of genetically altered but histologically normal cells from the mucosa (Crawford 2008). These transitional cells (intermediate cell zone) function to allow the bladder to stretch when full and shrink when empty. Long-term irritation of the bladder by infectious agents or foreign bodies cause the transitional epithelium to change into squamous or flattened cells, which gives rise to squamous cell carcinoma. Adenocarcinoma arises from malignancy in the cells that make up the mucus-secreting glands in the bladder.

The associated risk factors for developing bladder cancer are smoking and chemical exposures at work. Smoking is associated with over 50% of bladder cancer cases in men and 52% in women (Freedman, Silverman et al. 2011). A linear relationship exists between tobacco smoking and the risk of developing bladder cancer (Boffetta 2008). The chemical 2-Naphthylamine in cigarette smoke has been shown to increase bladder cancer risk. In addition, exposure to chemical

carcinogens, such as benzidine, in the workplace greatly increases the risk of bladder cancer. People in occupations that deal with dyes, leathers, rubbers, pesticides and fertilizers are predisposed for bladder cancer. Another risk factor for the development of bladder cancer is schistosomiasis, a parasitic disease caused by several species of trematodes. *Schistosoma* embed their eggs into the lamina propria and muscularis propia of the bladder wall and provoke a severe inflammatory response and fibrosis, thus increasing the risk of bladder cancer. In areas with low prevalence of schistosomiasis, 90% of diagnosed bladder cancers are transitional cell carcinoma, with the remaining 10% are squamous and adenocarcinoma. However, in areas where there is a high prevalence of schistosomiasis, such as Egypt, Sudan and countries in the east Africa, squamous cell carcinoma is the most frequent type of bladder cancer.

Various genetic alterations, such as mutations in v-Ha-ras Harvey rat sarcoma viral oncogene homolog (H-Ras), v-Ki-ras2 Kirsten rat sarcoma viral oncogene homolog (K-Ras), neuroblastom RAS viral (v-ras) oncogene homolog (N-Ras), Fibroblast growth factor receptor 3 (FGFR3), (Phosphatidylinositol-4,5-biphosphate 3-kinase, catalytic, alpha polypeptide (PIK3CA) and tumour protein p53 (p53) have been found associated with an increased risk of bladder cancer (Kompier, Lurkin et al. 2010). FGFR3 and p53 alterations are mutually exclusive, and they characterize two different genetic pathways in urothelial cell carcinoma pathogenesis (van Rhijn, van der Kwast et al. 2004). FGFR3 mutations are frequently found in low-stage or low-grade tumours and are related to favourable disease outcome. On the other hand, p53 mutations are frequently found in

invasive urothelial cell carcinoma as well as in high-grade superficial tumours, including carcinoma *in situ*, the putative precursor of invasive urothelial cell carcinoma. Patients with p53 mutations present with adverse disease parameters and poor prognosis. In addition to these genetic alterations, bladder cancer patients who exhibit high expression of autocrine growth factor receptors have significantly lower survival rates (Korman, Peabody et al. 1996).

Diagnosis and treatment

The most common signs of bladder cancer are hematuria (blood or blood clots in the urine) as well as voiding symptoms and pain that develop above the pubic bone or in the flank region due to pressure of the urine against the back. Thus, urine tests, imaging tests and cytoscopy are used to aid in the detection of bladder cancer. Urine cytology is used to detect for abnormal cells that shed from the lining of the bladder. Cytoscopy serves as a tool to examine the lining of the bladder and urinalysis is used to detect for the presence of white and red blood cells under the microscope. Other laboratory tests, such as BTA Trak and BTA Stat assays are conducted to detect the bladder cancer biomarker bladder tumour-associated antigen (BTA) in urine samples. Nuclear Matrix Protein No.22 (NMP-22) is another urinary marker of bladder cancer that can be detected using commercial assays. Tumour masses are detected using intravenous pyelogram (IVP), an x-ray examination. In this procedure, the injected radiopaque dye

(contrast agent) collects in the kidney and gets excreted into the bladder. X-rays are taken as the dye moves through the urogenital system to examine the structure of the bladder and detect the presence of abnormal masses. Computed tomography (CT) scanning is also used to detect masses and determine if the cancer has spread to other regions. Biopsy is used to excise any abnormal tissue if observed, which is processed for histological examination to confirm or exclude the presence of cancer cells.

Staging of bladder cancer is determined by the TNM (tumour, node, metastasis) method of classification. The tumour (T) stage describes the layers of tissue affected within the bladder wall. Ta, T1 and Tis stages describe early bladder cancer in which cancer cells have not invaded into the muscle layer, while T2, T3 and T4 describe later stages of cancer progression. Ta is used to describe a non-invasive papillary carcinoma found on the inner lining of the bladder, whereas T1 refers to a tumour embedded within the lamina propria but not yet invaded the muscle layer. Tis describes non-invasive flat carcinoma (flat carcinoma in situ, CIS) Ta and T1 tumours form mushroom-like protrusions while Tis (CIS or carcinoma in situ) forms flat lesions on the inner lining of the bladder. The flat lesions comprise cells in the mid- to upper epithelium with high cytologic grade. T2 describes a tumour that has invaded into the muscle layer, T3 describes tumour growth through the muscle layer into the fatty layer surrounding the bladder, and T4 describes tumour growth that has disseminated from the bladder to other organs. The second part of the classification involves the lymph node (N) stages, describing the number of involved lymph nodes and the region affected. N0

describes no cancer found in any lymph nodes, N1 refers to one affected lymph node in the pelvis, N2 refers more than one lymph node affected in the pelvis, and N3 refers to one or more lymph nodes affected in the groin. Finally, the metastasis (M) stage describes the spread of the cancer to another organ. M0 refers to no metastasis whereas M1 refers to metastasis found in other parts of the body, usually the bones, lungs or liver.

The grade of bladder cancer is determined by the morphology and growth rate of the cells. Grade 1 cancers have cells that display normal cell morphology and are slow growing. Grade 2 cancers comprise moderately differentiated cells that proliferate faster than those in low-grade tumours. Grade 3 cancers have poorly differentiated cells with even higher proliferative rates.

Advanced bladder cancer, known as invasive bladder cancer, consists of T2, T3 and T4 tumours. Patients with invasive bladder cancer are treated with radial cystectomy and proximal lymph node removal. This is followed by chemotherapy and radiation to lower the chance of relapse at a distant site. In more advanced T4 tumours, bladder cancer is treated with chemotherapy to shrink the primary tumour before radial cystectomy and radiation therapy.

Various chemotherapeutic agents are used in combination for the treatment of bladder cancer. The three main chemotherapeutic regimens for invasive bladder cancer are CISCA, CMV and MVAC. The CISCA regimen is a combination of Cisplatin, Doxorubicin and Cyclophosphamide for a cycle of 21-28 days

(Sternberg, Bracken et al. 1977). The CMV regimen consists of a combination of Cisplatin, Methotrexate and Vinblastine for a cycle 21 days (Harker, Meyers et al. 1985). The MVAC regimen is a combination of Methotrexate, Vinblastine, Doxorubicin and Cisplatin for a cycle of 28 days ('chemo regimen'). For non-invasive, high-grade bacillus Calmette-Guerin (BCG)-refractory bladder cancer, sequential intravesical combination chemotherapy consisting of gemcitabine and mitimycin C is used (Lightfoot, Breyer et al. 2013).
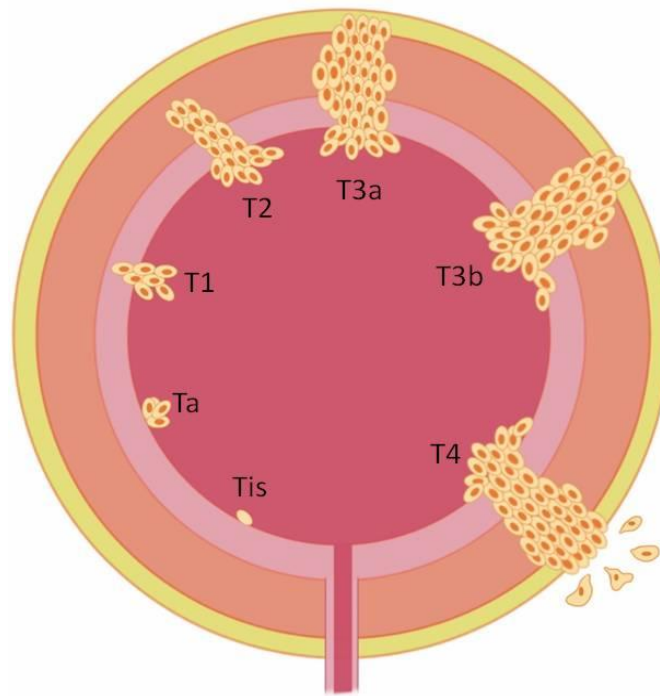
Figure 4: Illustration of bladder cancer tumour stages.
Bladder cancer is staged using the TNM (tumour, nodes, metastatsis) classification system. 'T' is followed by numbers and/or letters to describe the extent to which the primary tumour has grown through the bladder wall. Tis: Non-invasive flat carcinoma (flat carcinoma in situ, CIS); Ta: non-invasive papillary carcinoma; T1: the tumour has grown from the inner lining of the bladder to the lamina propria but not yet invaded the muscle layer. T2: The tumour has grown into the muscle layer. T3: the tumour has grown past the muscle layer into the fatty layer. T3a: the tumour spread to the fatty tissue can only be seen by using a microscope. T3b: the tumour spread to the fatty tissue is large enough to be detected by imaging tests or seen/felt by the surgeon. T4: tumour has spread beyond the fatty layer.

Bladder cancer and growth factors

Growth factors contribute to tumorigenesis by increasing tumour cell proliferation, angiogenesis and invasion. Certain growth factors and their cognate receptors have been found associated with bladder cancer progression. For example, EGFR was first characterized in superficial and invasive bladder cancer in 1989 (Smith, Fennelly et al. 1989). The over-expression of wild-type EGFR and abnormal secretion of EGF preceded the physical detection of transitional cell carcinoma. The degree of EGFR over-expression in bladder tumours correlates with the tumour stage and grade (Khaled, Bahnassy et al. 2009).

Activating point mutations of FGFR3 have also been identified in approximately 75% of low-grade and low-stage bladder carcinoma. Mutations in FGFR3 are common in papillary bladder cancers, suggesting that FGFR3 mutations occur early in the development of non-invasive bladder cancer (Cappellen, De Oliveira et al. 1999; Hernandez, Lopez-Knowles et al. 2006). Up regulation of FGFR signalling is also detected in tumours with oncogenic FGFR3 gene fusions (Williams, Hurst et al. 2013).

Elevated levels of HGF have been detected in the serum and tissues of patients with bladder cancer. Muscle-invasive cancer patients have higher serum levels of HGF than do superficial cases. Among all bladder cancer patients, those with metastatic bladder cancer have the highest levels of HGF in the serum and tissue. Decreased disease-free period and overall survival rates are reported for patients

with high serum levels of HGF as compared to those with similar disease state but lower HGF serum levels (Smolen, Sordella et al. 2006).

Since haematuria is usually associated with advanced bladder cancer, the VEGF pathway is to be critically important in the process of angiogenesis. Studies have shown that protein expression of VEGF in bladder cancer tissues and serum levels of VEGF correlate with increased tumour stage (Bernardini, Fauconnet et al. 2001; Yang, Chu et al. 2004). In particular, VEGFR2 expression correlates with pathological stage in human urothelial carcinoma cell lines and bladder tumours (Xia, Kumar et al. 2006).

Objectives

In this thesis, an *in vitro* bladder cancer model was used to investigate the interaction of microenvironment and carcinoma cells. Chapter 1 describes the establishment of an *in vitro* bladder cancer model that readily engages EMT when induced. When NBT-II carcinoma cells are challenged with EGF and HGF, NBT-II carcinoma cells not only undergo EMT but also express a common set of genes that is responsible for tumour progression. Interestingly, some of the EGF and HGF regulated genes are highly associated with invasive bladder cancer. The role HGF play in bladder tumour progression is further examined. The transcriptomics of NBT-II carcinoma cells at multiple time-points after HGF induction was investigated. The level of transcriptional activity is highest during the window

from which the cells disperse to the point they gain motility. Expression profiling analysis indicates that HGF initiates other signal transduction pathways to acquire and sustain a mesenchymal phenotype. A downstream effector, Smad2 is implicated in this HGF induction system and is regulated by both MAPK and TGFbR1. This chapter also describes the difference in the role of the linker and C-terminus region of Smad2.

Chapter 2 is divided into 2 parts. The first part of Chapter 2 describes an EMT inhibitor screen in which small molecular weight kinase inhibitors were utilised to interfere with downstream signalling systems to c-Met (HGFR). This screen identified inhibitors that target c-Met, MEK, PI3K and TGFRβ. The shortlisted inhibitors were able to block EMT and transwell migration. In the second part of Chapter 2, we utilised an *in vivo* orthotopic bladder cancer mouse model to test the potential of a TGFβRI inhibitor in delaying cancer progression. The *in vivo* model shows that carcinoma bladder wall invasion was delayed in inhibitor treated mouse. In chapter 3, the significance of these findings and the impact they have on therapy will be discussed.

Chapter 2: Experimental procedures

Cell lines and culture conditions

The transitional cell carcinoma cell lines HT1376, J82, NBT-II, T24, TCCSUP, UM-UC-3 were obtained from the American Type Culture Collection (ATCC; catalog no. CRL-1472, HTB-1, CRL-1655, HTB-4, HTB-5, CRL-1749). Cells were routinely cultured in Dulbecco's Modified Eagle Medium (Gibco, Life Technologies) supplemented with 10% fetal bovine serum (FBS, HyClone Thermo Scientific), 1 µg/ml puromycin (Sigma) and 100 units/ml penicillin-streptomycin (1× pen-strep, Invitrogen). Cultured cells are regularly tested for mycoplasma contamination.

Reagents and preparation of compound plates

For each growth factor-induced EMT in NBT-II cells, we optimized the final growth factor concentrations to be 20ng/ml EGF (Sigma), 4ng/ml HGF (Calbiochem) for EMT inhibitor screen, 5 ng/ml HGF for all other experiments and 150ng/ml IGF-1 (R&D Systems).

Test compounds were purchased from various vendors (Selleck Chemicals, Sigma Aldrich, SYN|thesis MedChem, and Tocris Bioscience). Compound stocks were assembled in 96-well V-bottom plates (Greiner). For screening studies, test compounds at both 0.25 mM and 1.0 mM concentrations in DMSO were prepared, with each occupying a single well in columns 2–11 of the stock plates. For dose response studies, test compounds were prepared in duplicate wells and

serially diluted in DMSO, starting with a 1.0 mM concentration. Stock plates were stored at $-20^{\circ}C$ and thawed to room temperature before use.

Stable transfection

NBT-II were stably transfected with mcherry-fluorescent H2B plasmid (Addgene deposited by Robert Benezra) using lipofectamine2000, according to manufacturer's protocol (Invitrogen), followed by selection for single clones by supplementing 1mg/ml neomycin (Sigma) to the medium.

NBT-II/ UM-UC-3 were stably transfected with Smad2dnL and Smad2dnC plasmid (Addgene deposited by Joan Massague and Rik Derynck) using lipofectamine2000, according to manufacturer's protocol (Invitrogen), followed by selection for single clones by supplementing 1ug/ml puromycin (Invitrogen) to the medium.

UM-UC-3 were stably transfected with pGl4.51 luciferase 2/CMV vector (Promega) using lipofectamine2000, according to manufacturer's protocol (Invitrogen), followed by selection for single clones by supplementing 1mg/ml neomycin (Sigma) to the medium. Luciferase activity was measured with luciferase assay (Promega).

Immunofluorescence

NBT-II cells were seeded at a density of 100 cells per well on Ibidi 8 well μ-slides and grown for four days to form colonies. Cells were pre-treated with HGF or EGF and then fixed with 4% paraformaldehyde and stained with mouse anti-rat Desmoplakin (Millipore; clone DP2), mouse anti-human Vimentin (Abcam; clone V9) and mouse anti-Smad2/3 (BD Transduction Laboratories; clone 18/Smad2/3) primary antibodies. A goat anti-mouse antibody conjugated to Alexa Fluor 488 (Invitrogen) was used as a secondary antibody. Fluorescent images were captured with a Leica DM6000b Inverted microscope and monochrome coolsnap HQ2 camera (microlambda).

DNA microarray

Total RNA was purified from NBT-II cells using RNeasy mini kit (Qiagen). RNA concentration was determined using NanoDrop 1000 Spectrophotometer (Thermoscientific) and RNA integrity was measured using the Agilent Bioanalyzer 2100 (Agilent). 5ug of total RNA was used to generate sense-strand cDNA using Ambion® WT Expression Kit protocol (Ambion) with Applied Biosystems Vertic 96 well Thermal Cycler (Applied Biosystems) followed by fragmentation and labelling using the Affymetrix GeneChip® WT Terminal labelling kit protocol (Affymetrix) before loading onto the Affymetrix Rat Gene 1.0st Array (Affymetrix). The probe array was incubated for 16 hours at 45°C at constant rotation (60r.p.m). The washing and staining procedure was performed in

the Affymetrix Fluidics Station 450 (Affymetrix). Microarrays were then scanned using GeneChip® Scanner 3000 7G (Affymetrix).

DNA microarray data analysis

Probe set intensities were normalized with unified efficient Lowess correction (Ballman, Grill et al. 2004). Normalization was performed on all 24 microarrays, followed by a log2 transformation. Log2 probe intensities of below 6 were filtered off from the analysis. About 53% of the probe-sets pass as present in each sample. Significant genes were chosen with criteria of FDR 0.01 and a minimum fold change of 1.2.

Gene score analysis – finding Differentially Expressed Genes (DEG)

The method reported by Zeisel A et al (Zeisel, Amir et al. 2010) was used to estimate intensity-dependent noise in the data and to estimate p-values. This method assumes that the noise in the data has a normal distribution and is intensity dependent. Genes were filtered according to temporal variation to find genes that have at least one time point with a fold change of at least 2 compared to its initial value at t=0. P-values for differential expression of each gene, at every time-point − comparing treated vs. control, based on intensity-dependent estimation of the noise was computed. An improved Benjamini-Hochberg (Benjamini and Hochberg 1995) estimate of the False Discovery Rate (FDR) was used (Zeisel, Zuk et al. 2011) Genes with FDR below 0.05 and with a minimal

fold change value of 1.5 at the specific time-point were identified as DEGs. Gene score was computed: score= number of time-points at which a given gene is differentially expressed.

Functional annotation and pathway enrichment analysis

In order to assign biological interpretation to gene lists, gene set enrichment analysis was performed using the DAVID online tool, to identify both significantly dominant biological processes and pathways (Huang da, Sherman et al. 2009) (Huang da, Sherman et al. 2009)

Wound healing assay

NBT-II cells were seeded at a density 2×10^5 cells/ml in each well of a 12 well-plate (NUNC) and transfected with 20nM of siRNA (Smad2, Smad3 and Smad4) (Qiagen) for 48 hours. 3 wounds were made for each sample using a yellow pipette tip, and wound closure was imaged at 0 hour and after 24 hours. Area of the wound was measured using ImageJ software. Total area migrated by the cells was calculated by subtracting the area measured at 24 hour from the area of the wound measured at 0 hour.

Fractionation assay

NBT-II cells were seeded at a density of 0.5 x10^6 cells per 10cm cell-culture treated dish (NUNC) and grown for four days to form colonies. Cells were pre-treated with HGF or HGF + A83-01 before harvesting. Cells were tripsinized and the number of cells in each sample was quantified. Equal number of cells was pelleted for each sample. Fractionation was performed using Qproteome cell compartment kit (Qiagen), according to manufacturer's protocol.

Transwell assay/Boyden chamber

5 x10^5 of cells were seeded on Matrigel (BD biosciences) coated polycarbonate membrane insert (6.5 mm in diameter with 8.0um pores) that hung above medium supplemented with or without HGF in a Transwell setup (Costar) and incubated for 24 hours at 37°C. The upper side of the insert was swiped with cotton bud to remove the non-motile cells and the cells at the underside of the insert were stained with calcein AM (Invitrogen) for an hour in the incubator. The stained cells were then trypsinized and the number of migrating cells in each well was quantified by fluorescence reading using Tecan100 (Tecan).

Spot migration assay

NBT-II cells were trypsinized and concentrated to a density of 5×10^6 cell/ml in CO_2-independent medium (Invitrogen) supplemented with 10% FBS. The cell

suspension was then evenly dispensed into the wells of 2 columns of a 96-well V-bottom plate. Using a robotic liquid-handling station (Bravo, Agilent Technologies), 0.5 µl of cell suspension was transferred from the 2 columns of the cell suspension-loaded plate and deposited into the center of the wells of 2 columns of a blank 96-well polystyrene tissue-culture treated clear bottom, black assay plate (Corning #3904). This process was repeated six times so that all 96 wells of the assay plate were deposited with a cell suspension spot. The plate was then sealed to minimize evaporation of the cell suspension spots and transferred to a 37°C, 5% CO_2 incubator to allow for cells to attach to the culture surface. After 1 hour, the plate was gently washed with medium once to remove unattached cells, refreshed with 100 µl of assay medium (DMEM supplemented with 10% FBS and 1× pen-strep), and then further incubated to allow for cell-cell contacts to establish in the cell colonies.

After 4 hours of incubation, the cell colonies for each well were imaged using a confocal microplate imager (MetaXpress Ultra, Molecular Devices) with 10×Plan Fluor objective, 561 nm laser excitation and 593/40 nm emission filter configuration. Four tiled, non-overlapping images were acquired around the center of each well, and were then stitched together during image analysis to generate a montage covering an area of 3.2 mm×3.2 mm. These images (T1) represent the initial state of the cell colonies before EMT induction.

After the T1 images were acquired, 1 µl of test compounds were transferred from compound stock plates and added to the assay plates. Appropriate negative

controls (1 µl DMSO) and positive controls (1 µl 1.0 mM compound in DMSO) were also added into columns 1 and 12 of each assay plate, respectively. The assay was optimized to use AG1478, JNJ-38877605 and BMS-536924 as reference positive control compounds for EGF-, HGF- and IGF-1-induced EMT, respectively. The cultures were then further incubated overnight.

The next day, 50 µl of growth factor-containing medium was added to each well of the assay plates. The cultures were then incubated for another 24 hours, to allow for EMT and sufficient cell motility/dispersion to occur in the cell colonies.

Finally, the cell colonies were imaged again using the microplate imager, as described above. These images (T2) represent the final state of the cell colonies after compound treatment and EMT induction. The acquired T1 and T2 image sets for each assay plate were then sent for image analysis.

Image analysis routine

The acquisition of each well was obtained by four adjacent field images with no interstice in between. Each field image was loaded and nuclei were initially segmented independently of other fields to prevent artifact at the field border. Nuclei segmentation was achieved by combining a wavelet transform which is robust to noise and inhomogeneous background, and a watershed algorithm based on intensities to split nuclei clusters. Mask of nuclei segmentation of the different fields were then stitched together in order to obtain a large segmentation of the whole well. Cell bodies were estimated by applying a morphological dilation on the nucleus segmentation using a disk of 30 pixels (48 µm) in diameter. In cells

that were contiguous, such as in a cell colony, nuclei segmentation dilation will result in the formation of continuous region areas with surrounding cells which can then be identified as colonies. In general, a well will contain one big colony (corresponding to the initial cell spot) and several much smaller colonies (corresponding to single cells, small cluster of cells, dust and contamination). Only nuclei contained in the biggest colony were kept and subsequently analysed. A spreading coefficient was derived from nuclei positions in order to measure how much the colony had dispersed. The spreading coefficient is defined as the standard deviation of the cell positions in the cell colony relative to the center of the colony:

$$sp = \frac{1}{\#Col} \sum_{c \in Col} \sqrt{(c_x - Col_x)^2 + (c_y - Col_y)^2}$$

where **Col** indicates all cells of a colony, **#Col** is the total cell number, [**Col$_x$, Col$_y$**] is the average position of all nuclei in the colony, [**c$_x$, c$_y$**] is the position of the cell c. The coefficient **sp** is homogenous with a distance and indicates the relative cell dispersion from the colony center.

Total cell number and spreading coefficient values for each well were exported into an Excel sheet. The Cell Count Ratio (CCR) and Cell Dispersion Ratio (CDR) values were calculated by combining data calculated from T1 and T2 images for each well, while the normalized CDR or CDR% of each well calculated by taking the CDR values of negative and positive controls as the control limits:

$$CCR = \frac{\#Col_{T2}}{\#Col_{T1}}; CDR = \frac{sp_{T2}}{sp_{T1}};$$

$$CDR\% = \frac{CDR - CDR_{pos}}{CDR_{neg} - CDR_{pos}} \times 100\%$$

where **CDR$_{pos}$** and **CDR$_{neg}$** are the average CDR values of the negative and positive control wells respectively in each test plate (Inglese, Shamu et al. 2007).

EMT time-lapse video

EMT inhibitory effects of selected compounds were validated by NBT-II epithelial colony time-lapse videoscopy. NBT-II cells were plated onto a 12-well plate (BD) at a low density of 2000 cells per well in 1 ml of assay medium. Cells were allowed to grow and form epithelial colonies for a period of 4 days. The cultures were then refreshed with assay medium containing growth factor (EGF or HGF) prior to video imaging. Video imaging of individual cell colonies was performed using a video microscope incubator system (Axiovert-200M, Carl Zeiss). Time-lapse images were taken at 5 min intervals for 18 hours. Tracking of cells was performed with the particle tracking function in Metamorph software (Metamorph).

Western blots

Cells were lysed with protease/phosphatase inhibitor (Calbiochem) -containing RIPA buffer (Sigma). Proteins were separated in 8% polyacrylamide gels and transferred to PVDF membranes (Millipore). Membranes were blocked in 5%

BSA (Sigma) and incubated at 4°C overnight with MMP-13 (Millipore), E-cadherin (BD), α-tubulin (Sigma) and pSmad2 245/250, pSmad2 467, Smad4, Smad3, pc-MET, c-MET, pEGFR, EGFR, pIGFR-1, IGFR-1, pERK 1/2, ERK (Cell Signaling) primary antibodies. Membranes were then developed with HRP-conjugated secondary antibody (Amersham) and ECL substrate (Millipore). The blots were scanned using G:BOX Chemi XT16 (Syngene).

Bladder cancer animal models

Orthotopic model

All animal work adhered to the Agency of Science Technology and Research (A*STAR), Institutional Animal Care and use Committee (IACUC), guidelines on animal use and handling. 6 to 8 weeks old female balb/c nude (nu/nu) mice were used. General anesthesia was induced in the mice with inhaled isoflurane (4% for induction, 1-2% for maintenance) and maintained via nosecone. Sterile ophthalmic ointment is applied to the animal's eyes and a heating platform is used to maintain body heat. The urine of the animals was removed by applying gentle pressure on the bladder. Using a lubricated 24-guage intravenous catheter (Braun) connected to a 1ml syringe (BD) with the needle stylet removed, the mouse urethra was catheterized. A pair of forceps was used to gently lift the vulvar folds. A 45 degree angle was initially adopted to cannulate the urethra following which a shallower angle was taken to pass the catheter through the urethra into the bladder. Care was taken not to perforate the urethra or bladder. 100ul of PBS was

instilled into the bladder to wash the lumen. 100ul 0.2% Trypsin was instilled in the lumen for a maximum of 30 minutes. Following which the bladder was washed three times with 100ul PBS. 100ul of a 5x10^6 UMUC3-Luc2 cells was instilled into the bladder and the catheter and syringe left in place. The mouse was maintained under general anesthesia for 3 hours before the catheter and syringe was removed.

Subcutaneous model

Xenografts were generated by injecting 0.1ml of 2.5x10^6 of UMUC3-Luc cells subcutaneously into the dorsal flanks of female BALB/c nude mice (6 to 8 weeks old). Animal body weight and physical signs were monitored during the experiments. Tumour size was measured weekly by vernier caliper. The tumour volume was calculated, with the formula: [length x width2]/2.

Bioluminescent Imaging

General anesthesia was induced in mice with vaporized isoflurane and maintained via nose cone. Bioluminescence imaging was performed using the IVIS Spectrum Imaging System 200 (Xenogen) 10 minutes after an intraperitoneal injection of 150mg/kg firefly D-Luciferin in 200uL of PBS. A digital grayscale image was acquired followed by an acquisition and overlay of a pseudocolor image representing the spatial distribution of detected photons emerging from active luciferase within the mouse. Signal intensity was quantified in photons per second

per region of interest. Imaging was performed weekly for 5 weeks after tumour inoculation.

Histological procedures

4% paraformaldehyde was delivered via a catheter into the mouse bladder lumen and was retained for 10 minutes. Following which the mouse urethra was tied and the whole bladder was excised and placed into 4% paraformaldehyde overnight at 4^oC. The fixed bladder was paraffin embedded and paraffin blocks were cut at 6um thickness per tissue section. Bladder tumours were deparaffinized before hematoxylin and eosin (H&E) staining.

Colony formation assay

The soft agar assay consisted of 3 layers. 0.6ml bottom layer of 0.6% agar in RPMI (Gibco, Life Technologies) supplemented with 10% fetal bovine serum (FBS, HyClone Thermo Scientific), was dispensed into each well of a 24-well plate and allowed to solidify at room temperature. The middle layer (0.5ml) consisted of 0.36% agar with UM-UC3 carcinoma cells in RPMI medium supplemented with 10% fetal bovine serum was plated above the bottom layer and allowed to solidify at room temperature. The top layer consisted of 0.5ml/well of RPMI medium supplemented with 10% fetal bovine serum and compounds. Experiments were set up in triplicates and incubated at 37^oC in a humidified incubator with 5% CO2 for 2 weeks.

Statistical analysis

Error bars in CDR dose response plots in the EMT inhibition screen represent standard deviation of replicate samples. CDR IC_{50} values were calculated through sigmoidal curve fitting of CDR dose response plots using GraphPad Prism software. Statistical tests used are described in the individual figure legends. Prism (GraphPad Inc.) and Excel (Microsoft) softwares were used for calculations and graphing. P values less than 0.05 were considered statistically significant.

Chapter 3: Results

Part 1: Progression scheme of high grade superficial tumours to the muscle invasive state in bladder cancer.

Introduction

Neoplastic transformation of urothelial cells gives rise to urothelial carcinomas broadly classified into non-muscle invasive (Ta and T1) and muscle invasive ($\geq$ T2). Patients diagnosed with bladder carcinoma often suffer from recurrent tumours. At present, the mechanism leading to bladder cancer is still poorly understood and our knowledge about progression from low stage/grade to high stage/grade tumours is also limited. Much effort has been made to understand the etiology of bladder cancer and it has revealed that urothelial carcinoma develops through a multistep process, accumulating genetic alterations during progression.

Non-muscle invasive tumours are difficult to eradicate and have diverse prognosis. Low grade Ta tumours rarely progress to muscle invasive tumours but frequently recur while high grade Ta and T1 tumours display a higher risk of progression. Tumours progressing to muscle invasive carcinomas are life threatening as these tumours often lead to extensive metastasis. These observations prompt to identify molecular mechanisms that govern the progression of high grade tumours in order to treat patients with a more specific therapeutic regimen.

EMT is an important process in high grade bladder tumours. It is characterized by a down-regulation of the E-cadherin adhesion molecule and of proteins associated with cell polarity along with up regulation of fibronectin, vimentin and MMPs. EMT induced by TGF-β and growth factors such EGF family members and HGF is associated with loss of differentiation and increased migration, invasion and angiogenesis. Dissecting the EMT process into functional modules might provide an insight to a better understanding of the progression of high grade tumours.

In order to study the events leading to cancer cell dissemination, we have chosen to study an *in vitro* bladder cancer cell model which exhibits a transition from bona fide epithelial, forming cobblestone colonies to migratory single mesenchymal cells. The cell line model designated Nara Bladder Tumour-II (NBT-II) carcinoma cell line was established from a rat bladder carcinoma. Wistar rats were given the carcinogen, BBN(N-butyl-N-(4-hydroxybutyl) nitrosamine) at a concentration of 0.05% in drinking water for 20 weeks to induce bladder tumours (Toyoshima, Ito et al. 1971). The tumours produced by this carcinogen resemble invasive human bladder cancer in histology, etiology and in kinetics. Bladder tumours in rodents are often Tis and were of high grade with invasive potential. NBT-II carcinoma cells present a favourable model to work with for *in vitro* studies. NBT-II cells can undergo EMT in response to several different growth factors and extracellular matrix proteins (Valles, Boyer et al. 1990); (Tucker, Boyer et al. 1991); (Bellusci, Moens et al. 1994); (Petit, Boyer et al. 2000)

The oligonucleotide microarray technology offers the possibility to quantify expression levels of thousands of genes in parallel. DNA microarray analysis has emerged as an important tool to identify genes that are differentially expressed in normal and disease state. An in-depth analysis of microarray expression profiling can provide 1) association studies which aim to construct a panel of genes or biological pathways implicated, 2) class discovery which aims to discover clusters based on molecular data and 3) prediction studies which aims to classify patients based on clinical endpoints and drug response. In our study, DNA microarray technology is utilised to dissect step by step the EMT process enabling the discovery of step-wise activation of biological pathways critical in the progression of high grade superficial tumours to muscle invasive state.

Results

NBT-II carcinoma cells undergo EMT in response to EGF and HGF.

NBT-II cells treated with epidermal growth factor (EGF) or hepatocyte growth factor (HGF) for 24 hours undergone EMT. The edge of untreated colonies was well defined with cells displaying an epithelial morphology and retaining cell-cell contacts; while the edge of colonies treated with EGF or HGF was disrupted with cells acquiring a mesenchymal morphology accompanied by the loss of cell-cell contacts (Figure 5).
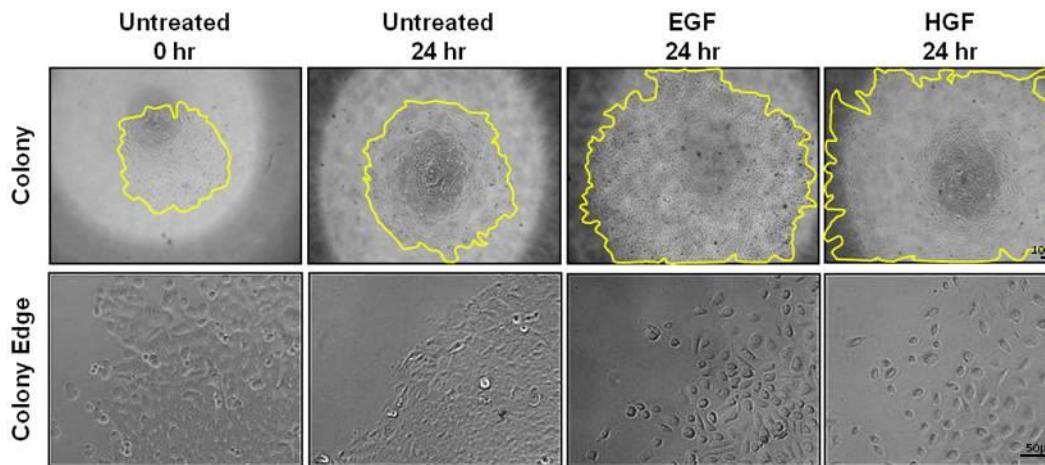
Figure 5: EGF or HGF disrupts cell-cell contacts and induce morphological changes in NBT-II cells.
NBT-II cells (5000 cells per well/96 well-plate) were seeded onto the center of each well to compact for 5 hours before incubation with growth factors (20ng/ml EGF, 5ng/ml HGF) for 24 hours. Colony: phase contrast pictures taken at 4x magnification; Colony edge: phase contrast pictures taken at 10x magnification.

Desmoplakin redistributed from the membrane cortex to the cytoplasm, indicating loss of cell-cell contact; and Vimentin increased after 24 hours of EGF or HGF treatment, indicating EMT (Figure 6A). To assess motility, NBT-II cells were tracked for 18 hours using time-lapse microscopy. As seen in Figure 6B, NBT-II cells treated with EGF and HGF travelled significantly further (EGF: 764μm, HGF: 634 μm vs Ctrl: 203 μm) with an increase velocity (EGF: 60 μm/hr, HGF: 50 μm/hr vs Ctrl:15 μm/hr) (Figure 6C).
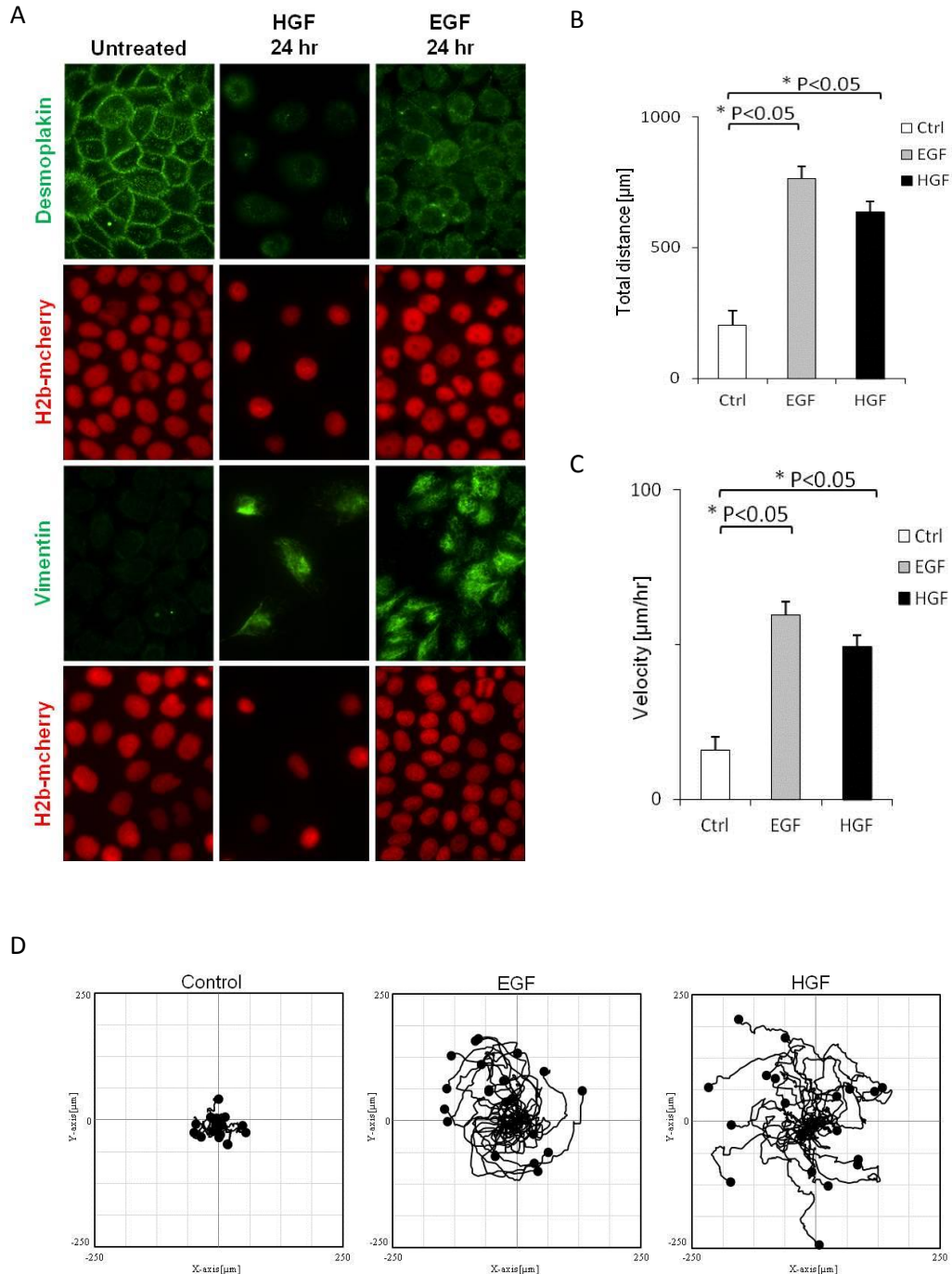
Figure 6: EGF and HGF induce MT in NBT-II cells.
(A) NBT-II carcinoma cells were grown for 4 days to form cell colonies before the start of experiment. Cell colonies were then treated with HGF (5ng/ml) or EGF (20ng/ml) for 24 hours. Top panel, Green: Desmoplakin (cell-cell contact); Third panel, Green: Vimentin (intermediate filament); Red: H2b (nuclear stain). Images are representative of 3 independent experiments. (B) illustrates the individual tracks of 30 cells in the colony. (C) and (D) show an increase in velocity and distance travelled by NBT-II cells treated with EGF/HGF. Bars represent mean + SEM. *p<0.05 , two-tailed t-test.

Gene expression profiling was performed on NBT-II cells treated for 24 hours with EGF and HGF to identify differential gene expression correlating with that of the morphological and behavioural changes induced by growth factor in NBT-II cells. Transcriptome analysis provided a list of 383 genes regulated by both EGF and HGF (Figure 7A). Among the genes that were regulated by EGF and HGF, transcriptome analysis also identified a subset of genes that were closely related to EMT. The expression of these genes was validated using quantitative reverse transcription polymerase chain reaction (qRT-PCR). An up-regulation of mesenchymal markers such as Matrix metalloproteinase 3 (Mmp3), Serpin peptidase inhibitor, clade e, member1 (Serpine1) and Zinc finger E-box binding homeobox 1 (Zeb1) and a down-regulation of epithelial markers such as Desmoplakin (Dsp), Keratin 19 (Krt 19) and Occludin (Ocln) was observed (Figure 7B). Taken together, the data demonstrated that NBT-II cells can undergo morphological and behavioural changes characteristic of epithelial mesenchymal transition and hence demonstrated its relevance as an *in vitro* model for this study.
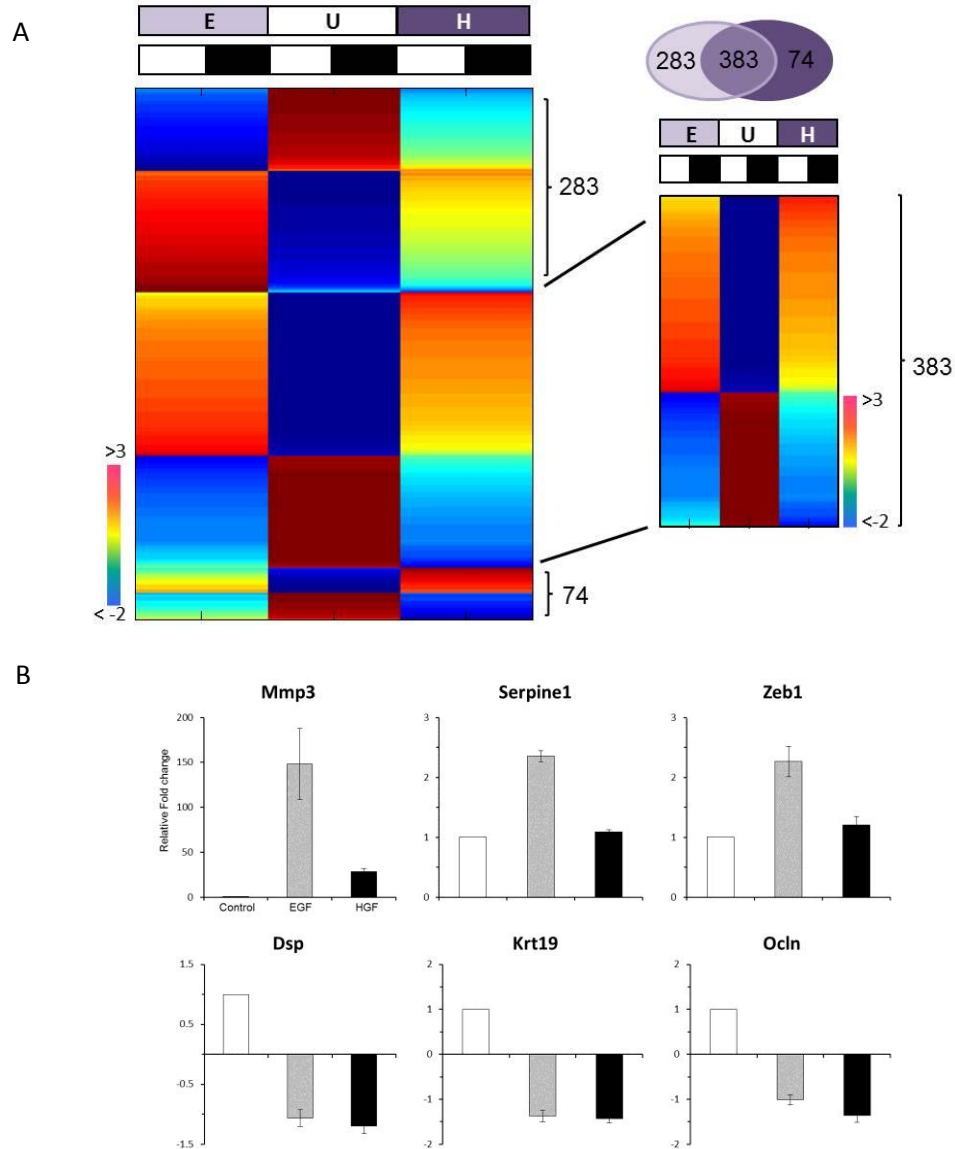
Figure 7: Transcriptomic analysis revealed common genes induced or repressed by EGF and HGF.

(A) The differential expression level for each of the growth factor (E/H) treated samples is provided relative to the untreated (U) samples. A set of 383 common genes showed significant over-expression/down-regulation in the presence of EGF/HGF. E= EGF; H= HGF. Arrays were analysed in duplicates: white bar = repeat 1; black bar = repeat 2. (B) Further analysis of the 383 genes revealed a subset of EMT-related genes. Real-time PCR analysis with reverse transcription showing fold induction of Mmp3, Serpine1, Zeb1 and fold reduction of Dsp, Krt19 and Ocln messenger RNAs in NBT-II cells treated with EGF/HGF. Data are normalized with the expression levels of housekeeping genes and represent the mean of 3 independent experiments. Bars represent mean $\pm$ SEM.

NBT-II carcinoma cells in response to EGF and HGF engage in processes relevant to tumour progression

Gene ontology analysis revealed that the 383 genes participated in biological processes typical of tumour progression such as actin cytoskeleton organization, cell migration and cell proliferation (Table 1). Pathway analysis indicated focal adhesion, ECM-receptor interaction and ErbB signalling as the top three networks (Table 2). Genes of these networks regulate cell-substrate adhesion and affect the stability of cortical actin which are both important for EMT and migration. Up-regulation of ErbB family ligands as well as v-myc myelocytomatosis viral oncogene homolog (Myc) and PI3K contribute to cell survival. Moreover, down-regulation of tumour suppressors like Grhl3, Gata3, Id4, Hoxd10 and Bhlhe40 were observed among the 383 genes (Appendices). Taken together, the data demonstrated that under the influence of growth factors, NBT-II cells can recapitulate certain aspects of tumour progression.

Table 1: Biological processes engaged when induced by EGF/HGF.

Biological process	EGF	HGF
Actin cytoskeleton organization	+	+
Cell adhesion	+	+
Cell communication	+	+
Cell motion/migration	+	+
Cell proliferation	+	+
Enzyme linked receptor protein signaling	+	+
Epidermal growth factor signaling	+	+
Programmed cell death	+	+
Regulation of phosphorylation/protein kinase activity	+	+
TM receptor protein tyrosine kinase signaling	+	+
Wound healing	+	+

Table 2: Top 3 pathways in EGF/HGF induced NBT-II cells.

Pathway	Genes	FDR (Benjamini)
Focal adhesion rno04510	FLT1, PIK3CB, PIK3CD, ACTN1, ITGA2, ITGA3, VCL, LAMB3, CCND1, LAMA3, LAMB2, LAMA5, PPP1R12A, LAMC2, ZYX, THBS2	0.00065
ECM-receptor interaction rno04512	LAMB3, LAMB2, LAMA3, CD44, LAMA5, ITGA2, LAMC2, ITGA3, THBS2	0.01003
ErbB signaling pathway rno04012	EREG, PIK3CB, PIK3CD, HBEGF, TGFA, AREG, NRG1, MYC	0.05515

NBT-II carcinoma cells induced by EGF and HGF express genes found in advanced stages of bladder cancer

Since constitutively activated growth factor receptors and elevated serum levels of growth factors were causal factors for invasion and metastasis in cancer, the list of 383 gene list was further explored by comparing it with 7 published human bladder cancer microarray data sets comprising 400 patients. This analysis identified a set of EGF/HGF driven genes (Table 3) that were deregulated in invasive bladder cancer. This further affirms the role EGF and HGF play in bladder cancer progression towards enhanced malignancy.

Table 3: Identification of a subset of genes implicated in invasive bladder cancer.

Name	Symbol	Up/Down-regulated	Reference
Actinin, alpha 1	Actn1	Up-regulated	Riester et al., 2012
Amphiregulin	Areg	Up-regulated	Blaveri et al., 2005
Caveolin 1	Cav1	Up-regulated	Rajjayabun et al., 2001
Chemokine (C-X-C motif) ligand 1	Cxcl1	Up-regulated	Kawanishi et al., 2008
Cyclin D1	Ccnd1	Up-regulated	Watters et al., 2002
Dual specificity phosphatase 6	Dusp6	Up-regulated	Blaveri et al., 2005
Early growth response 1	Egr1	Up-regulated	Modlich et al., 2004
ETS-domain protein	Elk3	Up-regulated	Modlich et al., 2004
FOS-like antigen 1	Fosl1	Up-regulated	Modlich et al., 2004
High mobility group AT-hook1	Hmga1	Up-regulated	Modlich et al., 2004
Integrin, alpha 3	Itga3	Up-regulated	Modlich et al., 2004
Laminin, gamma 2	Lamc2	Up-regulated	Modlich et al., 2004
Matrix metallopeptidase 3	Mmp3	Up-regulated	Blaveri et al., 2005
Prostaglandin-endoperoxide synthase 2	Ptgs2	Up-regulated	Mohammed et al., 1999
Thrombospondin 2	Thbs2	Up-regulated	Blaveri et al., 2005
v-myc myelocytomatosis viral oncogene homolog	Myc	Up-regulated	Watters et al., 2002
Jun D proto-oncogene	Jund	Down-regulated	Modlich et al., 2004
Keratin 19	Krt19	Down-regulated	Modlich et al., 2004

Changes in cell morphology and motility observed post HGF induction

Muscle-invasive bladder cancer patients have higher serum levels of HGF than patients with superficial ones. To address the impact of HGF signalling on bladder cancer progression, subsequent studies will focus on the contribution of

HGF to the changes in cell morphology, motility and differential gene expressions. To investigate the dynamic changes in phenotype during HGF-induced mesenchymal transition, images of NBT-II carcinoma cells were taken at an interval of 5 minutes for 48 hours and compiled into a movie using Axiovision software. Under the influence of HGF treatment, coherent sheets of epithelial NBT-II carcinoma cells progressively dissociated, leading to single cells with increased spreading and lamellipodial activity. The time-points were recorded when an observable change in morphology and behaviour of NBT-II carcinoma cells was detected. NBT-II carcinoma cells remained in the epithelial state after 2 hours of HGF treatment and engaged into locomotion within 3-4 hours following HGF induction. 4 hours post HGF treatment, NBT-II carcinoma cells enter a meta-stable state in which epithelial colonies were disrupted and each cell can alternatively remain stationary or locomote; and 9 hours post HGF induction, NBT-II carcinoma cells reached a mesenchymal state in which the scatter effect was preeminent and NBT-II carcinoma cells migrated out of the colonized area (Figure 8A). To assess motility for the 6 defined time-points (0, 2, 4, 6, 9, 24 hours), NBT-II carcinoma cells were tracked for an hour at each time-point using timelapse microscopy. NBT-II carcinoma cells that entered the meta-stable state migrated with a 2-fold increase in velocity as compared to cells in the epithelial state (Figure 8C). NBT-II cells in the EMT-ed state travelled significantly further (Figure 8D) with an increase velocity (Figure 8C) that resulted in larger total displacement (Figure 8E).
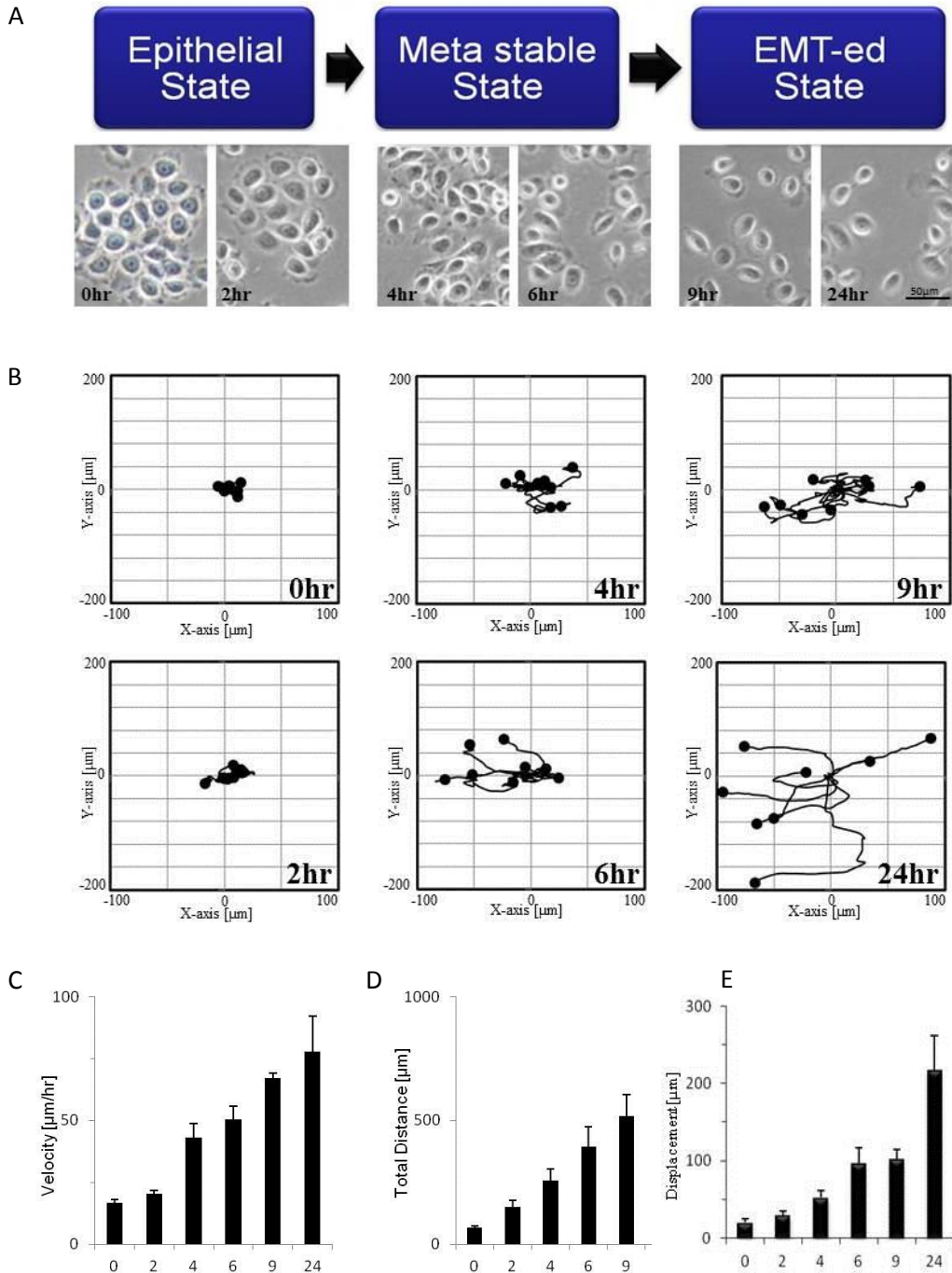
Figure 8: HGF induced subsequent changes in cell morphology and cell migration.
(A) NBT-II carcinoma cells were grown for 4 days to form cell colonies. The cell colonies were subsequently treated with HGF (5ng/ml) and imaged at 2, 4, 6, 9, 24 hours post HGF. (B) illustrates the individual tracks of 8 cells in the colony. (C), (D) and (E) show an increase in velocity, distance travelled and displacement of NBT-II cells treated with HGF over the period of 24 hours. Bars represent mean + SEM.

Sets of genes with sustained expression shift NBT-II cells towards a more invasive state

In an attempt to investigate how cancer cells shift towards a more malignant state under the influence of a growth factor, gene expression profiling was performed on NBT-II cells treated with HGF for the 6 defined time-points. Gene scores were computed and 326 genes (226+76+24 numbers represented in red in Table 4) were observed with sustained expression over 3 or more time-points. Detailed analysis was performed on these 326 genes as these genes might provide clues to the mechanism of tumour progression. Pathway analysis indicated that ErbB, p53, MAPK signalling and focal adhesion related pathways were altered (Table5). Dysregulation of ErbB, MAPK and p53 pathways promote cell survival and apoptosis evasion (Witsch, Sela et al. 2010) (Plati, Bucur et al. 2008). Focal adhesion related pathway regulates cell motion and invasion processes (Huttenlocher and Horwitz 2011). Gene ontology analysis also revealed biological processes related to migration like regulation of cell motion (GO:0051270) and branching morphogenesis (GO:0049754) (Table 6). For example, genes up-regulated in this analysis were often over-expressed in metastatic cancers. Down-regulation of FGFR3 gene expression was also observed in the microarray analysis. Down regulation of FGFR3 together with alteration of p53 pathway suggested that NBT-II carcinoma cells under the influence of HGF shifted towards a pro-invasive state, consistent with the current bladder cancer findings in which tumours switch from Ta or T1 stages to invasive stages with a shift in

FGFR3 and p53 status (Neuzillet, Paoletti et al. 2012) (van Rhijn, van der Kwast et al. 2004).

Table 4: Gene Score: the frequency of a gene detected over 6 time-points

FDR, Fc score	1	2	3	4	5	6
0.05, 1.5	660	325	226	76	24	0

Score 1: gene appear once in the 6 time-points
Score 2: gene appear twice in the 6 time-points
Score 3: gene appear 3 times in the 6 time-points
Score 4: gene appear 4 times in the 6 time-points
Score 5: gene appear 5 times in the 6 time-points
Score 6: gene appear in all 6 time-points
For example, 660 genes with score 1 means 660 genes are detected once in the 6 time-points studied.
FDR: false discovery rate
Fc : fold change

Table 5: pathway analysis for 326 genes revealed 4 top pathways.

Pathway	Genes	FDR (Benjamini)	AFDR*100 (FDR)
ErbB signaling pathway rno04012	CDKN1A, EREG, HBEGF, TGFA, AREG, NRG1	0.397	10.616
p53 signaling pathway rno04115	CCNB1, CDKN1A, CCNB2, SERPINE1, CCNG2	0.472	19.153
MAPK signaling pathway Rno04010	DUSP5, FGFR3, DUSP1, DUSP10, IL1A, RASA1, TGFB1, DUSP6, NGF	0.750	45.934
Focal adhesion rno04510	LAMA3, FLT1, PDGFC, LAMC2, PXN, FN1, MYL9	0.820	61.438

Table 6: GO analysis for 326 genes revealed 4 top pathways.

GO term	Genes	FDR (Benjamini)
GO:0051270 Regulation of cell motion	FLT1, PTPRM, PDPN, CHST3, IRS1, CXCL12, CXCL10, CITED2, TRIB1, LAMA3, GAB1, TGFBR3, HBEGF, CYR61	0.005028
GO:0007173 Epidermal growth factor receptor signaling pathway	EREG, GAB1, HBEGF, TGFA, AREG	0.00992
GO:0008283 Cell proliferation	PPARD, PDPN, TSPAN5, CSPG4, BRCA2, IL24, GDNF, CXCL12, LGR4, IL23A, EREG, TGFBR3, AREG, ASPM, ERCC1	0.010795
GO:0008544 Epidermis development	FRAS1, TXNIP, PPARD, BARX2, PTGS2, FLG, TGM1, GAB1, SPRR1AL	0.02379
GO:0048754 Branching morphogenesis of a tube	EDNRA, SPRY2, WNT4, FLT1, AREG, GDNF, CXCL12, CYR61	0.031858

Expression profiles reveal sets of genes at different time-points, sequentially contributing to malignancy

To delve deeper, detailed analysis was performed on genes that were differentially expressed at each time-point. Analysis indicated that the dominating signalling pathway was MAPK at 2 hours post HGF treatment, followed by ErbB and TGFb signalling pathways (Table 7). Genes that regulate adherens junctions and tight junctions (Claudin 4 (Cldn4), Actinin, alpha 1 (Actn1), Tight junction protein 2

(Tjp2)) were affected, suggesting NBT-II carcinoma cells were prone to undergo dissociation.

Table 7: Pathway analysis revealed dominant pathways at each time-point.

2 hr	4 hr	6 hr	9 hr	24 hr
MAPK signaling pathway rno04010	ErbB signaling pathway rno04012	Focal adhesion rno04510	Focal adhesion rno04510	ErbB signaling pathway rno04012
Adherens junction rno04520	MAPK signaling pathway rno04010	Regulation of actin cytoskeleton rno04810	Regulation of actin cytoskeleton rno04810	p53 signaling pathway rno04115
ErbB signaling pathway rno04012	TGF-beta signaling pathway rno04350	Phosphatidylinositol signaling system rno04070	Leukocyte transendothelial migration rno04670	Phosphatidylinositol signaling system rno04070
TGF-beta signaling pathway rno04350	p53 signaling pathway rno04115	Leukocyte transendothelial migration rno04670	ErbB signaling pathway rno04012	TGF-beta signaling pathway rno04350
	Neurotrophin signaling pathway rno04722	ErbB signaling pathway rno04012	VEGF signaling pathway rno04370	ECM-receptor interaction rno04512
	VEGF signaling pathway rno04370	MAPK signaling pathway rno04010	p53 signaling pathway rno04115	
	Insulin signaling pathway rno04910	p53 signaling pathway rno04115	Axon guidance rno04360	
	Chemokine signaling pathway rno04062	Neurotrophin signaling pathway rno04722	ECM-receptor interaction rno04512	
	Jak-STAT signaling pathway rno04630	VEGF signaling pathway rno04370		

Cells at the meta-stable state showed the greatest number of differentially expressed genes with 419 and 449 genes observed at 4 and 6 hours post HGF treatment respectively (Figure 9). In addition to the 3 pathways mentioned above, 6 other pathways: p53, Neurotrophin, VEGF, Insulin, chemokine and Jak-Stat signalling pathways emerged at 4 hours post HGF treatment. At 6 hours post HGF treatment, TGFβ signalling was not detected by the analysis and instead Phosphatidylinositol signalling pathway was observed.   More genes were observed for regulating focal adhesion, cell cycle, junctional complexes, axon guidance and endocytosis. Genes that regulated B cell receptor and Natural killer cell signalling were also observed. At 24 hours post HGF treatment, ErbB, p53, phosphatidylinositol and TGFβ signalling pathways were detected. The emergence of TGFβ signalling pathway at 24 hours might indicate a switch in its tumour suppressor role to one that promotes tumour progression.   Genes that regulate focal adhesion formation and actin cytoskeleton reorganization were dominant throughout 6-24 hours post HGF treatment.
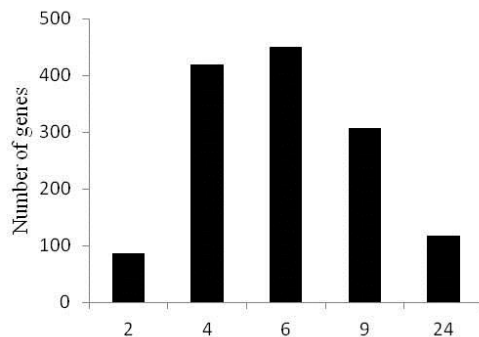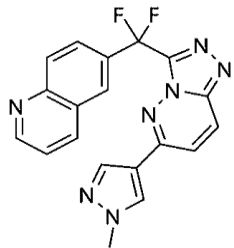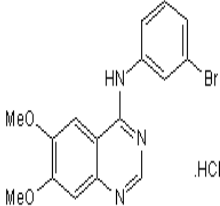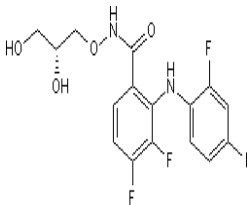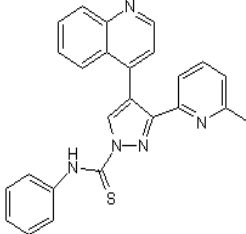
Figure 9: Number of differentially expressed genes at each time-point. Total number of differentially expressed genes was determined for each time-point peaking at 6 hours post HGF induction with 449 genes

To investigate if the pathways detected 2 hours post HGF were essential in the acquisition of the mesenchymal state, we compared NBT-II carcinoma cell colony dispersion by vehicle and targeted inhibitors (Table 8).

Table 8: Inhibitors used for drug treatment colony dispersion assay

c-Met inhibitor	EGFR inhibitor	MEK inhibitor	TGFβRI inhibitor
JNJ 38877605	PD 153035	PD 0325901	A83-01

We utilised the colony dispersion phenotype as readout since cell dissociation is the first step in the acquisition of a mesenchymal phenotype. Under normal growth conditions, NBT-II carcinoma cells grew to form an epithelial cell colony but with addition of HGF, NBT-II carcinoma cells acquired mesenchymal features and dispersed from the colony. In the presence of HGF, NBT-II carcinoma cells were treated with inhibitors of EGFR, MEK and TGFβRI and assessed if cell colonies remained intact or dispersed.

NBT-II carcinoma cells were induced by HGF and c-Met inhibitor was used as a positive control (intact cell colony). Colonies remained intact when cells were pre-treated with c-Met inhibitors overnight before addition of HGF. NBT-II cell colonies dispersed in the presence of EGFR inhibitor under HGF induction

61

(Figure 10) even though ErbB signalling was detected by the analysis. Colonies remained intact when cells were treated with MEK or TGFβRI inhibitor overnight before addition of HGF (Figure 11).
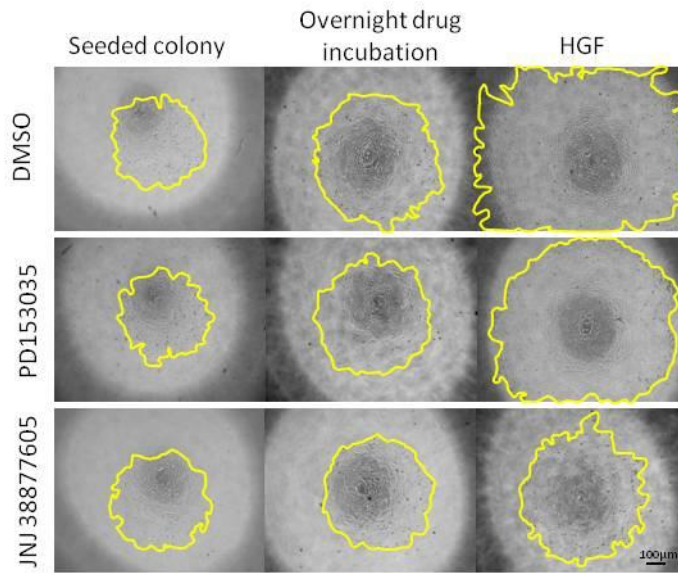
Figure 10: EGFR inhibitor failed to inhibit HGF-induced cell scatter.
$5x10^3$ NBT-II carcinoma cells were seeded onto each well center of 96 well-plates to form cell colonies for 4 hours before the start of experiment. Cell colonies were then treated overnight with DMSO (drug vehicle), 5μM PD153035 (EGFR inhibitor) or 4μm JNJ38877605 (c-Met inhibitor) before the addition of HGF (5ng/ml). Phase contrast images are representative of 3 independent experiments.

Next, instead of incubating cells with inhibitors before the addition of HGF, inhibitors were added to the culture 0.5, 2 and 5 hours after the addition of HGF to observe if the inhibitors were still able to abrogate the process of mesenchymal state acquisition. Colonies with the different treatment conditions were imaged 24 hours post HGF treatment (Figure 11). We observed that colonies remained compact when the colonies were treated with c-Met, MEK or TGFβR inhibitors

0.5 and 2 hours after addition of HGF. Cells in colonies undergo partial dispersion if MEK or TGFβR inhibitors were added after 5 hours of exposure to HGF. If MAPK and TGF-β pathways were inhibited within 2 hours of exposure to HGF, EMT was abrogated. The data suggested that subsequent activation of MAPK and TGFβ signalling pathways are required for EMT; and these two signallling modules are early events in the HGF induced cascade. Early inhibition of each of the two pathways can abrogate the EMT process but if the EMT process has been engaged (post 5 hours of HGF induction), blocking either of the two pathways will only yield modest effect.
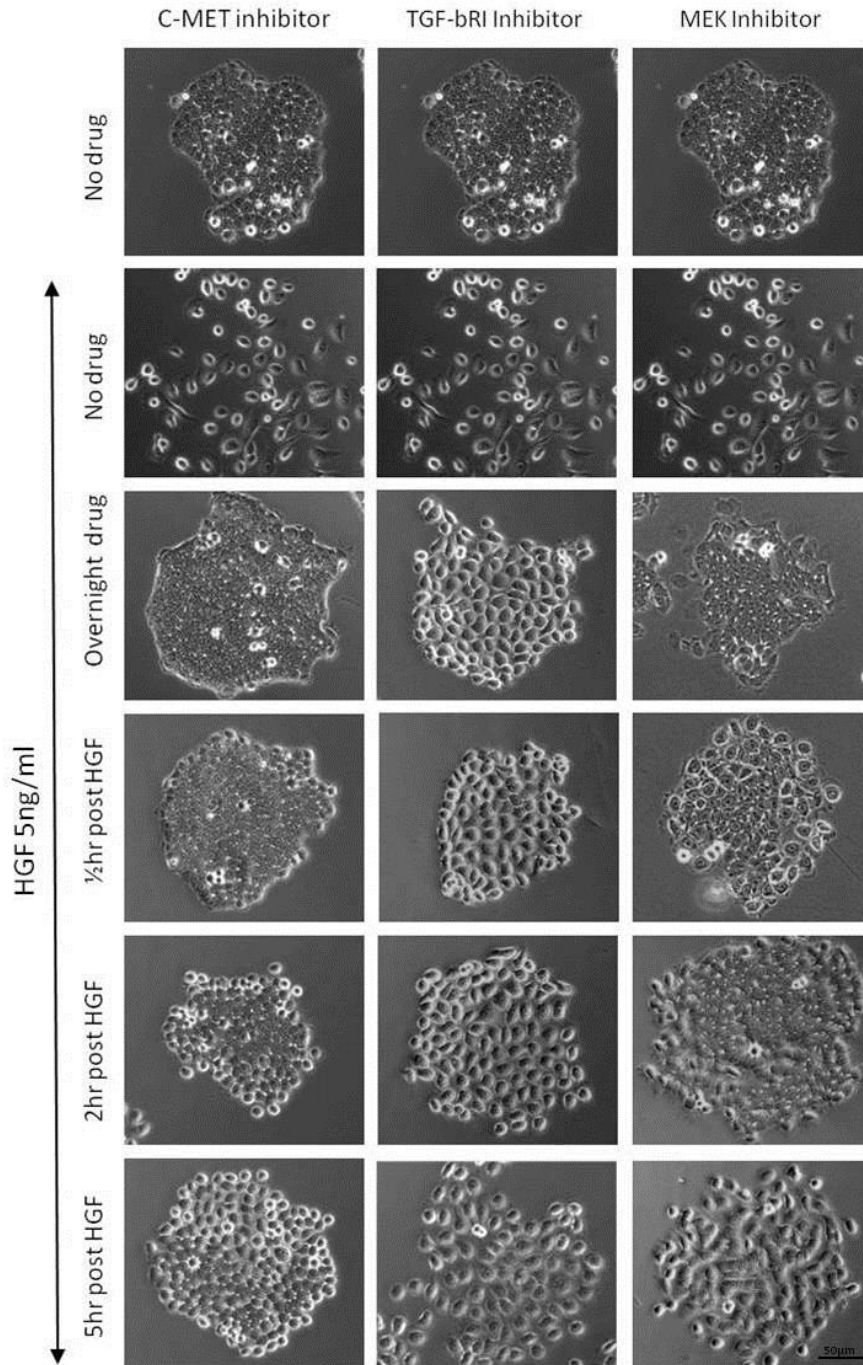
Figure 11: Inhibition of HGF induced cell dispersion with targeted inhibitors of TGFβRI and MEK.
NBT-II cells (100 cells per well) were plated for four days to allow for colony growth. No drug: NBT-II cells treated with DMSO (drug vehicle); Overnight drug: NBT-II cells were pre-treated overnight with inhibitors before addition of HGF; 0.5, 2, 5 hr post HGF: inhibitors were added 0.5 hour, 2 hours, 5 hours after the addition of HGF respectively. TGFbRI inhibitor: 10μM A83-01; MEK inhibitor: 2 μM PD0325901. Images are representative of 3 independent experiments.

MEK and TGFβRI act on a common downstream target

The most relevant target to investigate is Smad2 as both ERK (direct target of MEK) and TGFβRI phosphorylates Smad2. Specifically, the linker region of Smad2 is phosphorylated by ERK whilst the C-terminus is phosphorylated by TGFβRI (Hough, Radu et al. 2012) (Heldin and Moustakas 2012). siRNA knockdown of Smad2 was performed to assess if Smad2 is implicated in the HGF-induced EMT process. Small interfering ribonucleic acid (siRNA) knockdown for Smad2 was successful, yielding greater than 80% decrease in total Smad2 protein level (Figure 12A). siRNA knockdown of Smad2 prevented the dispersion of the HGF treated cell colonies (Figure 12B) and delayed the HGF-induced wound-closure (Figure 12E).

Both Smad2 and Smad3 are activated by TGFβRI mediated C-terminal phosphorylation; thereafter forming complexes with Smad4 before translocating to the nucleus where they bind other transcription factors to regulate the transcription of specific genes. Knockdown of Smad2-binding partners (Smad3 and Smad4) was performed. However siRNA knockdown for Smad3 was unsuccessful, yielding less than 20% knockdown in protein level (Figure12C) while siRNA knockdown for Smad4 lead to greater than 80% decrease in protein expression (Figure 12F). The siRNA knockdown of Smad4 resulted in a delay in wound-closure compared to the control (Figure 12G).
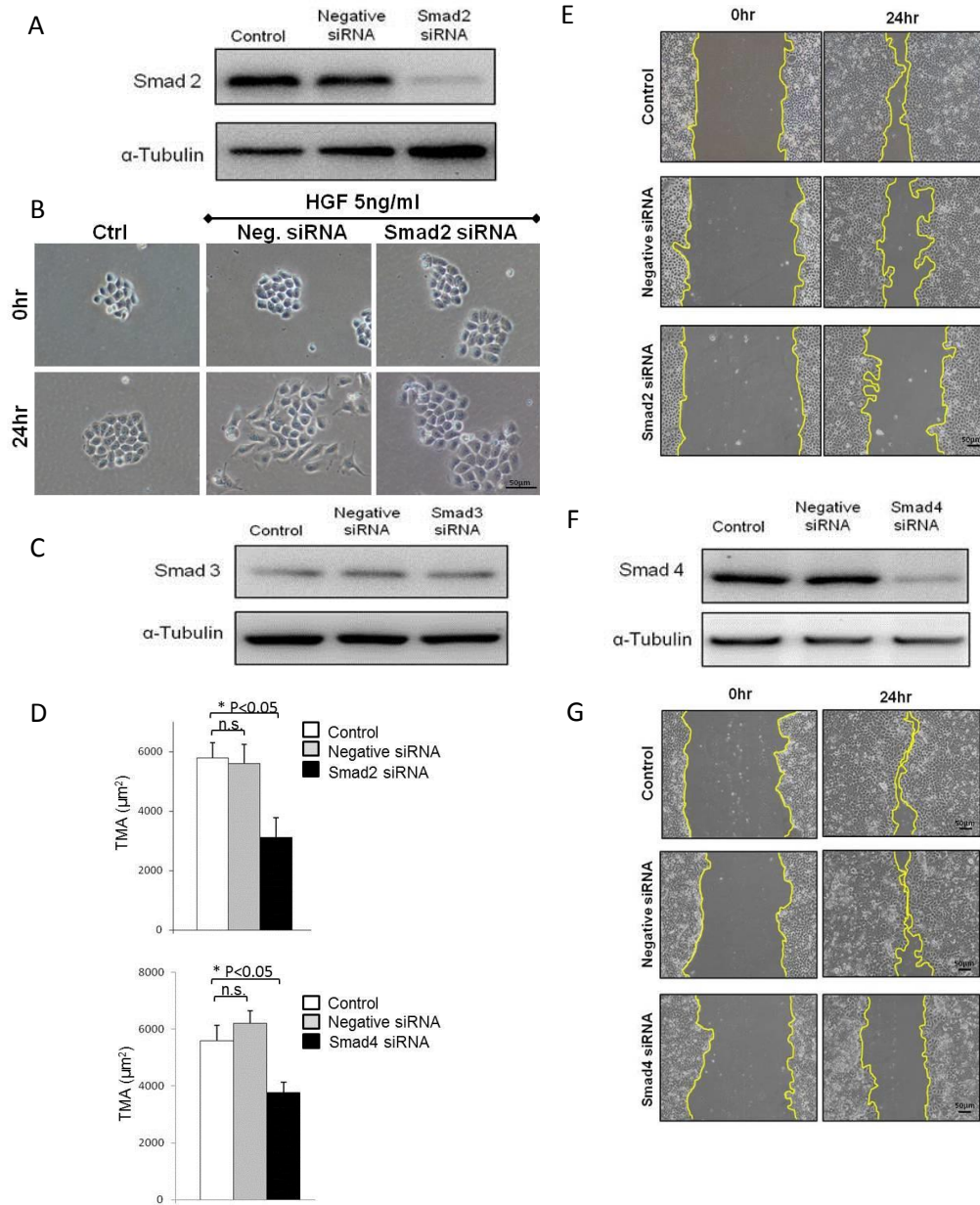
Figure 12: siRNA knockdown of Smad2 and Smad4 delayed HGF induced wound closure.

(A) Western blot analysis of protein levels of Smad2. (B) Colony dispersion assay of NBT-II cells transfected with Smad2 siRNA under HGF induction. (C) Western blot analysis of protein levels of Smad3 and Smad4 (F) after transfection with 50nM of their specific siRNA. A wound-healing assay was performed under HGF-treated conditions using NBT-II cells transfected with no siRNA (Control), negative siRNA, Smad2 siRNA (E) and Smad4 siRNA (G). Yellow lines mark the wound boundary. (D) Total Migration Area (TMA) is reduced in cells transfected with Smad2 siRNA and Smad4 siRNA. TMA is calculated by subtracting the area of the wound at 24hr from the area of wound at 0hr. n.s= not significant. Bars represent mean $\pm$ SEM. *p<0.05, two-tailed t-test. N=3 independent experiments.

In order to measure the area migrated by the cells, we subtracted the area of the wound at 24 hours from the area of the wound at 0 hour. The area occupied by migrated cells was significantly reduced when Smad2 or Smad4 (Figure 12D) were knockdown. These results further affirm the role of Smad2 in HGF-induced EMT and motility.

Using immunofluorescence labelling, Smad2 localized in the nucleus of NBT-II carcinoma cells 2 hours after HGF induction (Figure 13A). This HGF-induced Smad2 nuclear localization was inhibited with the addition of A83-01 (TGFβRI inhibitor), suggesting that the translocation of Smad2 to the nucleus is TGFβRI dependent.

Next, a fractionation assay was used to extract the cytoplasm and nuclear fractions from total cell lysates to study the level of phosphorylated Smad2 in each fraction for the different conditions. The fractionation assay similarly showed an increase in C-terminal phosphorylated Smad2 in the nuclear fraction 2 hours after the addition of HGF (Figure 13B). This increase was again inhibited with the addition of A83-01(TGFβRI inhibitor) which further affirmed that the translocation of Smad2 to the nucleus is TGFβRI dependent and TGFβRI mediated Smad2 C-terminal phosphorylation is critical for the translocation of Smad2 to the nucleus.
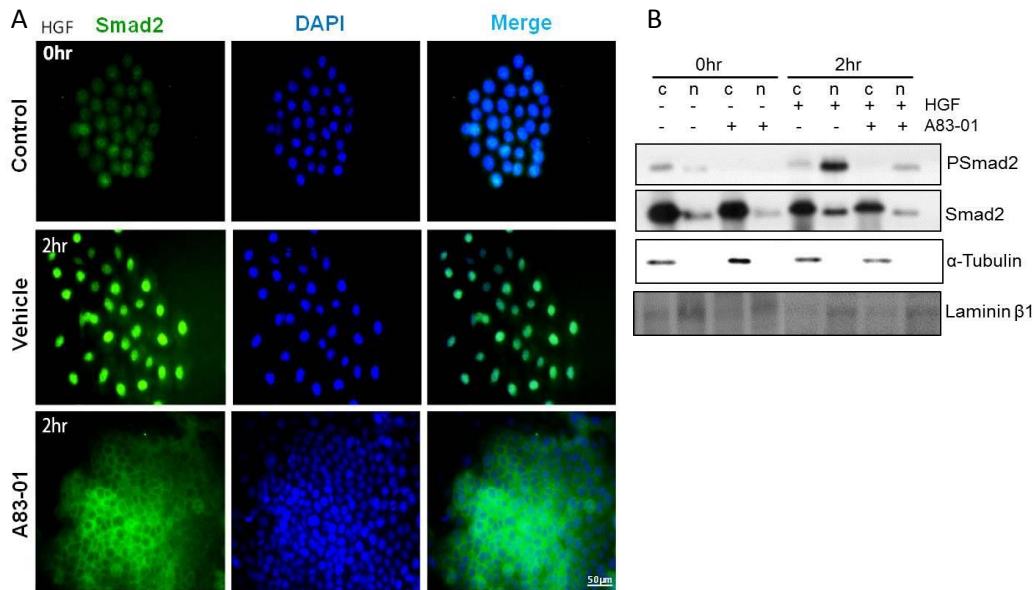
Figure 13: Nuclear translocation of Smad2 upon HGF induction is dependent on Smad2 C-terminus phosphorylation.
(A) NBT-II carcinoma cells were grown for 4 days to form cell colonies before the start of experiment. Cell colonies were pre-treated overnight with Vehicle (DMSO) or 10μM A83-01 (TGFbRI inhibitor) before addition of HGF (5ng/ml). Cultures were fixed 2 hours post HGF addition and stained for Smad2 protein. Green: Smad2; Blue: Dapi (nuclear stain). (B) Fractionation assay: Smad2 was observed in the nuclear fraction 2 hours post HGF addition. n: Nuclear fraction; c: Cytoplasmic fraction. PSmad2 : phosphorylation of Smad2 at C-terminus.

Smad2 is phosphorylated by ERK at the linker region and by TGFβRI at the C-terminus; the phosphorylation dynamics of the two regions (linker and C-terminus) of Smad2 might suggest how Smad2 is regulated. An increase in phosphorylation of the Smad2 linker region (Smad2 S245/S250/S255) was observed 0.5 hours after HGF induction, while an increase in the phosphorylation of Smad2 C-terminus (Smad2 S465/S467) was observed only 1 hour after HGF induction (Figure 14A). We hypothesized that the phosphorylation of Smad2 linker region might aid in the recruitment of Smad2 to TGFβRI for the

phosphorylation of Smad2 C-terminus. The administration of PD0325901 (MEK inhibitor) inhibited the activation of its direct target, ERK, thereby abrogating the phosphorylation of Smad2 linker region (Figure 14B). However, abrogating the phosphorylation of Smad2 linker region resulted in an unexpected increase in the phosphorylation of the Smad2 C-terminus (Figure 14B), suggesting that the Smad2 linker phosphorylation might inhibit the phosphorylation of Smad2 C-terminus.

We also observed that a decrease in the pERK1/2 (phosphorylated ERK1/2) was accompanied by a decrease in the phosphorylation of the Smad2 linker region and an increase in the phosphorylation of the Smad2 C-terminus 1 hour after HGF induction (Figure 14A). This led to the conclusion that ERK1/2 may function like a switch to regulate the phosphorylation of Smad2 C-terminus via Smad2 linker phosphorylation and thereby affecting Smad2 function.

A
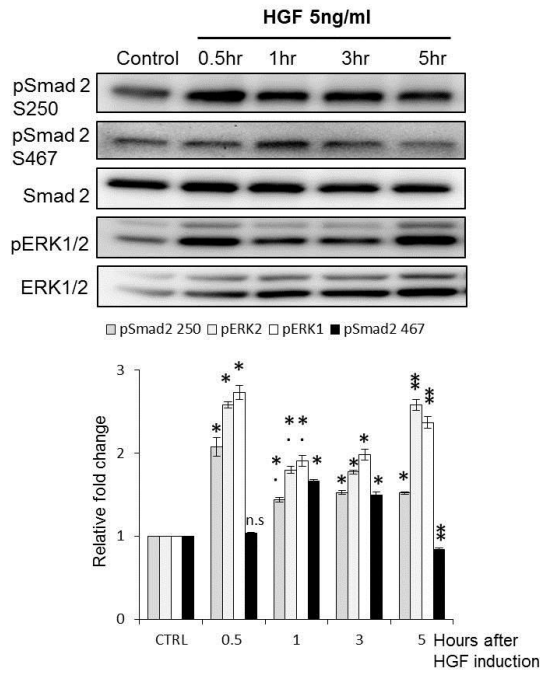
Figure 14: Phosphorylation of Smad2 linker region inhibits the phosphorylation of Smad2 C-terminus.

(A) Top panel: Immunoblots for pSmad2 S250 (linker region S245/S250/S255), pErk1/2 displayed activation within 0.5 hour (lane 2) by HGF; pSmad2 S467 (C-terminus region S465/S467) activation at 1hour (lane3) by HGF. Bottom panel: graph that display the fold-induction of phosphorylating pSmad2 S250 (white), pERK1 (light grey), pERK2 (dark grey) and pSmad2 S467 (black) compared to control (CTRL). The trend of pErk1/2 (Grey bars) is opposite to that of pSmad2 S467 (black bars). Data represent the mean of two independent experiments. Bars represent mean $\pm$ Standard Deviation. *= p-value < 0.05 when compared to control.

⁎ = p-value < 0.05 when compared to 0.5 hours after HGF induction.

⁎ = p-value < 0.05 when compared to 3 hours after HGF induction.
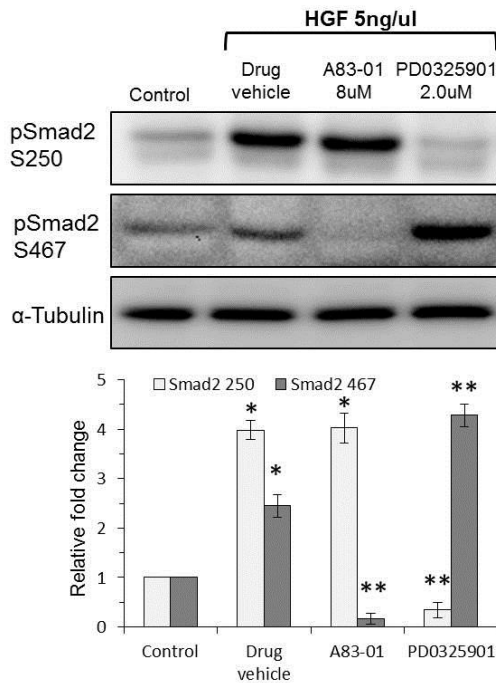
(B) Immunoblots for pSmad2 S250, whose induction by HGF is inhibited by PD0325901 (MEK inhibitor); activation of pSmad2 S467 was inhibited by A83-01 (TGFβRI inhibitor) but augmented by PD0325901. Drug vehicle: DMSO. α-Tubulin acts as loading controls. Data represent the mean of three independent experiments. Bars represent mean $\pm$ Standard deviation. *= p-value < 0.05 when compared to control. **= p-value <0.05 when compared to drug vehicle.

B

To investigate the role of the two phosphorylated Smad2 regions (linker and C-terminus) in the EMT process, human bladder carcinoma cells (UM-UC-3) were treated with either MEK inhibitor (PD0325901) or TGFβRI inhibitor (A83-01); and tested for the expression of EMT markers Snail-1, Zeb1 and Twist (Figure 15). The addition of PD0325901 (MEK inhibitor) abrogated the phosphorylation of ERK1/2 resulting in a non-phosphorylated Smad2 linker region accompanied by a decrease in Snail-1 and Zeb1 protein levels (Figure 15A). Furthermore, the abrogation of the Smad2 linker phosphorylation was accompanied by an increase in the phosphorylation of the Smad2 C-terminus with an increase in Twist protein level (Figure 15A). To study if the increase in Twist was due to the increase in Smad2 C-terminus phosphorylation, we treated UM-UC-3 with A83-01 (TGFβRI inhibitor) and PD0325901 (MEK inhibitor) in combination. With the addition of A83-01, a decrease in Twist protein level was observed (Figure 15B). The data showed that phosphorylation of the linker region of Smad2 regulated Snail-1 and Zeb1 while phosphorylation of the C-terminus regulated the expression of Twist.
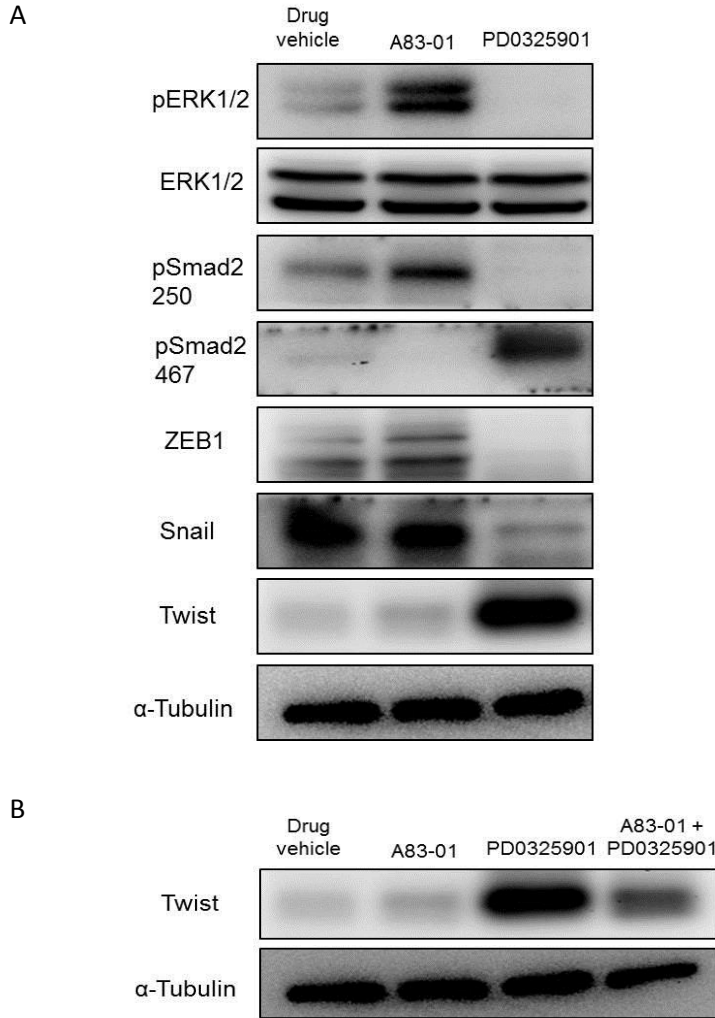
Figure 15: Regulation of EMT markers by Smad2 linker and C-terminus region.
Human bladder carcinoma cells (UM-UC-3) were cultured with culture medium containing either drug vehicle (DMSO), 10μM A83-01 (TGFβRI inhibitor) or 2μM PD0325901 (MEK inhibitor) for 3 days. (A) Immunoblots of Zeb1 and Snail, whose expression is diminished with the abrogation of phosphorylation of pSmad2 S250 (linker region S245/S250/S255) upon PD0325901 (MEK inhibitor) treatment; Twist expression is up-regulated with an increase in pSmad2 S467 (C-terminus region S465/S467) phosphorylation (lane3). (B) Immunoblot of Twist, whose protein level increases in the presence of PD0325901 and is diminished when cells are treated with PD0325901 and A83-01 in combination. α-Tubulin acts as loading controls.

To investigate if phosphorylation of the linker and c-terminus regions in Smad2 is required for tumour initiation and sustenance, the human UM-UC-3 bladder carcinoma cell line was transfected with a cDNA construct plasmid that harboured mutations to abrogate the phosphorylation of the Smad2 linker region (Smad2 dnL) or the Smad2 C-terminus region (Smad2 dnC). The stably transfected cells were subcutaneously injected into the flanks of nude mice and observed for tumour growth. Cells that harboured Smad2 dnL plasmid were rarely tumorigenic with tumour forming in only 1 out of 5 mice (Figure 16A). Cells that harboured Smad2 dnC plasmid were tumorigenic with tumours forming in all mice (Figure 16A). Tumour volume of tumours derived from Smad2 dnL transfected cells was not significantly different from the tumour volume of tumours derived from Smad2 dnC transefected cells. However, the growth rate of the tumours derived from Smad2 dnL or Smad2 dnC transfected cells was significantly slower than tumours that derived from empty vector transfected cells; thus resulting in significantly smaller tumours compared to the tumours derived from empty Vector L or empty Vector C respectively (Figure 16B). These data suggested that the phosphorylation of the Smad2 linker region is important for the tumorogenicity of the UM-UC-3 cells.
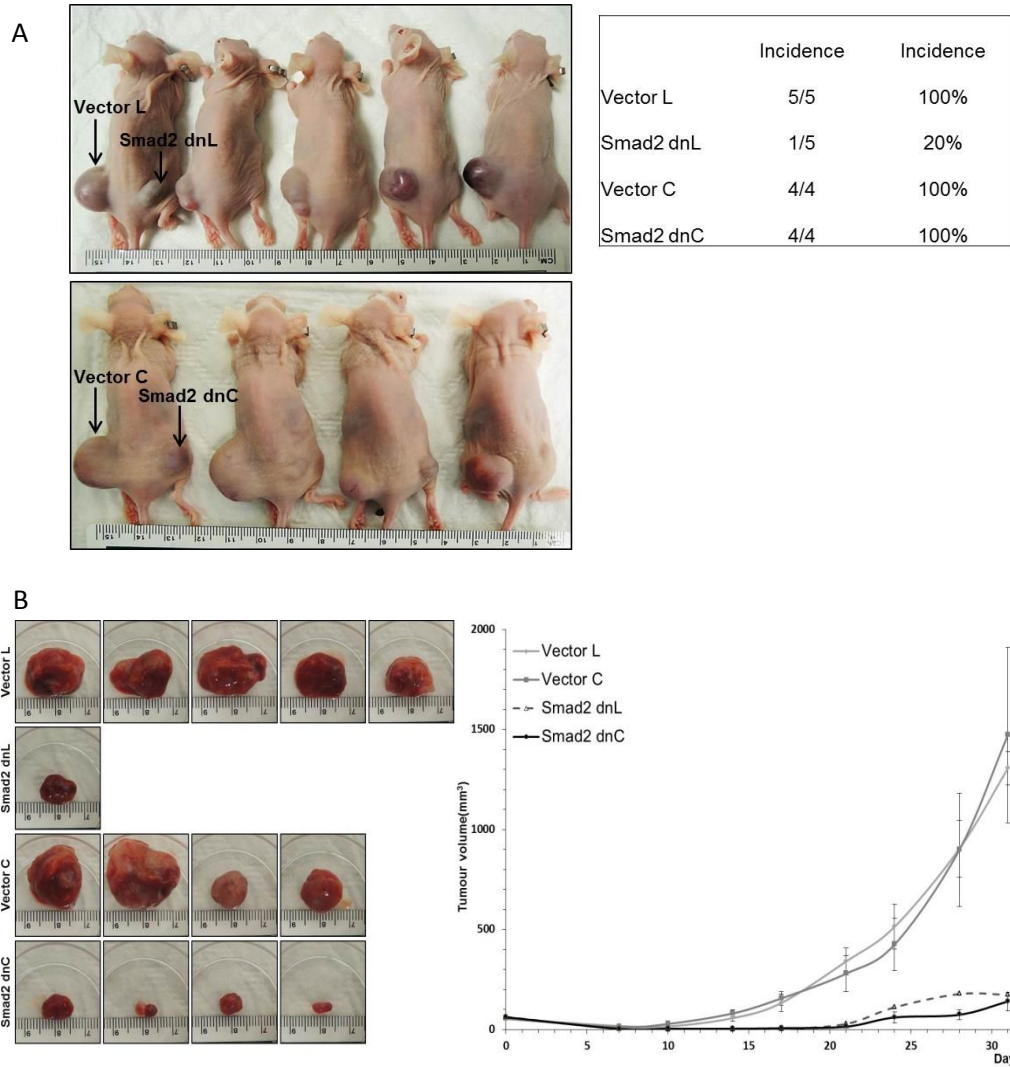
Figure 16: Abrogation of the phosphorylation of the Smad2 linker region and C-terminus region reduces tumorigenicity and tumour growth respectively.
Four UM-UC-3 stable cell lines were generated by stably transfecting UM-UC-3 cell line with Smad2dnL (non-phosphorylating Smad2 linker region) or Smad2dnC (non-phosphorylating Smad2 C-terminus region) plasmid or their respective empty vectors (Vector L or Vector C). Each stable cell line was subcutaneously injected into the dorsal flanks of female athymic mice to form tumours. (A) Top panel: Mice were subcutaneously injected with Vector L stable UM-UC-3 cells on the left flank and Smad2dnL stable UM-UC-3 cells on the right flank.(N=5) Bottom panel: Mice were subcutaneously injected with Vector C stable UM-UC-3 cells on the left flank and Smad2dnC stable UM-UC-3 cells on the right flank. (N=5, 1 died) Right panel: Incidence of tumour formation for each stable cell line was calculated. (B) tumour volume was closely followed for 31 days, measurements taken twice every week. (D) Mice were euthanized and tumours were extracted. Bars represent the mean and error bars indicate SEM (n=5).

74

Discussion

This study identified common transcripts regulated by both EGF and HGF signalling. A subset of the identified common transcripts was reported to be involved in invasive stages of bladder cancer. A gene of particular interest is HMGA1 that belongs to the high-mobility group A (HMGA) protein family. HMGA1 is a non-histone chromatin factor and several studies demonstrated that HMGA proteins have a critical role in neoplastic transformation. In pancreatic cancer, HMGA1 is over-expressed in >90% of primary pancreatic cancer, with low level in early precursor lesions. Over-expression of HMGA proteins is associated with a highly malignant phenotype, representing a poor prognostic index. HMGA1 cooperates with different molecules for tumour progression. HMGA1 cooperates with K-RAS to induce migration and anchorage-independent growth in cells. HMGA1 induces the expression of COX-2 and cells become non-tumorigenic *in vivo* when HMGA1 is repressed. HMGA1 inhibits p53-mediated mitochondrial apoptosis by disrupting the binding of p53 and Bcl-2 though physical interaction with Bcl-2. HMGA1 was also reported to enhance cellular reprogramming from a somatic cell to a fully pluripotent stem cell. Since some cancer cells are considered to exhibit stem cell properties, further studies are required to investigate if HMGA1 contribute to poorly differentiated, stem-like cancers.

Through the differential gene expression profile from each step of the EMT process, we were able to unravel the chronological activation of signalling modules termed the c-Met kinetic signature. The data reported in this chapter

displayed the streamlined events in response to HGF for acquisition of invasiveness in carcinoma cells. Although most of the identified genes are already known to associate with cancer, the majority of them have not been reported as induced in TCC. Some of the gene families (for example, genes related to cell adhesion, cell proliferation and immune response) identified in this study were also reported in studies performed on pooled tumour samples that represent different stages and grades (Thykjaer, Workman et al. 2001). The limitation of the study is the absence of cancer microenvironment which filters c-Met's involvement in processes like angiogenesis –a potent contributor to metastasis.

We have also shown that Smad2 acts as a common downstream target of both ERK and TGFβRI in the c-Met driven system to regulate the expression of EMT markers (Figure 17); and Smad2 linker region is important for tumorigenicity and Smad2 C-terminus is important in tumour growth. In addition, knocking down the Smad2 protein abrogates wound-closure, demonstrating the importance of Smad2 in HGF-induced cell migration.

In summary, this study provided insights into the stepwise dysregulation of pathways which might be useful for designing therapeutics against high grade tumours with invasive potential. Further analysis and modeling of the data generated in this study are likely to result in the development of more sophisticated models of receptor-initiated signal transduction, endocytosis, trafficking and regulation. Future application of this stepwise analysis model to interrogate other processes like angiogenesis, regulation of miRNAs in cancer

progression and stepwise acquisition of chemoresistance may reveal mechanisms of pathogenesis in these systems. This may help to understand the role of each process in tumour progression, allowing the discovery of additional targets for therapeutics.
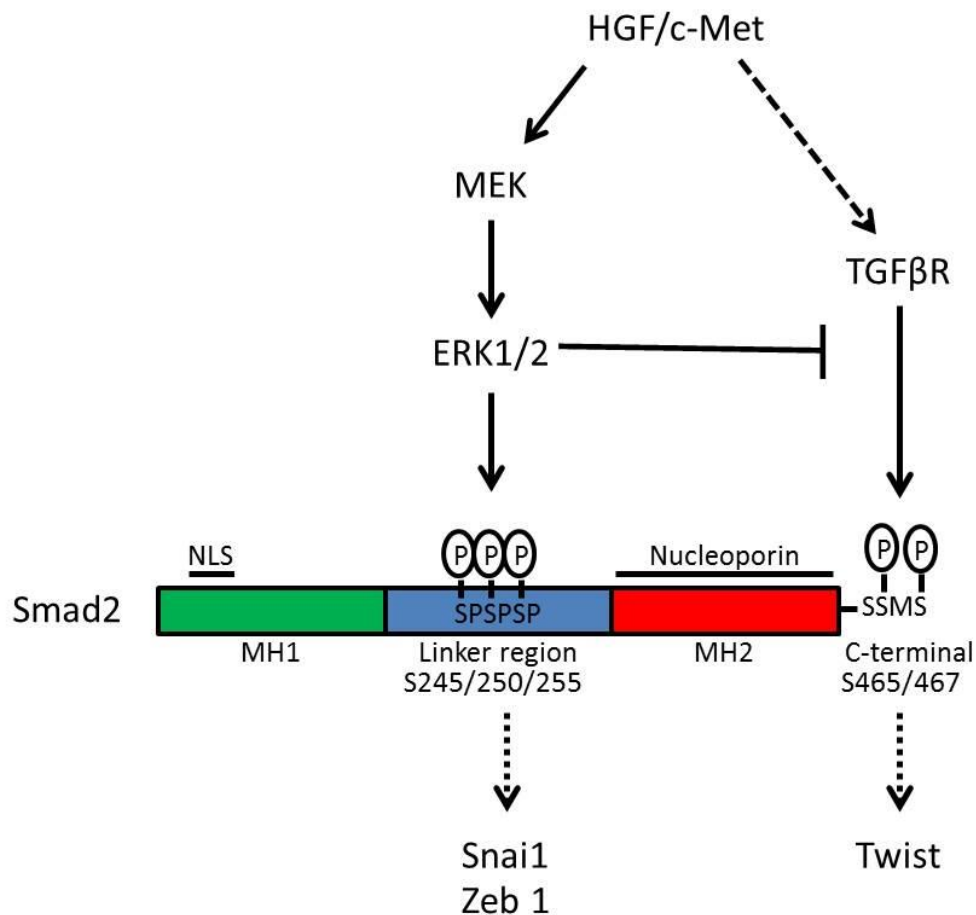
Figure 17: Diagram of Smad2 regulation by MEK and TGFβRI under HGF-induced conditions, regulating the expression of different EMT markers.
Under HGF induced conditions, ERK1/2 phosphorylates Smad2 linker region regulating Snail1 and Zeb1 expression while TGFβRI phosphorylates Smad2 C-terminus region regulating Twist1 expression. Both regions of Smad2 are important in EMT process and tumour progression.

Part 2: EMT inhibitor screening

Introduction

Bladder cancer progression is characterized by a massive invasion of carcinoma cells in the different layers of the bladder wall. Bladder cancer patients are reported to have elevated serum level of growth factors, namely hepatocyte growth factor (HGF), epidermal growth factor (EGF), transforming growth factor-beta (TGF-β) and insulin-like growth factor-1 (IGF-1), among others. These inducing agents act synergistically to promote tumour progression. The surrounding stroma cells secrete an array of cytokines and growth factors that aid in the metastasis of the primary tumour. (Thiery and Sleeman 2006; Moustakas and Heldin 2007)

Extensive efforts have been made in identifying agents that could affect carcinoma cell survival and proliferation. However as today progress has been slow. The classical treatment of bladder carcinoma recurrent superficial stages or high grade stage1 is still intravesical injection of Bacillus Calmette-Guerin an attenuated vaccine to boost non-specifically immune response. Mitomycin C is also often used as an anti-proliferative agent for these early stages. Different chemotherapeutic drugs are used in very advanced bladder cancers as adjuvant therapy following partial or radical cystectomy whenever possible. These agents include cis-platinum (cis-Pt) with or without 5FU mitomycin C. These agents can be used in combination with radiotherapy. Very advanced patients can also be

given gemcitabine and cis-Pt, M-VAC (methotrexate vinblastine doxorubicin cis-Pt) or cis-Pt and paclitaxel or docetaxel (Amercian Cancer Society Webpage). Many clinical trials explore combination therapies, phototherapy and targeted therapy such as erlotinib, an EGFR kinase inhibitor, in addition to the use of conventional chemotherapeutics (Clinicaltrials.gov). The drugs aforementioned were initially identified for their anti-proliferative activity. However, bladder cancer progression is not only determined by the ability of carcinomas cells to proliferate but also their invasive potential. Drugs that can limit the invasive potential of carcinoma cells may be more useful in the treatment of muscle invasive bladder cancer patients to delay tumour progression. Thus there is a need to search for agents that can limit the invasive potential of carcinoma cells as to complement the anti-proliferative agents.

Agents that inhibit EMT might aid in limiting the invasiveness of bladder carcinoma cells as EMT precedes invasion and metastasis. However, there are currently no available drugs that specifically inhibit EMT. In an attempt to identify such possible candidates, a library of kinase inhibitors was investigated for their effectiveness in inhibiting HGF, EGF and IGF-1 induced EMT. The kinase inhibitors were originally designed to combat oncogene addiction in carcinoma cells. Numerous carcinoma were found to over-express either wild-type or mutated kinases (Lemmon and Schlessinger 2010) (Schlessinger 2000) and these oncogenic kinases play important roles in sustaining tumour growth. Kinase inhibitors are selected for their ability to bind to the ATP-binding site of the dysregulated kinase thereby inhibiting phosphorylation and activation of the

signal transduction cascade responsible for sustaining tumour growth. Many preclinical studies showed the effectiveness of targeted small molecule inhibitors in limiting tumour growth. Examples include Gefitinib (EGFR inhibitor) for the treatment of non-small-cell lung cancer (Mok, Wu et al. 2009); and Imatinib Mesylate (PDGFR inhibitor) for the treatment of chronic myeloid leukemia (Hochhaus, Druker et al. 2008). Although these inhibitors were identified and optimized for their anti-proliferative properties, evidence suggests that some of these targeted small molecule inhibitors may also interfere with EMT; since the EMT program is governed by signalling pathways for which these small molecular weight compounds have been generated (Thiery and Sleeman 2006) (Chua, Poon et al. 2011). For example, Ki26894, an ALK5 inhibitor, has been shown to decrease the invasiveness and EMT of scirrhous gastric cancer cells (Shinto, Yashiro et al. 2010). Therefore, screening a library of kinase inhibitors might aid in the identification of possible candidates that can reduce the invasive potential of bladder carcinoma cells.

An EMT inhibition drug screening assay to identify EMT inhibitors was designed and developed in collaboration with Dr. Chua Kian Ngiap from assay development team of Experimental Therapeutics Center, A*STAR and the image analysis algorithm was developed by Dr. Victor Racine. This assay uses a model carcinoma reporter cell line (NBT-II) which was induced to undergo EMT initiated by different growth factors: EGF, HGF, or IGF-1. The inhibitors were screened for their EMT modulating properties through inhibition of growth factor induced EMT signalling.

Results

The design and assembly of EMT inhibition drug screening assay.

EMT inhibitory compound screen utilises a spot migration assay which measures the dispersion of cells in the presence of a test compound and an EMT inducer. H2B–mcherry transfected NBT-II stable cell line established in the lab was used for this assay. The red nuclei of the cells enabled the tracking of individual cell via live-cell fluorescent imaging. The cells were plated onto the center of each 96 well of clear bottom assay plates using a robotic liquid handling station at a concentration of 5million cells/ml. The cells were allowed to adhere for an hour before addition of more media to allow the cells to form a colony over 4-6 hour incubation period. The cells were then incubated overnight with low molecular weight compounds and subsequently treated with growth factor for 24 hours (Figure 18A). If cells remain epithelial and the colony is still intact after growth factor treatment, the tested compound is EMT inhibitory (Figure 18C).

5 test compounds were screened on each assay plate in the plate layout as shown in Figure 18B. Each assay plate had a column of positive and negative control for comparison. The column of negative control wells were treated with a growth factor (HGF/EGF/IGF) following the treatment of DMSO. The positive control columns were treated with a growth factor (HGF/EGF/IGF) following the treatment of their respective receptor's inhibitory compound that could inhibit the scatter function of that growth factor. For example, the c-Met inhibitor

81

(JNJ38877605) and the growth factor HGF; the EGFR inhibitor (AG1478) and the growth factor EGF; or the IGFR inhibitor (BMS536924) and the growth factor IGF. Images of the cell colony in each well were acquired prior to compound treatment, T1, and 24 hours after growth factor induction, T2, using a confocal microplate imager for comparison. The images obtained from T1 and T2 were sent for image analysis.

The effect of the test compounds were reported based on two parameters, cell count and cell dispersion (Figure 18D). The H2B-mcherry coloured cell nuclei were segmented using a wavelet decomposition scheme to remove inhomogeneous background and noise. A watershed procedure was then performed to redefine the boundary of any nuclei that failed to be separated by wavelet algorithm. All segmented nuclei with size that fell below the average size of all nuclei were removed from the analysis. The "cell count" of each well was computed by summing the total number of the segmented nuclei. The cell count ratio was calculated by taking cell count of T2/T1 of each well. The cell count ratio provided information on the proliferative status of the cell colony in response to the test compound. The cell count ratio of an analysed well below the threshold (proliferative index of 1.5) suggests that the test compound is cytotoxic and hence will be eliminated from the list. The "cell dispersion" of each colony is calculated by taking the standard deviation of the positions of all the cell nuclei with respect to the center of the cell colony in the analysed well.
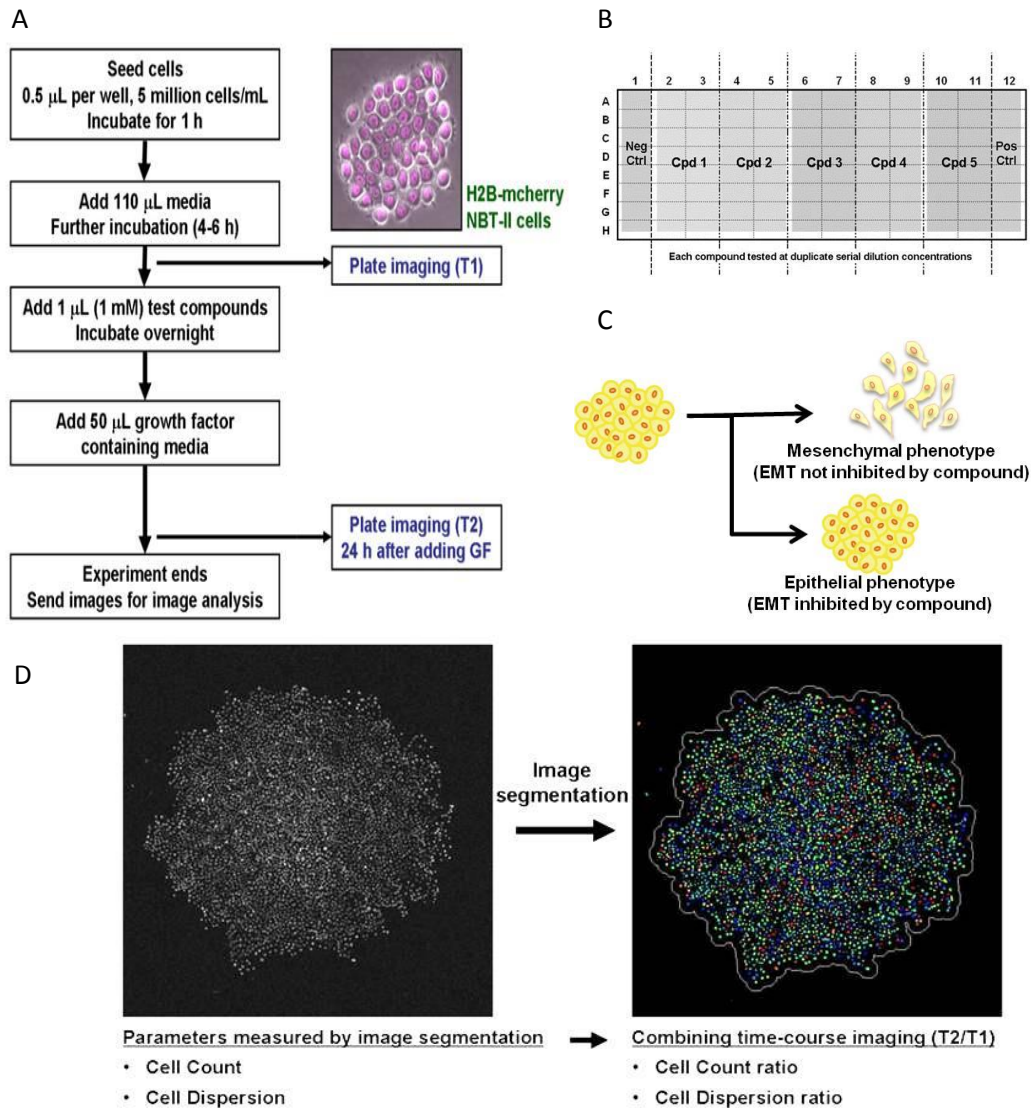
Figure 18: EMT spot migration screening assay overview.
(A) Screening assay workflow. Robot-assisted plating of H2B-mcherry transfected NBT-II cells into the well centers of 96-well plates. The initial plate image acquired at T1 served as the baseline reference for calculating the cell count ratio and cell dispersion ratio values for each well. The cells were treated with test compounds overnight using the plate layout (B) and further incubated for 24 hours with a growth factor to induce EMT. Final plate image acquired at T2 depicted the dispersion response of cells 24 hours after addition of the test compounds and growth factor treatment.   (C) EMT can be initiated and maintained in epithelial cells via growth factor signalling. The prevention of cell dispersion directly correlates to the propensity of a test compound to block an induced EMT signalling pathway. (D) Nuclei segmentation, which consists of a wavelet transform and watershed algorithm steps, was applied to identify all nuclei in the well. The nuclei segmentation mask was then dilated to generate merging region areas where distinct cell clusters could be isolated. Nuclei within the colony of interest were measured. Cell count was determined by the total nuclei count within the colony. Cell dispersion was determined by applying the spreading coefficient formula.

The X and Y coordinates of all cell nuclei were recorded and the average of the coordinates represented the center of the cell colony. The ratio of "cell dispersion" of T2/T1 corresponded to the scatter status of the cell colony. Cell dispersion ratio of an analysed well below the threshold (50%) suggests that the compound was successful in inhibiting the scatter.

The threshold values for both parameters were established using Tocris kinase library as the reference. All plates were normalized to cell dispersion ratio [Positive control=0% and Negative control =100%] and cell count ratio [Positive control =2.4]. A threshold for cell count ratio was set at 1.5 and the threshold for cell dispersion ratio was set at 50% of Negative Control/Positive Control Cell dispersion ratios range. A compound yielding cell count ratio ≥ 1.5 and cell dispersion ratio ≤ 50% of NegCtrl / PosCtrl Cell Dispersion ratios range in both low and high tested concentrations was considered as a hit (Figure 19).
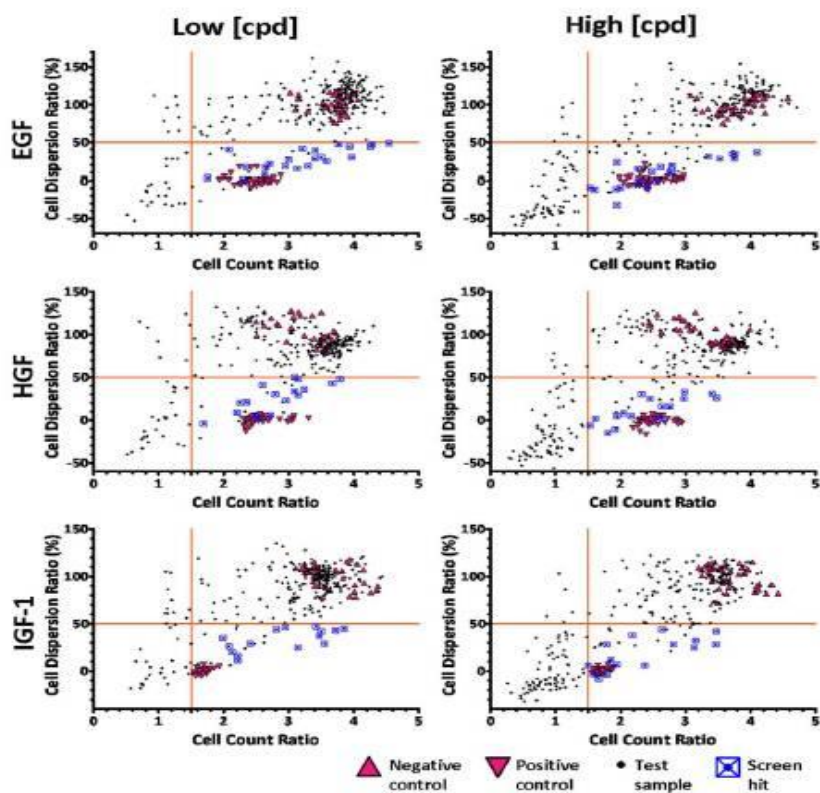
Figure 19: Cell dispersion ratio (CDR) vs. cell count ratio (CCR) plots.
The graphs illustrate the behavior of NBT-II cells treated with different test compounds and growth factors in the spot migration assay. CDR threshold was set at 50% CDR between positive control CDR and negative control CDR. CCR threshold was set at 1.5 growth rate. We assessed compounds that inhibit cell dispersion (less than CDR threshold) and do not severely inhibit cell growth (i.e. more than CCR threshold). To further refine our hits, the test compounds were run at a low and high concentration (1.67 and 6.67 mM, respectively). Hit compounds (crossed squares) were classified as test compounds that satisfy the CDR and CCR threshold criteria at both concentrations.

Table: 9 CCR and CDR(%) readings for shortlisted compounds

Compound Name	EGF (20 ng/mL)				HGF (4 ng/mL)				IGF-1 (150 ng/mL)			
	Cpd (1.67µM)		Cpd (6.67 µM)		Cpd (1.67µM)		Cpd (6.67 µM)		Cpd (1.67µM)		Cpd (6.67 µM)	
	CCR	CDR%	CCR	CDR%	CCR	CDR%	CCR	CDR%	CCR	CDR%	CCR	CDR%
A83-01	4	30	3.8	34	3.1	29	3	25	3.5	37	3.1	32
D4476	4.5	48	4.1	36	3.8	48	3.4	31	3.8	45	3.5	42
LY 364947	4.3	44	3.7	34	3.2	36	2.8	16	3.5	42	2.8	28
SB 431542	4.3	47	3.7	28	3.7	43	3.5	26	3.7	43	3.5	28
SD-208	3.6	25	3.5	28	3	23	2.6	16	3.5	29	3.1	25
AZD6244	3.4	28	2.8	9	3.1	48	3	33	2.8	44	2.6	44
CI-1040 (PD 184352)	3.5	30	2.3	-1	3.1	50	2.5	25	2.9	46	2.2	38
PD 0325901	2.3	1	2	-9	2.2	20	2	8	2	35	1.8	28
API-2	2.1	40	1.9	23	2.6	41	2.3	30	2	53	1.8	45
GDC-0941	3	18	1.9	-11	2.5	6	1.8	-15	2.2	16	1.6	-3
PI-103	1.8	3	1.6	-12	1.7	-4	1.5	-6	1.5	9	1.4	-2
PIK-90	2.6	17	2.6	17	2.3	21	2.2	5	2.4	29	1.9	12
ZSTK474	2.3	17	1.5	-9	2.2	9	1.6	2	2.1	20	1.5	6
AZD0530	3.1	15	1.9	-32	2.8	30	1.9	-11	2.2	11	1.7	-8
PP 1	3.8	47	2.8	11	3.1	34	1.9	5	3.1	25	1.8	-4
AG 1478 hydrochloride	2.7	21	2.5	11	2.8	67	2.8	65	3	72	3	68
BMS-536924	3.6	82	3	42	3.6	89	2.6	24	2.1	26	1.9	7
JNJ38877605	3.8	107	3.5	110	2.6	2	2.6	3	3.4	77	3.4	72

Peach- TGFβR inhibitors, Blue- MEK inhibitors, Purple- PI3K inhibitors,
Green- Src inhibitors, White- respective receptor inhibitor

Small molecular weight compounds that inhibited EMT induced by HGF, EGF, IGF-1 fall into 4 major classes of compounds.

The EMT drug screen shortlisted 4 major classes of compounds that successfully inhibited the HGF, EGF and IGF induced scatter. The activity level of c-Met, EGFR and IGFR were taken into considerations to eliminate compounds with off-target effects. To investigate if these shortlisted compounds affected the phosphorylation of the receptors, NBT-II carcinoma cells were pre-treated overnight with the shortlisted compounds (Table 9) and protein cell extracts were then collected after half hour treatment with HGF, EGF or IGF. Lysates treated with the shortlisted compounds were blotted for the phosphorylation of c-Met,

EGFR and IGFR. NBTII lysates with no growth factor treatment displayed a low endogenous level of phosphorylation of the three receptors. The band intensity increased with addition of the ligand and diminished with the receptor-targeted inhibitor (Figure 20).

A number of shortlisted compounds fall under the TGFβR class of compounds (Table 9 peach colour) and the shortlisted compounds were A83-01, D4476, LY364947, SB431542 and SD208. The phosphorylation of EGFR and IGFR were not affected by all compounds tested while D4476, LY364947 and SD208 abrogated the phosphorylation of c-Met; phosphorylation of c-Met was slightly augmented with A83-01 and slightly reduced with SB431542 treatment (Figure 20). Those compounds which inhibited the phosphorylation of c-Met were removed from the list as they were considered non-specific; hence, A83-01 compound was chosen to represent the TGFβR class of compounds for further validation.

The next class of compounds (Table 9 blue) tested was targeted against MEK and the shortlisted compounds were AZD 6244, CI- 1040 and PD0325901. All compounds in this class did not affect the phosphorylation of c-Met and IGFR, however, AZD6244 and CI-1040 resulted a reduction in the phosphorylation of EGFR (Figure 21). PD0325901 was chosen to represent the Mek class of compounds for further validation.

Figure 20: Several TGFβR targeted compounds affect the activity of c-Met, EGFR and IGFR.
Top panel: Immunoblot for pcMet (phosphorylation of c-Met), whose phosphorylation increases with the addition of the ligand (HGF) and diminished with JNJ38877605 (a specific c-MET inhibitor). The ligand-induced phosphorylation of c-MET is inhibited by D4476, LY364947 and SD208; slight augmentation of c-Met phosphorylation by A83-01 and slight reduction in c-Met phosphorylation by SB431542. Middle panel: Immunoblot for pEGFR(phosphorylation of EGFR) whose phosphorylation increases with the addition of the ligand (EGF) and diminished with AG1478 (a specific EGFR inhibitor). The ligand-induced phosphorylation of EGFR is not affected by the test compounds. Bottom panel: Immunoblot for pIGFR (phosphorylation of IGFR), whose phosphorylation increases with the addition of the ligand (IGF-1) and diminished with BMS-536924 (a specific IGFR inhibitor). IGF-1-induced IGFR phosphorylation is not affected by the test compounds. α-Tubulin acts as loading controls.
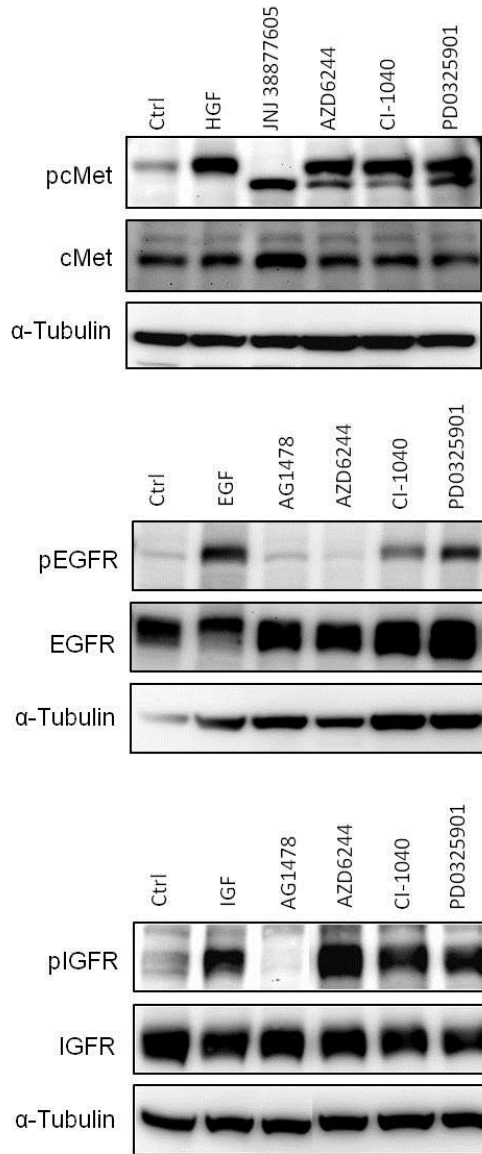
Figure 21: 2 MEK targeted compounds affect the activity of EGFR but not c-Met and IGFR.

Top panel: Immunoblot for pcMet (phosphorylation of c-Met), whose phosphorylation increases with the addition of the ligand (HGF) and diminished with JNJ38877605 (a specific c-Met inhibitor). MEK inhibitors do not affect the ligand induced phosphorylation of c-Met. Middle panel: Immunoblot for pEGFR(phosphorylation of EGFR) whose phosphorylation increases with the addition of the ligand (EGF) and diminished with AG1478 (a specific EGFR inhibitor). The ligand induced phosphorylation of EGFR is inhibited by AZD6244 and CI-1040. Bottom panel: Immunoblot for pIGFR (phosphorylation of IGFR), whose phosphorylation increases with the addition of the ligand (IGF-1) and diminished with BMS-536924 (a specific IGFR inhibitor). IGF-1 induced IGFR phosphorylation is not affected by the test compounds. α-Tubulin acts as loading controls.

The third class of compounds (Table 9 purple) tested were inhibitors of PI3K namely, API-2, GDC0941, PI103, PIK90 and ZSTK474. All compounds in this class caused an increase in phosphorylation of EGFR and IGFR; while API-2 and PI103 caused a reduction in ligand-induced c-Met phosphorylation (Figure 22). GDC0941 was chosen to represent the PI3K targeted class of compounds for further validation as GDC0941 presented lower cell dispersion ratios compared to PIK90 and ZSTK474 (Table 9).

The fourth class of shortlisted compounds (Table 9 green) consisted of Src inhibitors (AZD0530 and PP1). Both Src inhibitors, AZD0530 and PP1, caused a reduction in c-Met phosphorylation (Figure 23), suggesting the importance of an active Src protein in the maintenance of c-Met activity. The observations were similar to a report (Emaduddin, Bicknell et al. 2008) which showed a reduction in phosphorylation of Y1234/1235 c-Met by PP2, a pan SFK inhibitor. IGFR phosphorylation was not affected by the two compounds while PP1 interfered with the phosphorylation of EGFR. Therefore, AZD0530 was chosen to represent the Src inhibitors for further validation.
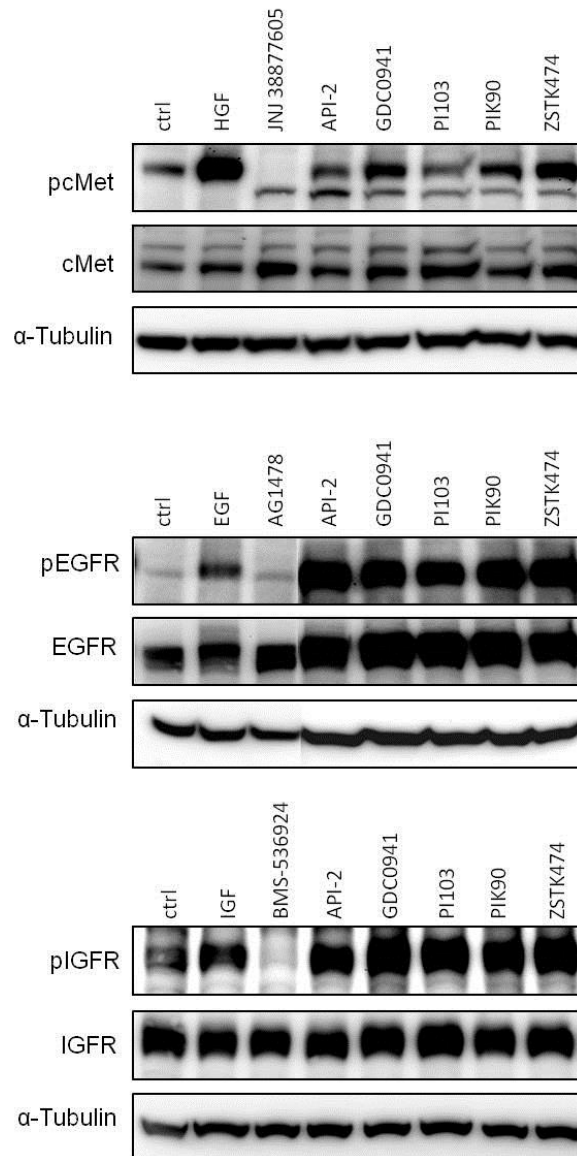
Figure 22: 2 PI3K targeted compounds caused a reduction in phosphorylation of c-Met, while augmenting EGFR and IGFR phosphorylation.

Top panel: Immunoblot for pcMet (phosphorylation of c-Met), whose phosphorylation increases with the addition of the ligand (HGF) and diminished with JNJ38877605 (a specific c-MET inhibitor). The ligand induced phosphorylation of c-MET is inhibited by API-2 and PI103. Middle panel: Immunoblot for pEGFR(phosphorylation of EGFR) whose phosphorylation increases with the addition of the ligand (EGF) and diminished with AG1478 (a specific EGFR inhibitor). The ligand induced phosphorylation of EGFR is not affected by the test compounds. Bottom panel: Immunoblot for pIGFR (phosphorylation of IGFR), whose phosphorylation increases with the addition of the ligand (IGF-1) and diminished with BMS-536924 (a specific IGFR inhibitor). IGF-1 induced IGFR phosphorylation is not affected by the tested compounds. α-Tubulin acts as loading controls.
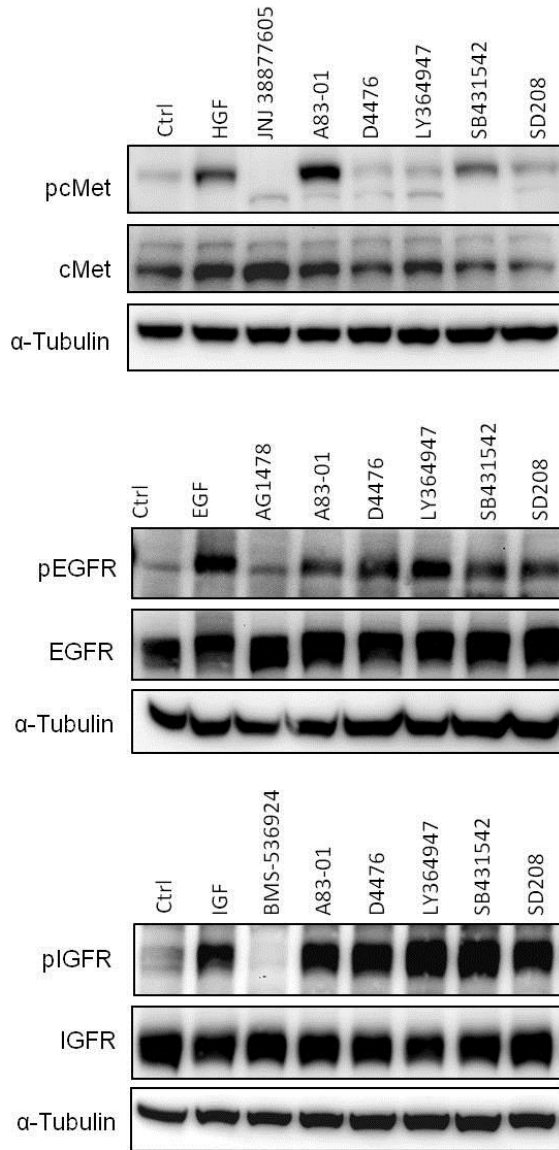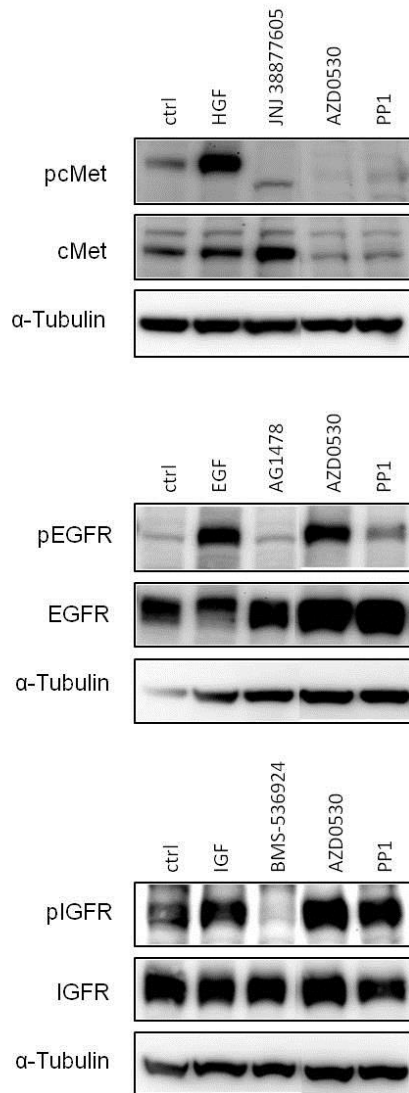
Figure 23: Both Src targeted compounds affect the activity of c-Met.
Top panel: Immunoblot for pcMet (phosphorylation of c-Met), whose phosphorylation increases with the addition of the ligand (HGF) and diminished with JNJ38877605 (a specific c-MET inhibitor). The ligand induced phosphorylation of c-MET is inhibited by both SRC inhibitors: AZD0530 and PP1. Middle panel: Immunoblot for pEGFR (phosphorylation of EGFR) whose phosphorylation increased with the addition of the ligand (EGF) and diminished with AG1478 (a specific EGFR inhibitor). The ligand induced phosphorylation of EGFR is inhibited by PP1. Bottom panel: Immunoblot for pIGFR (phosphorylation of IGFR), whose phosphorylation increases with the addition of the ligand (IGF-1) and diminished with BMS-536924 (a specific IGFR inhibitor). IGF-1 induced IGFR phosphorylation is not affected by the test compounds. α-Tubulin acts as loading controls.

The shortlisted representative compound from each class of inhibitors was tested for its relative potency in inhibiting growth factor induced EMT. We utilised the spot migration assay to measure the effectiveness of the shortlisted compound in inhibiting growth factor induced dispersion by determining the half maximal inhibitory concentration (IC_{50}). The four shortlisted compounds have IC_{50} in the nanomolar range (A83-01: 130nM, PD0325901: 20nM, GDC0941: 380nM and AZD0530: 510 nM) for HGF induced EMT; (A83-01: 69nM, PD0325901: 31nM, GDC0941: 740nM and AZD0530: 560 nM) for EGF induced EMT and (A83-01: 120nM, PD0325901: 8.9nM, GDC0941: 500nM and AZD0530: 240 nM) for IGF-1 induced EMT (Figure 24).
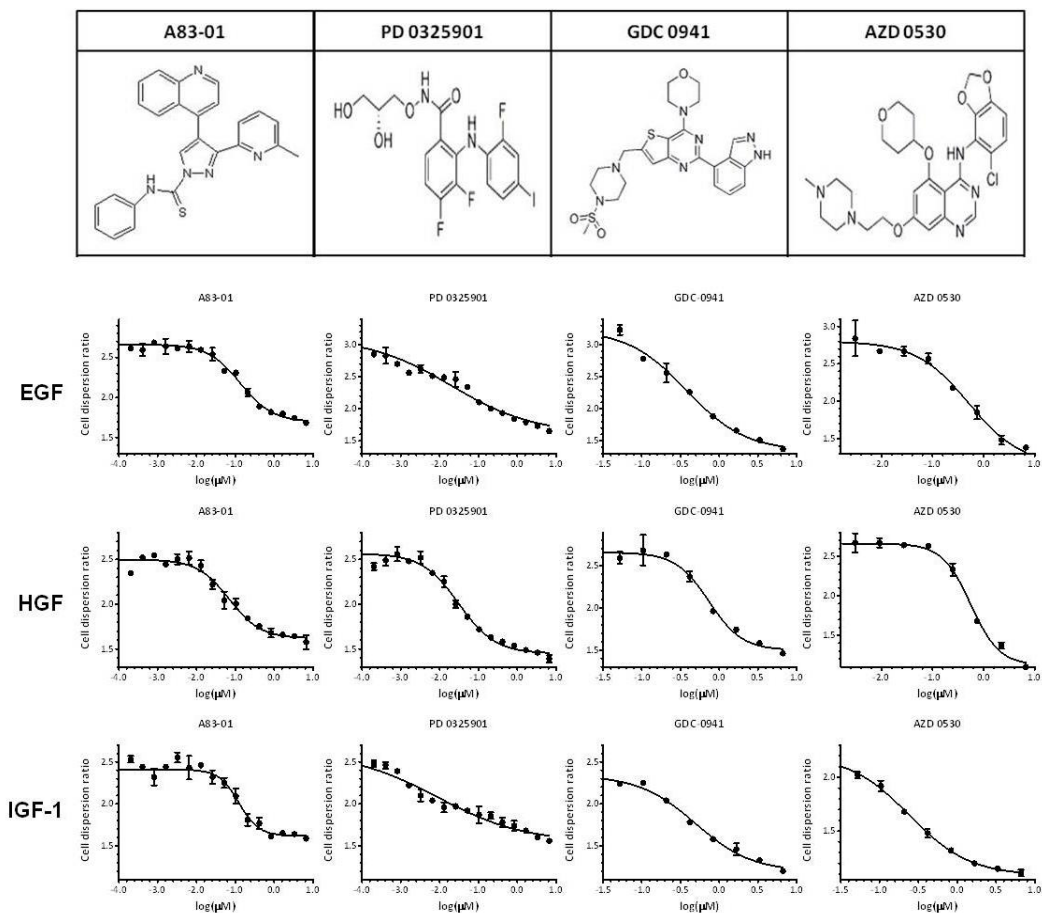
Figure 24: Relative propensity of the shortlisted compounds in inhibiting growth factor-induced dispersion.

Top panel: Structure of short-listed small molecular weight compounds; from left to right: A83-01 (TGFβRI inhibitor), PD 0325901 (MEK inhibitor), GDC 0941 (PI3K inhibitor) and AZD 0530 (Src inhibitor). Second to Fourth panel: Graphs were plotted Cell Dispersion Ratio (Y-axis) against log μM (X-axis). Graphs display the dose response curve of compounds in inhibiting growth factor induced dispersion. Second panel: Dose response curve to determine IC_{50} of short-listed compound in inhibiting EGF induced cell dispersion; from left to right: A83-01, PD 0325901, GDC 0941 and AZD 0530. Third panel: Dose response curve to determine IC_{50} of short-listed compound in inhibiting HGF-induced cell dispersion; from left to right: A83-01, PD 0325901, GDC 0941 and AZD 0530. Fourth panel: Dose response curve to determine IC_{50} of short-listed compound in inhibiting HGF-induced cell dispersion; from left to right: A83-01, PD 0325901, GDC 0941 and AZD 0530. The four compounds inhibit growth factor-induced EMT.

4 representative compounds of each inhibitor class show EMT modulating properties

NBT-II carcinoma cells were pre-treated with the representative compounds (A83-01, PD0325901, GDC0941, AZD0530) at 3 doses (0.5µM, 2µM, 8µM) overnight before induction by HGF, EGF or IGF-1 for 24 hours. Protein cell extracts were then blotted with antibodies against Mmp-13, a matrix metalloproteinase, and E-cadherin, the major adhesion molecule in adherens junctions. Mmp-13 is required for cell migration (Hattori, Mochizuki et al. 2009) and stromal expression of Mmp-13 contribute to invasion of carcinoma cells (Zigrino, Kuhn et al. 2009). Protein levels of Mmp-13 increased upon addition of HGF (Figure 25A), IGF-1 (Figure 25C) and modestly by EGF (Figure 25B). The IC_{50} AZD0530 (Src inhibitor) across all growth factors were approximately 500nM and therefore a dose-dependent reduction of Mmp-13 protein levels by AZD0530 was observed under EGF, HGF and IGF-1 induction. A modest dose dependent reduction of Mmp-13 was also observed with TGFβRI inhibitor (A83-01) under HGF and IGF-1 induction; the IC_{50} of this compound for both growth factors were approximately 100nM. The IC_{50} of MEK inhibitor (PD0325901) across all growth factors was below 40nM and hence a complete reduction of Mmp-13 was observed for all growth factors. Each of the representative compounds of TGFβRI, Mek, PI3K and Src inhibitors were able to reduce Mmp-13 protein levels except for PI3K inhibitor under EGF induction (Figure 25B).
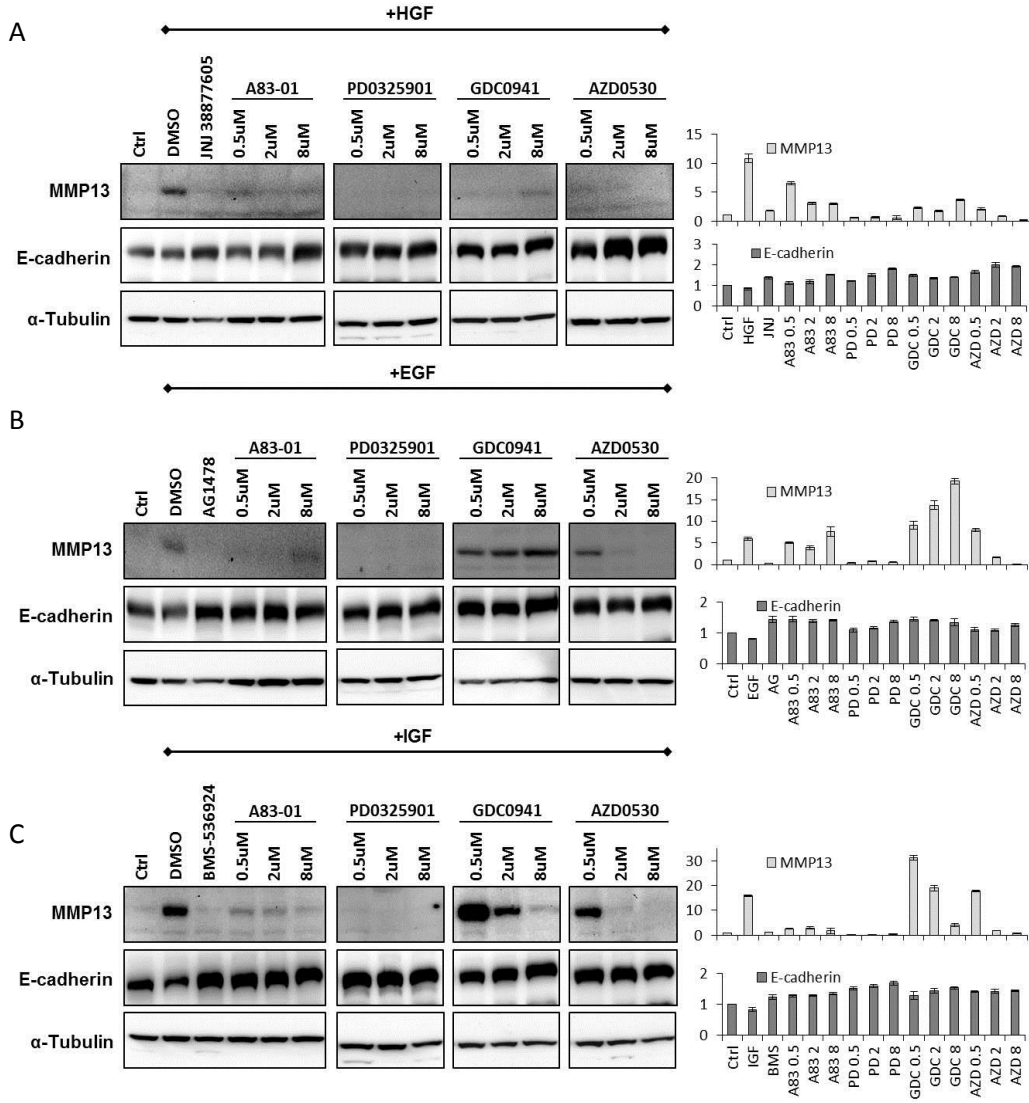
Figure 25: Modulation of EMT markers, E-cadherin and MMP13, by shortlisted compounds.

Immunoblot for MMP13 and E-cadherin, whose expression were modulated by EMT inhibitors under HGF (A), EGF (B), and IGF-1 (C) induced EMT conditions. E-cadherin expression levels decreased with growth factor addition compared with DMSO control, indicating cells have undergone EMT. However, the E-cadherin level was restored or augmented with increasing compound concentrations, due to EMT inhibition effected by these compounds. Conversely, addition of HGF and IGF-1 increased MMP-13 expression levels compared with DMSO control. In general, this increase in MMP-13 expression could be abrogated with the addition of the EMT inhibitors. Bars represent mean $\pm$ standard deviation. N=2.

These findings were consistent with previous reports showing that TGFβR, Src and Mek or its target, MAPK play a role in cell motility and tumour progression (Reddy, Nabha et al. 2003); (Wong, Chen et al. 2012); (Zhong, Chen et al. 2012). The 4 classes of compounds reduced the levels of Mmp-13, suggesting that these compounds lowered the cells potential in migration and invasion, consistent with the results of the screen. The cell lysates were then blotted for E-cadherin protein levels. All classes of compounds were able to augment the E-cadherin protein levels compared to growth factor treated ones. These results suggest that selective inhibition of MEK, PI3K, Src and TGFβRI could potentially revert EMT by restoring E-cadherin-mediated cell adhesion and reduce invasion through the inhibition of Mmp-13. . In addition, immunofluorescent labelling of Desmoplakins (epithelial marker) and Vimentin (mesenchymal marker) were included in the analyses to further confirm the EMT reversal induced by these 4 classes of compounds. (Appendix 5,6)

4 representative compounds reduced invasiveness of carcinoma cells.

The shortlisted EMT inhibitory compounds were validated for their ability to reduce the invasiveness of cells induced by growth factor exposure using a Boyden chamber assay. NBT-II carcinoma cells were added to the top compartment while the growth factor (HGF, EGF or IGF-1) was added to the bottom compartment to allow NBT-II carcinoma cells to invade the matrigel in response to the growth factors. Each of the representative compounds was added

to the top compartment and tested for its effectiveness in reducing the invasive properties of growth factor induced NBT-II carcinoma cells.

The traditional way of quantifying cells in this assay was to stain the cells with crystal violet dye and counting by eye under microscope. The traditional way is time consuming and prone to human error; therefore, we decided to stain the cells with Calcein AM and utilise a fluorometer for fluorescence quantification instead. To test whether quantification with fluorescence reading was acceptable in this assay, two independent transwell setups were done with identical conditions consisting of one control, one HGF-induced and one HGF+c-Met inhibitor (JNJ 38877605). One set of the experiment was stained with crystal violet while the other set was stained with Calcein AM. The relative fluorescence reading was consistent with the pictures of crystal violet stained cells (Figure 26A) showing that the use of Calcein AM and its fluorescence reading was acceptable for this assay.

The assay was extended to assess the ability of the 4 representative compounds to inhibit HGF, EGF or IGF-1 induced cell invasion. Greater number of NBT-II carcinoma cells under growth factor induction invaded the matrigel-coated insert compared to normal conditions (4.5 folds under HGF induction, 4.1 folds under EGF induction and 1.7 folds under IGF-1 induction) as shown in Figure 26B. Addition of the compounds (JNJ38877605 targeting c-Met, AG1478 targeting EGFR or BMS-536924 targeting IGF-1R) served as a positive control for each cognate receptors. Indeed, the addition of the positive control compounds decreased the number of cells that invaded the matrigel-coated inserts. All the

shortlisted compounds namely A83-01 targeting TGFβRI; PD0325901 targeting MEK; GDC0491 targeting PI3K; and AZD0530 targeting Src; successfully reduced the number of HGF, EGF or IGF-1-induced cells migrating through the matrigel-coated inserts (Figure 26B). Consistent with the screen, the shortlisted compounds were able to inhibit the *in vitro* matrigel invasion of growth factor induced NBT-II bladder carcinoma cells.
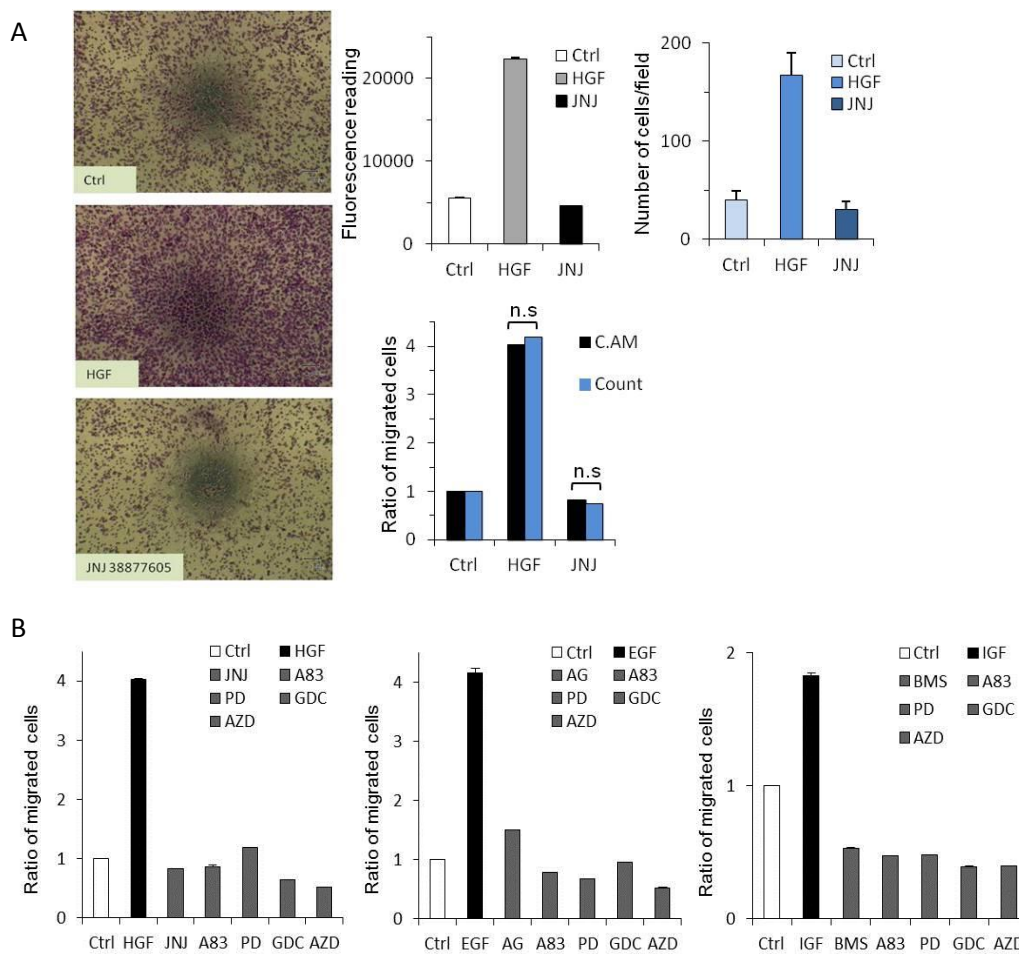
Figure 26: Shortlisted compounds inhibit growth factor induced invasive capabilities in NBT-II bladder carcinoma cells.

(A) No significant difference between the two detection methods used for quantifying cells that invaded through the matrigel-coated inserts in the boyden chamber assay. Left panel: Bright field images of crystal violet stained NBT-II cells that invaded through the matrigel-coated inserts. Graph with Y-axis (Fluorescence reading) displays the values detected by the Tecan Infinite M100 Pro microplate reader when the invaded NBT-II carcinoma cells were stained with Calcein AM and trypsinized

before reading. Greater number of cells invaded the matrigel-coated inserts with addition of HGF (about 4 fold increase compared to control). This invasiveness is inhibited by JNJ (JNJ 38877605), a specific compound for c-Met. The graph with Y-axis (Number of cells/field) displays the number of crystal violet stained NBT-II cells that invaded the matrigel-coated inserts, counted per field manually for each condition. The graph with Y-axis (Ratio of migrated cells) shows that there is no significant difference between the relative ratio calculated for the assay using Calcein AM fluorescence reading and assay using manual counting cells/field. (B) The shortlisted compounds A83 (A83-01), a specific inhibitor for TGFβRI; PD (PD0325901), a specific inhibitor for MEK; GDC (GDC 0491), a specific inhibitor for PI3K; and AZD (AZD0530), a specific inhibitor of Src inhibit the HGF/EGF/IGF-1 induced *in vitro* matrigel invasion. Left: Graph displaying the relative ratio of cells that undergo HGF induced matrigel invasion; positive inhibitor control: JNJ. Middle: Graph displaying the relative ratio of cells that undergo EGF-induced matrigel invasion; positive inhibitor control: AG (AG1478), a specific inhibitor for EGFR. Right: Graph displaying the relative ratio of cells that undergo IGF-1 induced matrigel invasion; positive inhibitor control: BMS (BMS-536924), a specific inhibitor for IGF-1R. n.s= not significant.

A TGFβRI EMT signature is found in c-Met driven EMT

MEK, PI3K and Src are known downstream targets of growth factors; however the activation TGFβRI pathway has not been described in HGF, EGF and IGF signalling. Data from the drug screen concluded that TGFβRI inhibitor (A83-01) could inhibit growth factor induced EMT; hence an expression profiling was performed to uncover the TGFβRI EMT signature in this c-Met driven system. Under induction of HGF, the gene expression profile of TGFβRI inhibitor (A83-01) treated cells was compared with Vehicle (DMSO) to identify genes affected by TGFβRI signalling under HGF induction. Two analyses were performed in order to identify the TGFβRI EMT signature in the c-Met driven system. The first analysis was to identify the genes regulated by HGF in which expression profile of cells treated with DMSO in absence of HGF was compared with that of cells

treated with DMSO and HGF. The second analysis was to compare profiling of DMSO+HGF versus A83-01+ HGF treated samples to identify the genes affected by the inhibition of TGFβRI. The overlap of the genes from the two analyses delivered 280 HGF-deregulated genes whose expression was reverted back to values comparable to control with TGFβRI inhibition. This list of 280 genes described the TGFβRI EMT signature under c-Met driven conditions (Figure 27A). However, 177 genes failed to recover their gene expression towards the level at control state when A83-01 was added. In addition, Zeb1 was among the 177 genes which expression was lowered but not 100% reverted by A83-01 compound. This group of 177 genes was less efficiently regulated by TGFβ receptor than the group of 280 genes in the presence of HGF. Thus the TGFβRI EMT signature was defined by the 280 genes.

To investigate the role of this TGFβRI EMT signature in HGF induction system, a gene ontology analysis on the 280 genes was performed with DAVID, a Functional Annotation Bioinformatics Microarray Analysis software provided free online by the National Institute of Allergy and Infectious Diseases (NIAID), at the National Institute of Health in Bethesda Md USA. The major pathways identified by the analysis were focal adhesion, ECM-receptor interaction and ErbB signalling (Table 10). Some of the 280 genes affected processes like cell motion, morphogenesis of branching structure, cell adhesion and actin cytoskeleton organization (Table 11).

Table 10: 3 top pathways engaged by genes from the TGFβRI EMT signature.

Pathway	Genes	FDR (Benjamini)
Focal adhesion rno04510	FLT1, PIK3CB, PIK3CD, ACTN1, ITGA2, ITGA3, VCL, LAMB3, LAMA3, VEGFA, PPP1R12A, LAMC2, ZYX, THBS2	3.89E-04
ECM-receptor interaction rno04512	LAMB3, LAMA3, CD44, ITGA2, LAMC2, ITGA3, THBS2	0.028455
ErbB signaling pathway rno04012	EREG, PIK3CB, PIK3CD, HBEGF, TGFA, AREG, NRG1	0.029293

Inhibition of TGFβRI reduced the expression level of Lamc2 also known as Laminin-5, Vcl (vinculin) and Itga2/3 (integrins) which are important players at focal adhesion sites. Laminin 5 induced cells to form large lamellae-like areas (Dogic, Rousselle et al. 1998) and NBT-II carcinoma cells when exposed to laminin-5 undergo locomotion. Another gene identified critical for HGF induced cell migration was HB-EGF (heparin-binding EGF-like growth factor). The membrane bound HB-EGF was reported to regulate cell- matrix interactions while the soluble form increased HGF induced cell migration (Singh, Tsukada et al. 2004). Inhibition of TGFβRI reduced the expression level of HB-EGF. A reduction of HB-EGF could perturb cell migration. In conclusion, A83-01 compound showed certain EMT inhibiting features and the TGFβRI EMT signature governs the protein machinery for migration and invasion processes for c-Met-driven EMT.

Table 11: Major biological processes affected by 280 genes of the TGFβRI EMT signature.

GO term	Genes	FDR (Benjamini)
GO:0051270 regulation of cell motion	PTPRM, FLT1, PDPN, ACTN1, ITGA2, ABHD2, VCL, LAMA3, ETS1, PTK2B, RRAS2, VEGFA, HBEGF, CYR61, IGFBP5	6.49E-04
GO:0042127 regulation of cell proliferation	PTGS2, ALDH3A1, CASP3, PTGES, PTK2B, HLX, SERPINE1, TGFA, FOSL1, ETV4, ODC1, PTPRM, FLT1, ITGA2, CENPF, NUPR1, EREG, ID2, DBP, F3, VEGFA, HBEGF, AREG, KCTD11, NGF, IGFBP5	0.003106
GO:0001763 morphogenesis of a branching structure	SPRY2, FLT1, CD44, VEGFA, SEMA3C, AREG, GDNF, ETV4, CYR61	0.023178
GO:0007155 cell adhesion	PVR, PTPRM, PDPN, PIK3CB, ACTN1, ITGA2, ITGA3, VCL, LAMA3, CD44, PTK2B, FAT1, LAMC2, MLLT4, RASA1, TTC39B, CYR61	0.050605
GO:0030036 actin cytoskeleton organization	RND1, NUAK2, PTK2B, FAT1, FHL3, ACTN1, RGD1560248, FHDC1, RASA1	0.113098

To further validate the microarray-based findings, 3 genes (Serpine1, p21 and Zyxin) were picked for analysis with western blot. Serpine1 also known as Plasminogen activator inhibitor-1 (PAI-1). PAI-1 was chosen for validation as it was identified as one of the gene transcripts in chapter one that contribute to tumour progression of bladder carcinoma cells; and it was found up-regulated in advanced stages of bladder cancer. Low concentration of PAI-1 was sufficient to modify the actin cytoskeleton and focal adhesions, promoting cell migration (Degryse, Neels et al. 2004). The second gene validated was CDKN1a also known as cyclin-dependent kinase inhibitor 1 or CDK-interacting protein 1 (p21/Cip1). p21 is a transcriptional target of the tumour suppressor gene, p53, and mediates the p53-dependent cell cycle G1 phase arrest (Abbas and Dutta 2009). Other than an effector of anti-proliferative signals, p21 can also display anti-apoptotic effects through direct binding and inhibiting the transactivation activity of the transcription factors: E2F transcription factor 1 (E2F1), signal transducer and activator of transcription 3 (STAT3) and Myc. The third gene validated was Zyxin which is a zinc-binding phosphoprotein that concentrates at focal adhesions; and its proline rich N-terminal domain mediates actin polymerization. Zyxin may be a potential effector protein that contributes to locomotion by modulating the actin cytoskeletal organization. Protein levels of PAI-1, p21 and Zyxin were elevated under HGF induction and decreased upon A83-01 (TGFβRI inhibitor) addition. The protein level of PAI-1 protein was reduced by A83-01 to a greater extent compared to p21 and Zyxin (Figure 27B).
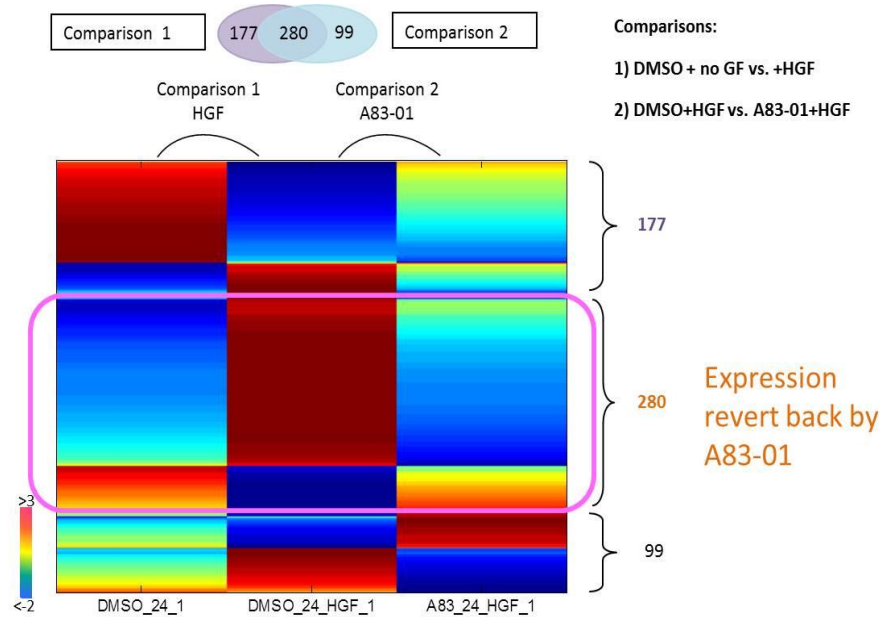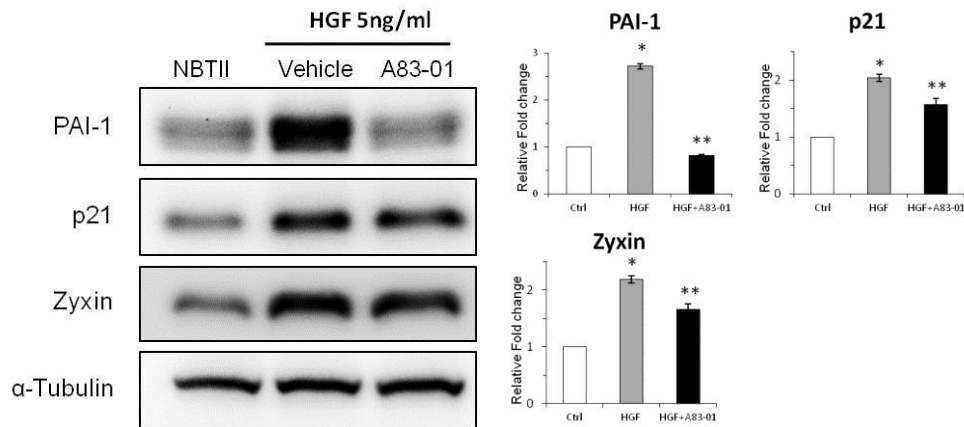
Figure 27: The TGFβRI EMT signature in c-MET driven EMT.
(A) The unsupervised clustering of the mean intensities in the two repeats of each condition:1) DMSO (drug vehicle) without (GF) growth factor versus DMSO+HGF and 2) DMSO+HGF versus A83-01+HGF. The addition of A83-01 (TGFβRI inhibitor) reversed the effect of the growth factor (HGF) for a group of 280 genes; A83-01 failed to revert a group of 177 HGF driven genes back to control conditions; and 99 genes were the side-effects of the drug. (B) Western blot analysis of protein level of PAI-1, p21 and Zyxin in NBT-II carcinoma cells treated with or without 2.5uM of A83-01 in the presence of 5ng/ml of HGF for 24 hours. The addition of A83-01 reverted the HGF induced PAI-1 protein expression; and to a lesser extent, p21 and Zyxin. Intensity of each western blot band was measured and normalized against band intensity of α-Tubulin for each sample; relative fold change for each protein was calculated by comparing protein band intensity of vehicle or A83-01 against control. α-Tubulin was used as a loading control. Bars represent mean $\pm$ standard deviation. N=3. *= p-value <0.05 when compared to control. **= p-value <0.05 when compared to HGF treated.

Part 3: Validation of a TGFβRI inhibitor using an orthotopic bladder cancer model

Introduction

The goal standard for treatment of superficial stage transitional carcinoma is transurethral resection possibly followed by chemotherapy or intravesical immunotherapy treatment. However, the high rate of recurrence and the potential to the progress as muscle-invasive raise much concern for the follow-up patients. There is a need to evaluate novel treatment strategies that can improve the efficacy of the current treatment. Testing of new therapeutic agents or drug regimens cannot be done initially in the clinics unless preclinical trials provide a rationale to change the current treatment modalities. As of today, there are two preclinical murine bladder cancer models: 1) the chemically induced bladder cancer model and 2) the xenograft model which involves the transplantation of human transitional carcinoma or carcinoma cells into immunodeficient or immunocompetent mice. Transitional carcinoma cells can be implanted to form heterotopic tumour (subcuetaneous injection) or orthotopic tumour (intravesical instillation). The xenograft model is preferred as it permits the labeling of carcinoma cells before implantation to allow the real-time tracking of carcinoma cells in the animal. The subcutaneous model is useful in the investigation of tumourigenicity while the orthotopic model is useful in the study of tumour progression as carcinoma cells form tumours that reside in the organ of origin, providing a favourable model for evaluation of new treatment modalities. Part 2

of this chapter describes the optimization of a murine orthotopic bladder cancer model that is used to evaluate the effectiveness of the shortlisted TGFβRI inhibitor (A83-01) in limiting the invasive potential of bladder carcinoma cells.

Results

Choosing the appropriate cell line for the establishment of an orthotopic bladder cancer model relevant to our study

To study the invasive behaviour of the carcinoma cells *in vivo*, we started with the selection of bladder cell line originating from high grade tumours with high invasive potential. Since the expression level of c-Met was found to correlate with tumour grade in human bladder cancer patients and poor prognosis was associated with high c-Met expression levels, it is preferable that the cell line chosen have a relatively high expression of c-Met with c-Met activity. Therefore, we assessed the level of c-Met expression across a panel of 4 commonly used human bladder carcinoma cell lines: HT1376, T24, J82 and UM-UC-3; and observed that UM-UC-3 human bladder carcinoma cells expressed relatively higher levels of c-MET compared to the other human bladder carcinoma cell lines (Figure 28A). Furthermore, c-Met is constitutively active in UM-UC-3 (Figure 28B).

To investigate if c-Met expression of the bladder carcinoma cells correlates with their invasive behaviour, a matrigel-coated boyden chamber was used to compare the invasiveness of a low c-Met expressing human bladder carcinoma cell line HT1376 with a high c-Met expressing human bladder carcinoma cell line UM-UC-3. 2.3 folds more UM-UC-3 carcinoma cells invaded the matrigel layer compared to HT1376 carcinoma cells (Figure 28C). This data demonstrated that higher levels of c-Met expression correlates with increased invasive behaviour of

bladder carcinoma cells; and the levels of c-Met expression can be a measure of

invasive potential in bladder carcinoma cells.
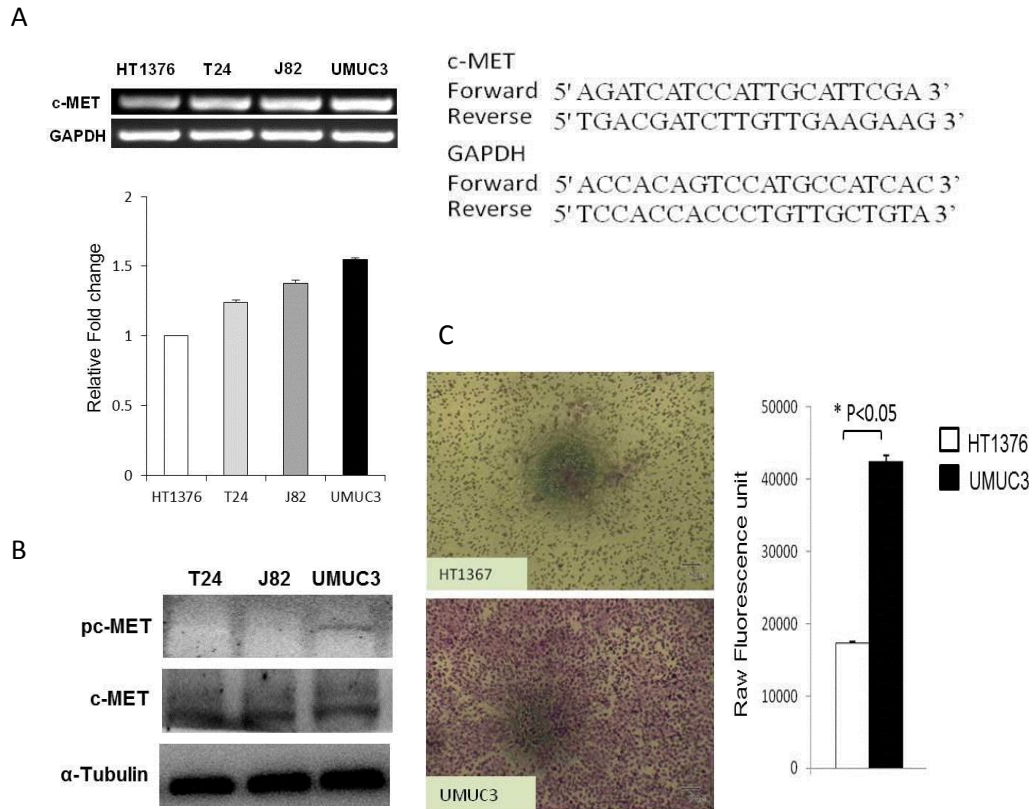
Figure 28: c-MET expression level correlates with invasiveness in bladder carcinoma cell lines.
(A) Left panel: Semi-quantitative RT-PCR was used to amplify fragment (410bp) of c-Met from mRNAs of 4 human transitional cell carcinoma cell lines (HT1376, T24, J82 and UM-UC-3 (UMUC3)). The graph displays the relative fold change in c-Met expression of T24, J82 and UM-UC-3 compared to HT1376. Right panel: forward and reverse primer sequence for human c-Met and Gapdh. (B) Immunoblot for c-Met phosphorylation (pc-MET) shows that c-Met is constitutively phosphorylated in UM-UC-3 under resting state. c-Met is not activated in T24 and J82 cell lines. α-Tubulin was used as a loading control. (C) Left panel: crystal violet staining of HT1376 and UM-UC-3 cells that invaded the matrigel in the boyden chamber. Right panel: Fluorescence quantification of Calcein AM stained HT1376 and UM-UC-3 cells that invaded the matrigel in the boyden chamber. Bars represent mean + SEM. *p<0.05, two-tailed t-test. N=3 independent experiments.

The tumorigenicity of HT1376, T24, J82 and UM-UC-3 carcinoma cell lines were observed using a subcutaneous model as tumours formed can be monitored and measured with a vernier caliper. Each carcinoma cell line was injected subcutaneously into the flank of 3 athymic mice and observed for tumour growth for 31 days. Only the tumours that were derived from UM-UC-3 carcinoma cells continued to grow and increase in volume (Figure 29). The invasiveness and tumorigenicity of UM-UC-3 bladder carcinoma cell line makes it an attractive cell line for the establishment of the orthotopic mouse bladder cancer model.
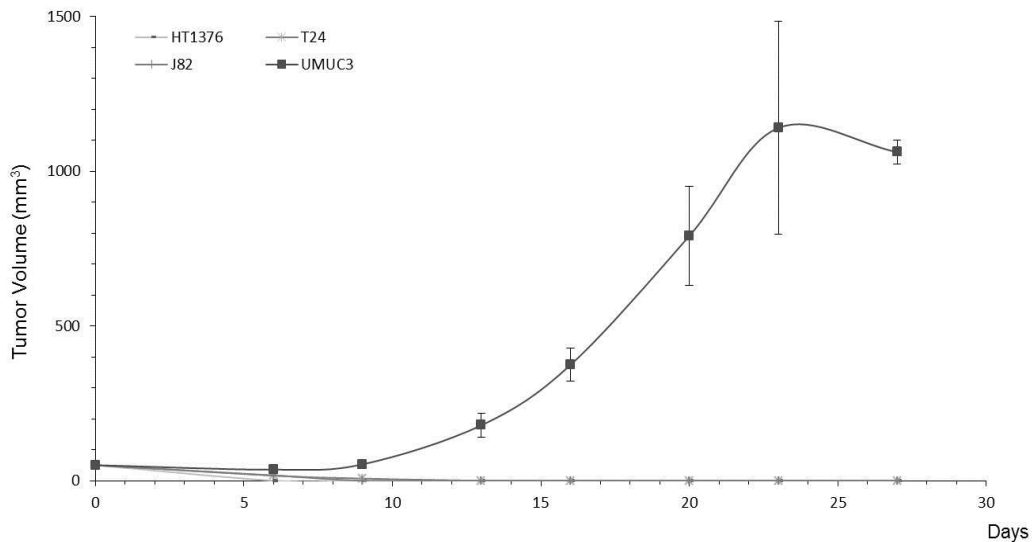
Figure 29: UM-UC-3 is tumourigenic *in vivo*.
4 human bladder cancer cell lines (HT1376, T24, J82 and UM-UC-3 (UMUC3)) were subcutaneously injected into the left and right flank of nude mice to form tumours, as described in materials and methods. The dimension of the tumours were measured twice a week using a digital vernier caliper; and the first measurement was taken a week after injection. HT1376 was not tumourigenic. Tumours formed by T24, J82 carcinoma cell lines regressed after 13 days. Tumours formed by UM-UC-3 carcinoma cell line grew and reached more than 1000mm^3 in less than 25 days. Tumour volume is calculated using the formula: (length x width^2)/2. Each point on the curve represents mean +SEM. N=6

UM-UC-3 carcinoma cells exhibit a spindle like morphology characteristic of mesenchymal cells. To determine the *in vitro* morphological changes of UM-UC-3 in response to A83-01 (TGFβRI inhibitor), UM-UC-3 carcinoma cells were treated with A83-01 and observed under a phase contrast microscope. In the presence or absence of HGF, UM-UC-3 carcinoma cells were observed to cluster and initiate cell-cell contacts under A83-01 treatment (Figure 30). It is important to note that UM-UC-3 carcinoma cells treated with HGF did not elicit a more mesenchymal phenotype, attributed to an already fully activated c-Met.
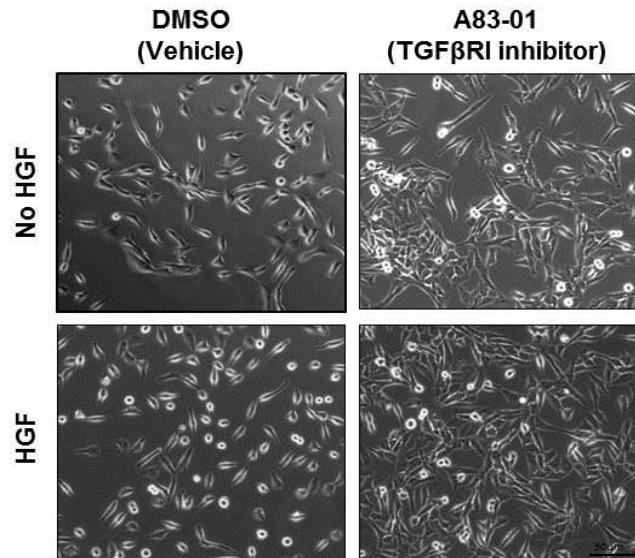
Figure 30: UM-UC-3 responds to A83-01 (TGFβRI inhibitor) and resumes cell-cell contacts with inhibition of TGFβRI.
Phase contrast images of UM-UC-3 cells treated with 10µM A83-01 in the presence and absence of 5ng/ml of HGF. Top Panel: UM-UC-3 carcinoma cells were incubated with DMSO (drug vehicle) or A83-01 (TGFβRI inhibitor) for 3 days and cell morphology was examined and photographed using a phase-contrast microscope. Bottom Panel: UM-UC-3 carcinoma cells were incubated with DMSO or A83-01 for 2 days prior to HGF treatment for 24 hours. HGF exposure did not induce any phenotype change as HGF receptor (c-Met) was constitutively activated in UM-UC-3 carcinoma cells. UM-UC-3 carcinoma cells treated with A83-01 initiated cell-cell contacts which were not observed in DMSO treated cells.

Method of tumour detection

Physical examination with bladder palpation and urine inspection are one of the methods to confirm tumour growth; however, when a tumour becomes palpable and haematuria is observed, it often represents a late stage of bladder cancer and efficacy of treatment might be compromised. In order to detect tumours and treat mice before clinical signs appear, non-invasive *in vivo* imaging (Bioluminescence, Fluorescence and MRI) is required. Bioluminescence is preferred as the image acquisition time is short and signal is strong. This technique involves a photo-imaging device that detects light signals that arise from the catalysis of the luciferin (substrate) by luciferase.

In order to detect the establishment and growth of UM-UC-3 tumours in the mouse bladder, UM-UC-3 carcinoma cells were generated to stably express a mammalian codon-optimized firefly luciferase2 that would react with its substrate (luciferin) for bioluminescence detection. When luciferin is intraperitoneally injected into the mice harbouring UM-UC-3-luc2 carcinoma cells in the bladder, luciferase of the UM-UC-3-luc2 carcinoma cells catalyse the oxidation of luciferin to oxyluciferin in the presence of ATP, Mg^{2+} and O_2 producing yellow-green light that shifts to red light *in vivo* at $37\,^{\circ}C$. The red light is detected by the bioluminescence imaging system, quantified and recorded in photons/sec.

Implantation technique

The stable cell line, UM-UC-3-luc2, was inoculated into the bladders of 6-8 week old-mice through an angiocatheter; and retained in the bladder lumen of mice for 3 hours (Figure 31). The lumen of the mouse bladder is lined with a film of mucin that consists largely of substances known as glycosaminoglycan (GAG). This GAG layer is thought to be the first line of defense of the urinary bladder against penetration into the bladder wall by bacteria and potentially harmful substances in the urine (www.ic-network.com/handbook.bladwall.html). Therefore, it is imperative that this GAG layer is disrupted or removed for UM-UC-3-luc2 cells to attach to the bladder wall. The bladder lumen of mice was pre-treated with 0.2% trypsin for 30 min to elute the intercalated proteoglycans from the luminal surface, thus increasing the tumour take rate of 0-10% to 40-60%.

The presence of tumours was confirmed using the bioluminescence *in vivo* imaging system a week after the implantation procedure (Figure 31).The major shortcoming of this procedure was the minimum incubation period of 3 hours that allowed UM-UC-3-luc2 cells to adhere to the bladder wall. During this incubation period, the mice were continuously under the influence of isoflurane induced anaesthesia. This prolonged anaesthesia inevitably resulted in an increased incidence of anaesthetic-related mortality.
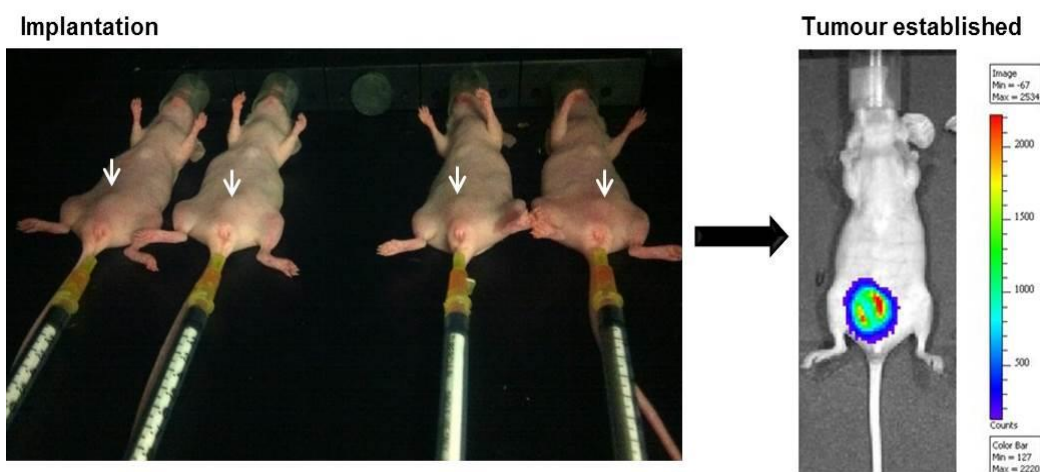
Figure 31: Orthotopic implantation and *in vivo* detection of bladder carcinoma.
Left picture: UM-UC-3 carcinoma cells harbouring the luciferase construct were instilled into the trypsin pre-treated bladder lumen via a 24G angiocatheter. UM-UC-3 carcinoma cells were incubated in the bladder lumen for 3 hours while mice were kept warm with a 37°C heat plate and subjected to 1.5% isoflurane anesthesia. White arrow shows the distended bladder during implantation. Right picture: Bioluminescent intensity (BLI) image of orthotopically inoculated UM-UC-3 cells in the bladder after one week of implantation. Luciferin was injected intraperitoneally into the mice to observe tumour take; luminescence would be detected from mice which had tumour established while no signal would be detected if UM-UC-3 carcinoma cells did not attach successfully.

Drug administration

Drug administration is a significant component in testing new therapeutic regimens and requires careful planning in optimizing the delivery of compound to the experimental animals while minimizing the potential adverse side effects. The route for administration of compounds is optimized for issues pertaining to compound stability, metabolism and excretion of compounds and compound solubility (selection of vehicle or solvent for drug delivery). The dosing

114

methodology which includes factors like frequency of administration and duration of treatment is critical as compounds have to be administered repeatedly and must not cause toxicity to the experimental animals.

Since TGFβRI inhibitor (A83-01) is highly insoluble in diluents like Carboxy methyl cellulose, 0.5% Tween 80 and Saline which were commonly used for drug administration, its dissolution was much improved using DMSO. The intravenous route requires the compound to be readily soluble in a vehicle that does not cause osmotic shock or toxicity to the animal. Intravenous injection of high percentage of DMSO is toxic to the animal and thus could not be used. The compound was thus administered intraperitoneally (150µg/200µl/body; DMSO: Saline (3:2, v/v)) or orally (800µg/200µl/body; DMSO: Saline (1:4, v/v)) to animals. The compound entered the bloodstream within half an hour after administration for both routes. To determine the final concentration of A83-01 that reach the blood stream and the time the drug takes to clear from the blood stream, blood samples were collected for analysis after 30 minutes, 2 hours and 4 hours after administration. . Drug concentration detected from the blood plasma was 1.2µM for oral administration at 30 minutes post administration and decreased to 0.3µM after 2 hours followed by 0.03µM after 4 hours; 4.25µM of A83-01 was detected in the plasma of mice 30 minutes after intraperitoneal injection and the plasma was cleared of the compound after 2 hours from the initial injection (Figure 32). The oral route was less efficient but the pharmacokinetics was more favourable over a longer period of time than intraperitoneal administration. However, when the compound present in the plasma was analysed using the HPLC technique,

double peaks were observed for the oral administration which suggested the possibility of a conjugated metabolite that might interfere with the outcome of the experiment.
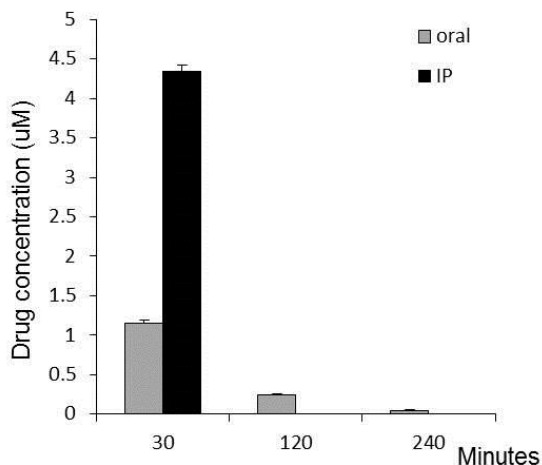
Figure 32: Comparison of A83-01 concentration in plasma of mice between oral and intraperitoneal administration.
The graph shows the concentration of A83-01 detected in the plasma of mice at 30 minutes, 2 hours and 4 hours after oral (grey bar) and IP (intraperitoneal) (black bar) administration. Mice were gavaged with 800ug/200ul/body (equivalent to 9.4mM) of A83-01 and the drug concentration detected in plasma was 1.2uM at 30 minutes; 0.3uM at 2 hours and 0.03uM at 4 hours after administration. For intraperitoneal administration, mice were injected with 150ug/200ul/body (equivalent to 1.7mM) of A83-01 and the drug concentration detected in the plasma was 4.2uM at 30 minutes.

The intraperitoneal route of administration is preferred as this method produced the highest bioavailability and circumvented the problem with enteral absorptive issues. The vehicle for A83-01 was referenced against a published study in which A83-01 was diluted in DMSO: Saline (3:2, v/v) (Minowa, Kawano et al. 2009). Since the pharmacokinetic data showed that A83-01 administered through intraperitoneal injection was cleared from the blood stream within 2 hours, A83-01 had to be administered with a daily dose of 150μg/body.

The efficacy of A83-01 in the treatment of the orthotopic bladder cancer model

Tumour growth was monitored weekly by measuring the bioluminescence intensity of the tumour using the *in vivo* bioluminescent imaging system. BLI reading was high (~ $1e^9$ photons/sec) on the day of instillation (Day 0) as a high number of cells were retained in the bladder; the BLI reading dropped tremendously after a week (Day7) due to the inability of a large number of cells to adhere to the bladder wall and undergo apoptosis or removed during urination. The BLI reading entered the linear phase after Day14 and this signifies successful implantation and tumour growth (Figure 33).
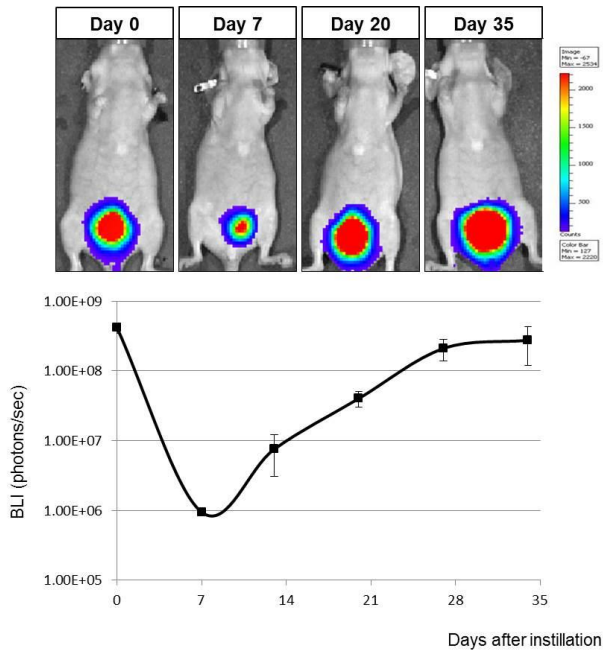
Figure 33: Monitoring *in vivo* tumour growth using bioluminescent imaging. Tumour was monitored weekly by peritoneally injecting mice with luciferin and imaged using bioluminescent imaging system. Top panel: BLI (bioluminescent intensity) image of mice from Day 0 to Day 35; Day 20 image represents the linear phase of the tumour growth (Day 14 to Day 28). Bottom panel: Graph illustrates the trend of the weekly measured BLI reading. A drop in BLI reading was observed at Day 7 in which most of the cells that did not detach were removed through urination; cells which attached gave a BLI reading. Tumour reached the linear phase after Day 14 and grew exponentially and reached a plateau after Day 28.

When tumours reach a bioluminescence intensity (BLI) of $5e^7$ photons/sec (~Day 17 post instillation), mice were paired according to their bioluminescence

117

intensity; and for each pair, for 2 weeks, the control mouse was treated with drug vehicle (DMSO: Saline (3:2, v/v)) while experimental one was treated with A83-01 diluted in DMSO: Saline (3:2, v/v).

Bladder tumours usually shed cells into the urine and therefore, the urine of mice was collected a week after treatment to detect morphological changes in the bladder carcinoma cells due to A83-01. The urine was placed in cell culture medium and observed the following day. The cells from urine of tumour bearing mice treated with A83-01 clustered together, initiating cell-cell contacts while those from mice treated with vehicle (DMSO) conferred similar morphology to the UM-UC-3 cell line (Figure 34A).

After 2 weeks of drug treatment, the tumors were fixed for 10 minutes by delivering 4% PFA via a catheter into the bladder before the bladder was surgically removed. The tumours were paraffin-embedded and the sections were Haematoxylin and Eosin stained and imaged. Carcinoma cells in mice treated with Vehicle were observed to invade through the bladder wall layers (Mucosa, Submucosa, Mucularis and Serosa) leaving behind pieces of untouched serosa (Figure 34B-C); while carcinoma cells of the A83-01 treated mice remained superficial (Figure 34D-G). Taken together, the data indicated that A83-01 induced a change in cell morphology and altered the invasiveness of carcinoma cells. TGFβRI targeted therapy might help to prevent invasion into the bladder wall for patients with high grade T1 tumours and could also be applied to delay progression in invasive bladder cancer patients.
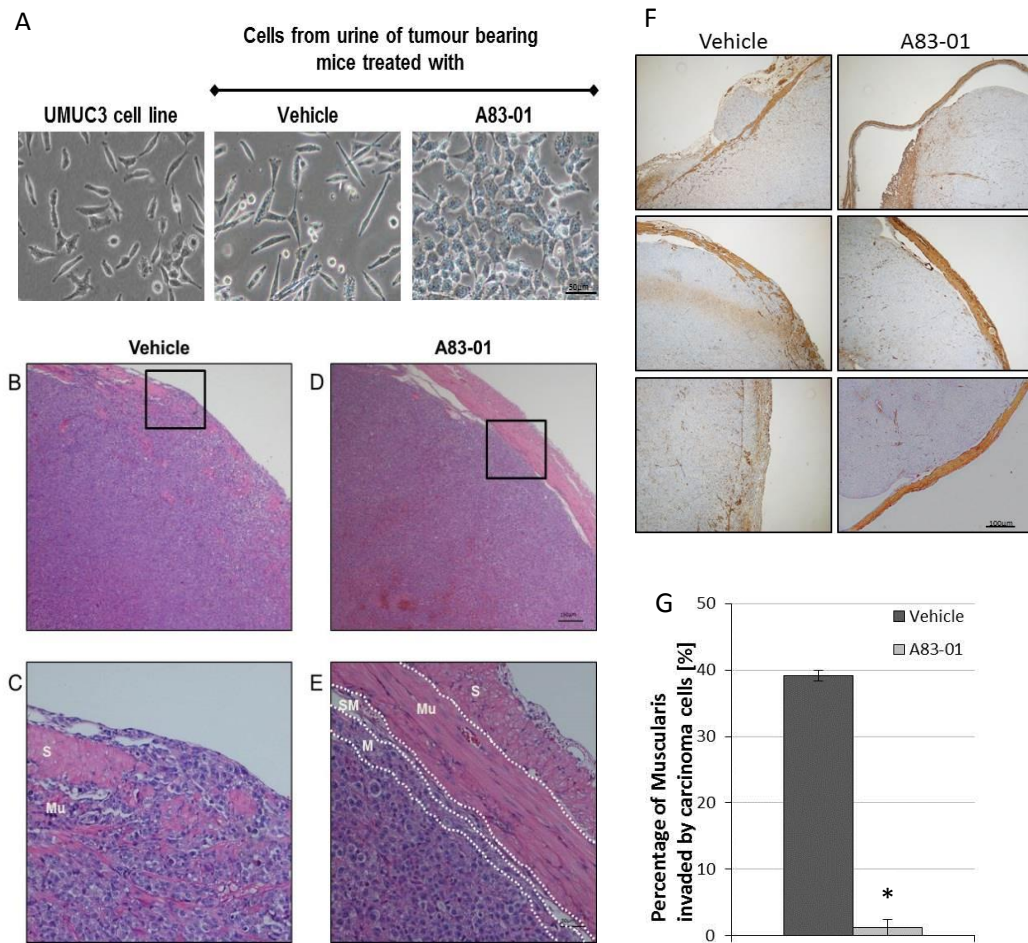
Figure 34: A83-01 affects the morphology of tumour-derived UM-UC-3 carcinoma cells and their ability to invade into the bladder wall.

(A) Urine of mice collected a week after treatment with Vehicle (DMSO: Saline (3:2, v/v)) or A83-01 were cultured in the incubator with culture media without drug for 5 days. Phase contrast images of cells that were shed into the urine of mice were taken and compared against the UM-UC-3 (UMUC3) carcinoma cell line. Cells from urine of tumour bearing mice treated with Vehicle were spindle-like, similar to the mesenchymal morphology of the parental UM-UC-3 carcinoma cell line; while those treated with A83-01 displayed different morphology which was observed to initiate cell-cell contacts. (B-E) Haematoxylin and Eosin staining of orthotopically established UM-UC-3 bladder tumours. (B) Mice treated with Vehicle displayed tumours with invasive phenotype in which UM-UC-3 carcinoma cells invaded the bladder wall. (C) Magnified insert of B showed that UM-UC-3 carcinoma cells invaded through the Mu (muscularis: muscle layer) and parts of the S (serosa); while (D) A83-01 treated UM-UC-3 carcinoma cells did not invade through the bladder wall. (E) Magnified insert of D showed that A83-01 treatment affected the invasiveness of UMUC3 carcinoma cells as cells were retained within the M (mucosa) and did not invade through the SM (submucosa), muscularis and the serosa. (F) Muscularis of bladders were histochemically labelled with anti-alpha smooth muscle actin (αSMA) and (G) the percentage of Muscularis invaded by UM-UC-3 was calculated using Image J analyses. Bars represent mean $\pm$ SEM. *=p-value <0.05.

119

Discussion

The EMT inhibition assay was adapted for high throughput screening of targeted compounds and a robotic liquid handler was programmed to consistently deposit cells onto a spot to form a cell colony/well reproducibly in multi-well plates. To the best of our knowledge, this method of generating cell colonies via confined spotting technique has not been previously attempted. Furthermore, this method requires much shorter time as compared to the common alternative method which require at least 3 days for sparsely attached cells to grow and form cell colonies. Another key advantage of this EMT screen is taking the entire well instead of representative microscopic views for analysis which greatly decreases sampling biasness. The two parameters (Cell Count Ratio and Cell Dispersion Ratio) measured colony compactness in numbers and this increases the confidence in hit identification.

Through the EMT drug screen, we discovered druggable targets TGFβRI, MEK, SRC and PI3K that might play significant role in EMT modulation and cancer progression. These four targets identified are crucial but does not represent all targets that are implicated in the EMT process. The library of compounds assembled for the screen comprised of a small subset of compounds that were developed by universities and the pharmaceutical industry and hence not a representative of all compounds identified to date. Efforts could be made to extend the EMT screen to include other diverse compound libraries for example

targeted compounds of metabolic diseases to allow the discovery of other potent EMT inhibitors.

We have shown that compounds targeting TGFβRI, Mek, PI3K and Src are inhibitory to EMT-inducing growth factors: EGF, HGF and IGF-1 in cell dispersion, cell migration and modulating EMT markers. However, the efficacy of these targeted compounds in inhibiting other EMT-inducing growth factors like PDGF and VEGF was not determined. These targeted compounds were not screened against VEGF-A and VEGF-B which were reported to induce EMT in bladder cancer cells as NBT-II cells did not produce a significant cell dispersion response (Appendix 7). Moreover, the effect of PDGF and VEGF are more pronounced *in vivo* than *in vitro* models due to the presence of endothelial cells.

We have identified the TGFβRI EMT signature in a c-Met driven system. This TGFβRI EMT signature comprise of genes that regulate focal adhesion and actin cytoskeleton reorganization. This signature provided evidence of the need for cooperation between TGF-β and HGF pathway in driving motility and invasion. The EMT signature identified here addressed the cell-substrate mechanism but lacked the cell-cell adhesion portion. It might be suggested that the cell-cell adhesion mechanism was impacted by the reorganization of actin cytoskeleton. Continuous effort has to be made to address this issue.

We have successfully used the orthotopic bladder cancer model to validate the efficacy of the TGFβRI inhibitor in limiting bladder wall invasion. This model provides a good model to study the first steps of bladder wall invasion as cells are

implanted superficially onto the wall lining. To the best of our knowledge, we showed it for the first time in bladder cancer that a receptor kinase inhibitor was able to delay the invasion of bladder carcinoma cells into the bladder wall. This observation further affirms the results from the screen and bridges the gap between *in vitro* cell-based experiments and preclinical models. The studies pave the road for using EMT inhibitors to treat invasive bladder cancers.

Chapter 4: Discussion

Metastasis

Epithelia neoplasia is initiated by genetic alterations leading to the inactivation of tumour suppressor genes and activating mutations of proto-oncogenes. Epigenetic changes are also critical in the transformation process by altering the expression level of key regulatory proteins including tumour suppressors. The transformed epithelial cells undergo considerable morphological changes, including partial loss of apico-basal polarity, actin microfilament and microtubule organization and exhibit uncontrolled proliferation leading first to a benign tumour mass before engaging into a malignant state. Angiogenesis is then initiated to support the metabolic needs of a malignant tumour mass once exceeding a few mm3. Subsequently, carcinoma cells still surrounded by a basement membrane designated as carcinoma in situ acquire additional genetic alterations and epigenetic modifications which can promote fragmentation and dissolution of the basement membrane allowing some carcinoma cells to invade into the surrounding stroma and intravasate into the blood or lymphatic vessels. Distant dissemination of carcinoma cells is an early event in tumour progression contrary to the accepted dogma that metastasis occur at a late stage of the disease. Circulating carcinoma cells that are able to escape cell death in the blood/lymph stream can potentially lodge in the parenchyma of distant organ to form micro metastases. Micrometastases are undetectable even using the most advanced

imaging techniques such as Magnetic resonance imaging (MRI) and Positron Emission Tomography (PET) scan. The disseminated carcinoma cells remain in a dormancy-like state due to a balanced rate of proliferation and apoptosis or acquire a senescent status. Carcinoma cells eventually can resume growth by unknown mechanisms thus generating clinically detectable macrometastases. The dissemination of carcinoma cells originating from the primary tumour to other parts of the body is life-threatening since most therapeutics regimens fail to prevent this process. The very low proliferative carcinoma cells in micro metastases are likely to be insensitive to chemo and targeted therapeutic agents and escape immune surveillance.

Metastasis was hypothesized to occur through the "seed and soil" theory introduced by Stephen Paget in 1889; in which the "seed" refers to the malignant cells that escape the primary tumour site and the "soil" refers to the microenvironment in which the carcinoma reside in the distant organs. Carcinoma cells in metastases differ from those in the primary tumour in their transcriptomic and genetic alteration profiles and this may be accounted by the possibility that metastatic carcinoma originate from carcinoma cells in the primary tumour at different times during tumour expansion and progress independently from those in the primary tumour. This genetic divergence is further accentuated by strong evidence for clonal heterogeneity in the primary tumours. These recent findings are in agreement with the original hypothesis formulated by Nowell for clonal selection during progression (Nowell 1976).

Metastasis process is not governed solely by genetic alterations; recent data have suggested additional layers of epigenetic control over cells that metastasize (Augoff, McCue et al. 2012); (Baylin and Ohm 2006). Epigenetic reprogramming is dynamic and reversible; mostly the abrogation expression of tumour suppressors. These epigenetic programs include the methylation of cytosines in CpG islands that can affect directly gene transcription; or in cooperation with histone posttranslational modifications can either activate or repress gene expression by modifying locally chromatin structure. In addition, more than 1500 micro RNA are critically involved in regulating levels of transcripts and proteins. Other non-coding RNAs are also recognized to modify the transcriptome.

Grading of carcinoma is established according to their proliferative rate, extent of anisokaryosis and to the degree of dedifferentiation. Grading is still mandatory today and the best indicator of prognosis with staging. Carcinomas that cannot form glandular-like structure but rather acquire a fibroblastic-like morphology are always of worse prognosis. This observation in addition to the fact that the initiation of cell migration is very often associated with an epithelial mesenchymal transition (EMT) during embryogenesis, has led to the hypothesis that carcinoma cells in the primary tumour may have co-opted such a mechanism to disseminate.

Carcinoma cells potentially can switch their phenotype from epithelial to mesenchymal or at least acquire an intermediate possibly metastable epithelial mesenchymal status before engaging into metastasis. The disseminated carcinoma cells can re-epithelialize in the distant sites or maintain a meta-stable state in

small metastases allowing carcinoma to disseminate from these secondary sites. EMT is a transient phenomenon and has been difficult until recently to capture in tumour biopsies. Such cells have now been documented in a large number of carcinoma of different origins. Among other evidence solitary colon carcinoma cells expressing nuclear β-catenin were identified at the invasive front within the stroma (Brabletz, Jung et al. 2001). The distribution of a large set of epithelial and mesenchymal markers has been established in more than 600 breast carcinoma samples revealing the presence of a significant number of carcinoma cells expressing mesenchymal markers. Circulating tumour cells in breast carcinoma patients were found to express a spectrum of EMT phenotypes (Powell, Talasaz et al. 2012). In the present study, EMT was found to have a role in the deregulated activation of invasive growth and metastasis of bladder carcinoma model cell lines.

Epigenetic reprogramming contributing to invasive growth is dependent on the environmental cues such as growth factors, oxygen content, nutrient availability and microenvironment composition. Although several cytokines and growth factors can promote cell proliferation, migration and protection from apoptosis, HGF optimally orchestrates the spatial and chronological events in this process. Moreover, HGF/c-Met signalling plays crucial roles in cancer progression, particularly in influencing tumour invasiveness and metastatic potential and down-regulation of c-Met decreased the tumourigenicity of cancer cells. It is challenging to pinpoint the period at which epigenetic reprogramming takes place *in vivo*, hence we attempted to uncover this process using an *in vitro* model of

EMT induced by HGF to analyse the transcriptome of cells undergoing phenotype switch. We identified a number of genes and pathways that are altered in the early steps (2 hour post-HGF treatment) in the EMT process. This early neoplastic process was observed with changes in expression of genes related to functional classes, such as interactors (Actg1, PVRL4, TGFβR2) of adherens junction proteins and interactors (MAGI3, Cldn4, Actn1, Tjp2) of tight junction proteins. ErbB, MAPK and TGFβ pathways identified here are often dysregulated in cancers. Similar to other reports, c-Met signalling activates ErbB signalling and also downstream MAPK signalling. However, it is intriguing to find that TGF-β signalling is activated at an early stage of the process. Although TGF-β is a potent inhibitor of cell proliferation, it is believed that in tumour cells, TGF-β pathway loses its anti-proliferative response and acquires a pro-oncogenic role. In this analysis, in the presence of HGF, TGF-β pathway assumes an oncogenic role as inhibition with TGFβR inhibitor abrogated cell dissociation. This finding correlates with other reports which show that TGFβ family ligands correlate with more aggressive phenotype of bladder cancer cell lines and deregulated TGFβ signalling led to enhanced migration and invasiveness of bladder cancer cells (Hung, Wang et al. 2008).

The metastable state was represented by pathways important for tumour sustenance and invasiveness. Alteration of p53 pathway and Phosphatidylinositol 4,5-biphosphate (PIP) pathway directly affects p53 and phosphatase and tensin homolog (PTEN) expression and stability. Mutation or alteration of p53 and PTEN expression were often found in tumours of advanced bladder cancer stages.

Mutations in p53 gene are associated with invasive phenotype and bad prognosis in bladder cancer. Genes that regulate focal adhesions Laminin, alpha 3 (Lama3), Lamc2, guanine nucleotide exchange factor Vav1 and Vav2 were deregulated. Lamc2 is highly expressed in advanced stages of bladder cancer. Although Vav1 and Vav2 proteins were not reported in TCC tumours, Vav1 was reported to be ectopically expressed in pancreatic adenocarcinomas, neuroblastoma and melanoma while Vav2 was observed to be a critical regulator of growth-factor stimulated motility in human cancers. The Jak-Stat pathway was also detected in this study and this pathway is linked to acute inflammation. The connection of inflammation to cancer progression and invasiveness is well established. VEGF pathway was up-regulated in this study and the VEGF pathway is highly responsible for angiogenesis in cancer, an important process in bladder cancer progression. Patients with T2/3 stages of bladder cancer usually have angiogenic tumours displaying blood lakes in tumours and blood in urine (Elfiky and Rosenberg 2009); (Shariat, Youssef et al. 2010).

TGF-β signalling is one of the modules which was then explored using phosproteomic analysis. A transient activation of TGF-β signalling via phosphorylation of Smad2 C-terminus serine residues was found to occur at an early stage following c-Met activation. The inhibition of this phosphorylation attenuated the migration and invasive potential of carcinoma cells. This is also seen in breast cancer cells in which a transient activation of TGF-β signalling is required to switch to an invasive phenotype. The activation of TGF-β signalling in this HGF-induced system is not clearly understood. The central dogma suggests

128

that TGF-β but not HGF induce the phosphorylation of Smad2 C-terminus while some reports showed C-terminal phosphorylation of Smad2 in response to HGF in a TGFβ-independent fashion. We have shown that the HGF-induced phosphorylation of Smad2 C-terminus is TGFβRI-dependent since TGFβRI inhibition leads to a decrease in Smad2 C-terminus phosphorylation. We have also demonstrated that activation of TGF-β signalling is mandatory for cells to disperse and migrate under the influence of two other growth factors EGF and IGF-I. Under the influence of these growth factors, TGF-β signalling promotes aggressiveness of carcinoma contrary to its suppressive role in normal cells. TGF-β signalling acts as a converging point for the three growth factors tested and should be taken into consideration when treating cancers with over-expression or constitutively active RTK.

In addition to Smad2 C-terminus phosphorylation, we have also investigated phosphorylation of the linker region and its impact on the phosphorylation of the C-terminus. ERK was found to phosphorylate Smad2 at the linker region in agreement with the observation with previous studies in which the linker region of Smad2 is phosphorylated at several serine/threonine residues through growth factor mediated MEK-ERK axis activation. Inhibition of MEK resulted in decreased cell migration, invasion and colony forming ability (Figure 34). The Smad2 linker region phosphorylated by ERK is suggested to be important for invasiveness as some reported the nuclear localization of Smad2 with phosphorylated linker regions in invasive late stage colorectal carcinoma (Matsuzaki, Kitano et al. 2009). However others have reported that

phosphorylation of Smad2 at both linker and C-terminus enhanced cell growth by up-regulation of c-Myc. It is unclear whether Smad2 linker or C-terminus region is fully responsible for the progression of bladder carcinoma as inhibition of phosphorylation of either one region results in smaller tumour size. However, we do observe that carcinoma cells with non-phosphorylating Smad2 linker (Smad2 dnL) were less tumorigenic compared to carcinoma cells with non-phosphorylating Smad2 C-terminus (Smad2 dnC). Inhibition of both regions' phosphorylations using a combination of compounds (A83-01 and PD0325901) greatly reduced the colony forming ability of carcinoma cells (Figure 34). In addition, inhibition of Smad2 linker phosphorylation led to an increase in Smad2 C-terminus phosphorylation and inhibition of Smad2 C-terminus phosphorylation led to an increase in phosphorylation of ERK and Smad2 linker region. The phosphorylations of the two regions of Smad2 are cross-regulated; such type of regulation is required for the progression in regulating cell growth and invasiveness.
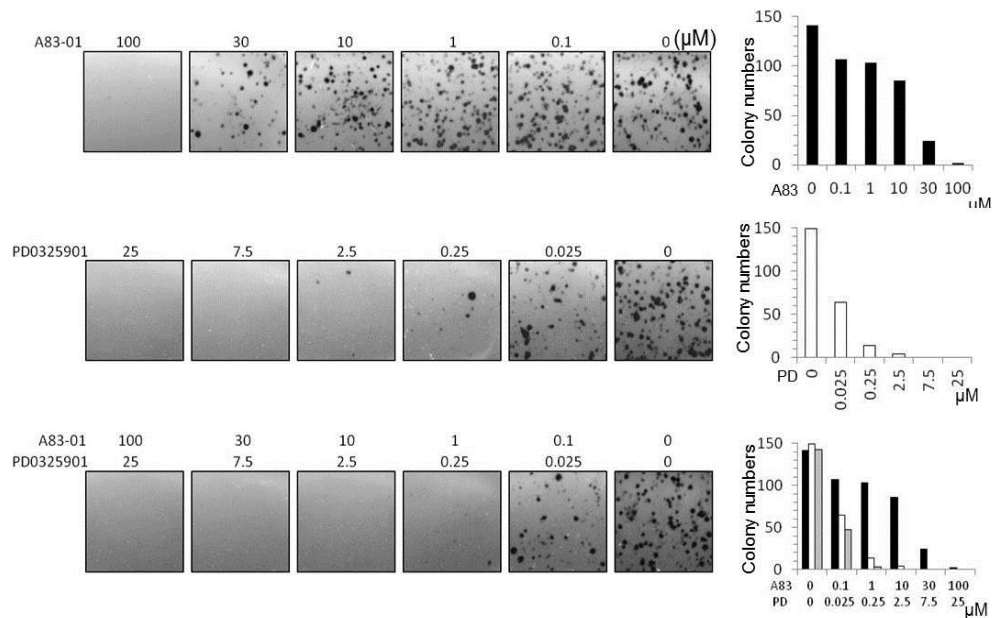
Figure 35: PD0325901 reduces colony forming ability.
Equal numbers of UM-UC-3 cells (5×10^4) were seeded into 24-wells pasltic dishes and treated with or without A83-01 (TGFβRI inhibitor) or PD0325901 (MEK inhibitor) at the indicated concentrations over a period of 14 days. Colonies were visualized by crystal violet staining. Top graph: Quantification of colony numbers in A83-01 treated UM-UC-3 carcinoma cells. Middle graph: Quantification of colony numbers in PD0325901 treated UM-UC3 carcinoma cells. Bottom graph: Quantification of colony numbers in A83-01 and PD0325901 treated UM-UC3 carcinoma cells. Quantification of colony number, representative of three independent experiments.

Knowledge in invasive growth and tumour progression led to the development of new compounds for targeted therapeutics. Most of the compounds were initially identified and optimized using proliferation inhibition assays. The ten major hallmarks of cancer were reviewed recently and constitute a logical framework to target cancer progression (Hanahan and Weinberg 2011). The 10 hallmarks of cancer include sustaining proliferative signalling, evading growth suppressors, resisting cell death, enabling replicative immortality, inducing angiogenesis, activating invasion and metastasis, genome instability and mutation, tumour promoting inflammation, avoiding immune destruction and deregulating cellular

131

energetics. Compounds that interfere with each of these hallmarks have been developed. There are a number of approved drugs targeting the capability to sustain proliferative signals via inhibition of the family of EGF receptors such as gefitinib (Iressa) or erlotinib (Tarceva), two EGFR kinase inhibitors used to treat lung cancers with mutated EGFR; and trastuzumab (Herceptin), an antibody against ErbB2 gene used to treat breast cancers. Some attempts have been made to target angiogenesis induction, mainly to destroy the vascularization in tumours. Several classes of angiogenic modulators such as anti-VEGF antibody (Avastin), a triple angiokinase inhibitor (BIBF-1120), MMP inhibitor (Neovastat), anti-endothelium drugs (combretastatins) were tested in clinical trials. Multiple approaches have been attempted to interfere with invasion and metastasis by designing drugs that target the ATP pocket of c-Met and developing neutralizing anti-HGF antibodies. Small molecular weight compounds such as PF04217903 and PF02341066 have reached phase1 clinical trial while JNJ38877605 reached phase2 clinical trial targeting advanced refractory tumours. Numerous clinical trials based on single tyrosine kinase inhibitors (TKI) have been conducted over the last decade demonstrating a significant albeit transient response to treatment. However, in the large majority of these patients resistance against the TKI therapy is eventually observed. This gain in resistance is partly due to the acquisition of novel mutations in the intended target or mutations in proteins downstream to the initial chosen target or activation of different pathways that empower carcinoma cells with the ability to survive. Lung carcinoma patients who initially responded to EGFR TKI treatment acquired resistance and cancer relapsed. Studies have

shown that the acquired resistance was a result of a secondary mutation in EGFR, T790M (Pao, Miller et al. 2005). In addition, attempts to investigate the cause of treatment failure revealed that the inhibition of any one of the receptors result in up-regulation of the other pathways. For example, EGFR TKI gefitinib resistant cells display IGF-1R hyper phosphorylation with constitutive association of (Insulin receptor substrate 1 (IRS-1) and PI3K that counteracts the ability of gefitinib in inhibiting cancerous cell growth (Guix, Faber et al. 2008). Baselga has also demonstrated that treatment with mammalian target of rapamycin (mTor) inhibitors result in up-regulation of IRS (O'Reilly, Rojo et al. 2006). Moreover, a given hallmark of cancer is governed by several partially redundant pathways, inhibition of one key element or pathway might not eliminate a hallmark capability completely. Selective co-targeting of multiple biochemical pathways or a common node might result in a more effective therapy.

We extended the concept of cancer hallmarks by adding EMT to the circuitry. Biochemical pathways that govern each cancer hallmark converge at some point and are implicated in the EMT process. We screened small molecular weight compounds initially designed to interfere with proliferation in an attempt to identify those that can inhibit EMT. Our laboratory in collaboration with Jean Pierre Abastado has thus demonstrated that the EMT inhibitors identified by our laboratory not only inhibit growth factor induced migration but also interfere with the actions of tumour promoting polymorphonuclear myeloid-derived suppressor cells (PMN-MDSCs) (Toh, Wang et al. 2011). Using this global approach, we target multiple hallmarks in parallel, combating proliferation, inflammation and

invasion and metastasis. With the right combination of drugs, new treatment modalities can be designed to target both the tumour and the microenvironment which may improve the efficacy of the current cancer therapeutics.

Therapeutic implications

Much effort has been made in the past decade to target the proliferative capability of carcinoma cells but all the therapeutic tools to date have limited efficacy and some therapeutic regimens may trigger additional processes which select for more aggressive and therapy-resistant cells. These carcinoma cells adapt and reduce their dependence on a particular hallmark and heighten the activity of other hallmarks leading to invasiveness and metastasis. This invasive and metastatic behaviour can be explained by cells seeking less hostile and new niches to renew tumour growth and also gain access to nearby pre-existing tissue vasculature. Mechanisms that govern invasion and metastasis are utmost important in elucidating the mechanisms of cancer pathogenesis. Our laboratory analysed the transcriptome of HGF-induced cells over time and uncovered the sequence of gene/pathway activation and the cascade of signalling events downstream to HGF/c-Met signalling. This study focussed only on a subset of the signal transduction pathways from one activated receptor and hence more exhaustive studies using this approach should be carried out to unravel the mechanisms and identify the signalling node responsible for invasive growth and metastasis. These

studies should provide valuable indicators for the development of new targeted therapies.

Inhibiting EMT: a strategy to target invasive growth and metastasis

Can invasive growth and metastasis be targeted? A concept emerged based on research in invasive growth and metastasis over the past decade implicating EMT as a process by which transformed epithelial cells can acquire attributes for invasion and metastasis. EMT is a multifaceted program and many biochemical pathways that affect other cancer hallmarks participate in the EMT process. It is difficult, however not impossible, to identify targetable EMT drivers. Advancing towards personalized medicine, administration of drugs will depend on the profile of the patient and the biopsies in which different tumours will display distinct deregulated pathways and certain enhanced hallmarks. A single agent can no longer be effective in the treatment of cancer due to the mechanisms activated by the carcinoma cells to survive. Combinatorial drug therapy may be a better option to target two or more hallmarks especially when EMT inhibitors are used. The notion of screening existing or newly developed compounds for their EMT inhibiting effects will aid in the establishment of a set of EMT inhibitors that may prove useful in executing combinatorial drug therapy.

Most logical targets for invasion and metastasis are c-Met and TGFβR, however not many advances have been made to target c-Met and TGFβR in the clinic. Strategies to inhibit TGF-β signalling include TGF-β antisense approaches that

showed reactivation of tumour-specific immune responses and patients become more susceptible to different therapeutic regimens (Iyer, Wang et al. 2005). TGFβ2 antisense oligonucleotide entered phase II/III trials to treat high grade gliomas and phaseI/II trials to treat pancreatic cancer. Monoclonal antibodies against TGFβ2 and TGFβ1 successfully completed phaseI/II trials. However, the success of targeting TGF-β signalling has been limited due to toxicity of drugs or to vast pleiotropic effects leading to physiological imbalances. The aim of the TGF-β targeted therapy must be directed against the double-edge sword of TGF-β to enable inhibition of the pro-oncogenic features and the proper restoration of anti-oncogeneic effects. Understanding the cross talk between TGF-β and RTK signalling is important for the development of proper anti-cancer concepts targeting TGF-β.

Options to inhibit HGF/c-Met signalling are kinase inhibitors designed to block the ATP pockets of c-Met and neutralizing antibodies designed to block ligand-mediated c-Met signalling. In some circumstances, c-Met can be activated in a ligand-independent manner and is required for tumour cell signalling and survival; and this was demonstrated by a report using RNA interference against c-Met (Shinomiya, Gao et al. 2004). Two laboratories have shown promising data in which one of the laboratory engineered a soluble form of c-Met and inhibited ligand-independent activation of c-Met (Coxon, Rex et al. 2009) while the other laboratory induced shedding of c-Met via a monoclonal antibody (DN30) that target the extracellular portion of c-Met, creating a decoy c-Met to prevent c-Met activation (Pacchiana, Chiriaco et al. 2010). Decoy c-Met impaired tumour cell

expansion and angiogenesis, inhibiting tumour growth and metastasis in mice. However, the duration of the experiment was not extended to document tumour relapse. Moreover, inhibition of a single receptor might lead to the up-regulation of other pathways; and TGFβRI was shown by our laboratory to be a converging point of growth factor signalling, a combination of c-Met antibody and a TGFβRI inhibitor might work more effectively to prevent cancer spread or relapse.

Another possible drug combination is MEK and TGFβR inhibitors. Cancers, especially bladder carcinoma, are found with frequent Ras mutations, rendering RTK inhibitors ineffective. A large body of literature suggests oncogenic RAS signalling plays an important role in switching TGF-β signalling from tumour suppressive to pro-oncogenic (Lehmann, Janda et al. 2000). Ras-MAPK signalling interferes with TGF-β signalling at the level of Smad2/3 activation and influences the composition of Smad-dependent transcription factor complexes, resulting in the transcription of a different set of genes. Ras and Smad-dependent transcription factors can also interact and cooperatively regulate transcription of target genes. Carcinoma cells in this case retain a functional TGF-β/Smad signalling; however the tumour suppressive functions were inhibited while malignancy increased. The mechanism of the synergy between oncogenic Ras and TGF-β signalling is just beginning to be resolved. In MDCK cells, Raf-mediated autocrine loop of TGF-β is required for the sustained activation of Raf-MAPK induced EMT and cell invasion. In human hepatocellular cells, hyper activation of MEK-ERK signalling inhibit the up-regulation of the NADPH oxidase, NOX4, a protein essential for mitochondrial-dependent apoptosis, allowing cells to escape

from TGF-β induced apoptosis (Caja, Sancho et al. 2009). The cooperation of oncogenic Ras and TGF-β signalling induced the secretion of PDGF and up-regulation of PDGF receptors upon EMT, activating PI3K and promoting β-catenin accumulation in the nucleus (Fischer, Fuchs et al. 2007). In pancreatic adenocarcinoma, oncogenic K-Ras-ERK signalling promoted TGF-β induced transcriptional down-regulation of Phosphatase and tensin homolog (PTEN) which causes an increase in cell proliferation and tumour expansion in pancreatic cancer (Chow, Quach et al. 2007). Animal studies demonstrated that TGF-β induced EMT is not sufficient for the acquisition of invasive features and requires activated Ras (H-RASV12) to alter the TGF-β response and confers metastatic potential (Zavadil 2009). Moreover, our data shows that inhibition of MEK results in K-Ras positive tumour shrinkage and tumour profile shows an increase in Smad2 C-terminus phosphorylation, potentially up-regulating the canonical TGF-β /Smad core signalling. However, our *in vitro* data shows that the effect of MEK inhibitors are compensated in the presence of growth factors, hence targeting MEK itself is not an effective option as the effect of the drug will be compensated by the growth factors present in the serum of cancer patients; and result in an inevitable relapse. Co-targeting of MEK and TGFβRI disrupts the oncogenic Ras-TGF-β signalling axis and aid in combating the compensating factors to improve prognosis.

Chemotherapeutics and EMT inhibition

Chemotherapy has been reported to induce EMT by several mechanisms in carcinoma cells. EMT has been recognized as a critical step in the process of metastasis leading to cancer spreading and treatment failure due to acquired resistance. Cisplatin-resistant human tongue carcinoma cell lines display mesenchymal features with enhanced invasiveness and motility attributed by down-regulation of EMT gene repressor miRNAs miR-200b and miR-15b. Ectopic expression of miR-200b and miR-15b with miRNA mimics effectively reversed the phenotype of EMT (Sun, Yao et al. 2012). Cisplatin-resistant ovarian carcinoma cells were found to overexpress EMT-related transcription factors, Snail 1, Snail 2, Zeb2 and Twist2, and reduction in expression of Snail 1 and Snail 2 resensitized the cells to cisplatin (Haslehurst, Koti et al. 2012). Chemotherapeutic drug, oxaliplatin, induced EMT through Fas signalling, resulting in a decrease in epithelial markers and an increase in mesenchymal markers accompanied by an increase in motility (Zheng, Cai et al. 2013). Chemotherapeutic agents such as cyclophosphamide and epirubicin in combination with 5-fluorouracil used for breast cancer treatment induced EMT by activating EGFR through elevated expression of amphiregulin, thereby inducing expression of Twist 1 and activation of NF-kB (Li, Chen et al. 2011).

In bladder cancer, coupling chemotherapeutics with EMT inhibition and anti-angiogenesis therapy might be a plausible solution. Muscle invasive bladder cancers are characterized by haematuria and the presence of blood lakes within the tumours, treatment regimens that interfere with angiogenesis should be

considered a feasible therapeutic strategy. Sequential treatment of mesenchymal human bladder carcinoma cells with vandetanib targeting VEGFR and EGFR displayed improved cisplatin sensitivity (Li, Yang et al. 2010). BIBF-1120, a triple angiokinase inhibitor, has been shown to inhibit tumour growth in lung and pancreatic preclinical models (Kutluk Cenik, Ostapoff et al. 2013). Post BIBF-1120 treatment of tumour tissues showed increased active caspase 3 with improved sensitivity to chemotherapy. However, it should be noted that tumour progression is dynamic and carcinoma cells have a tendency to reduce dependency for a certain hallmark and gain others; hence patients undergoing treatment have to be monitored closely to detect any switch in events to enable the implementation of other regimen.

Conclusion

In this study, we utilised an *in vitro* HGF-induced EMT in a bladder carcinoma model cell line to delineate the signalling pathways that drive invasiveness. Through a small molecular weight compound screen, we identified inhibitors of EGF, HGF and IGF-1-induced EMT. Using an orthotopic bladder cancer model, we showed that A83-01 (a TGFβRI inhibitor identified through the screen) delayed the invasion of human bladder carcinoma cells (UM-UC-3) into the bladder wall. Our gene expression profiling showed that HGF/c-Met signalling triggered other signalling pathways for EMT and tumour progression. HGF/c-Met signalling activates the MEK/ERK axis which in turn phosphorylates the Smad2 linker region, thereby regulating the expression of Snail1 and Zeb1. HGF/c-Met signalling results in the activation of TGFβRI (by an unknown mechanism) which in turn phosphorylates the Smad2 C-terminus region, thereby regulating the expression of Twist. In addition, we have shown that phosphorylated Smad2 linker region is important for tumorigenicity while phosphorylated Smad2 C-terminus region is important for invasive growth.
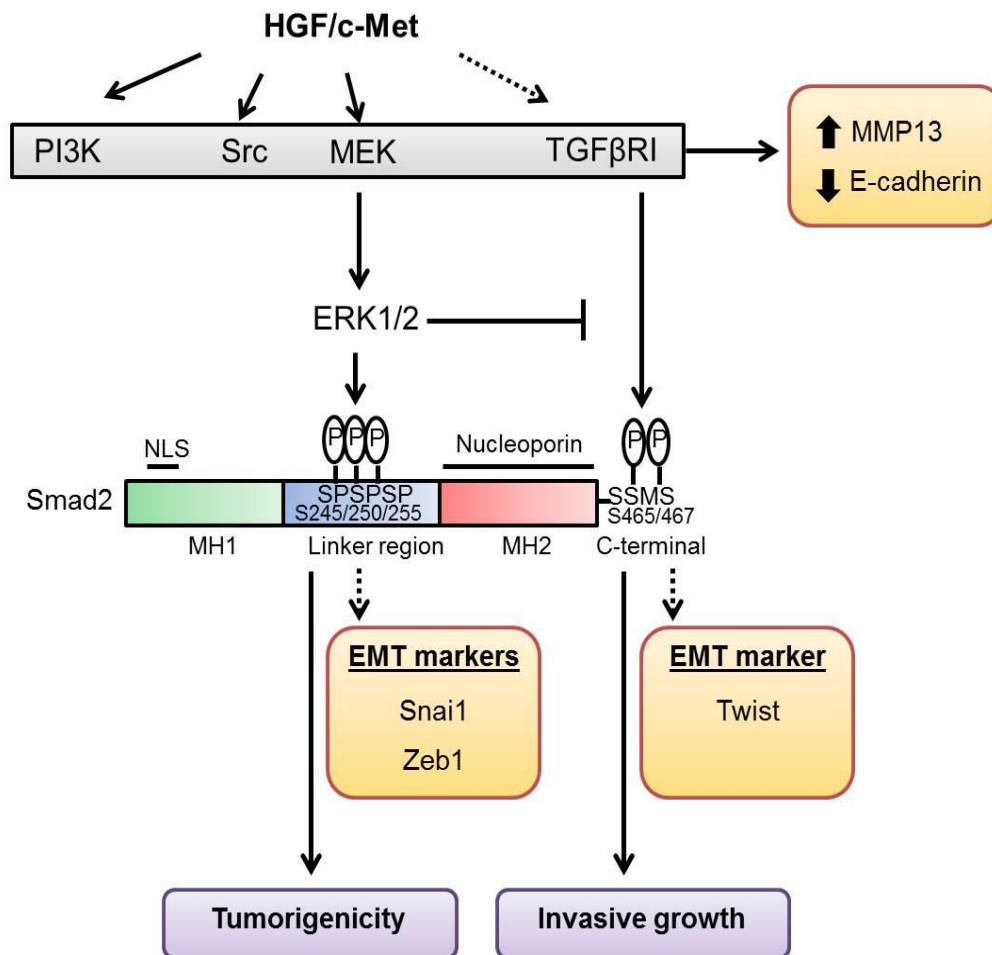
Figure 36: A proposed model for HGF/c-Met induced EMT and tumour progression.
Compounds targeting PI3K, Src, MEK and TGFβRI were identified in the small molecular weight screen. These compounds inhibited HGF-induced up-regulation of MMP13 and down-regulation of E-cadherin. HGF/c-Met signalling activates the MEK/ERK axis resulting in the phosphorylation of Smad2 linker region, thereby regulating the expression of Snai1 and Zeb1. HGF/c-Met signalling also activates the TGFβRI/Smad2 axis, resulting in the phosphorylation of the Smad2 C-terminus region, thereby regulating the expression of Twist. HGF/c-Met/MEK/ERK/Smad2 linker region axis might play a role in tumorigenicity; TGFβRI/Smad2 C-terminus axis might be important for invasive growth.

Bibliography

Abbas, T. and A. Dutta (2009). "p21 in cancer: intricate networks and multiple activities." Nature Reviews Cancer 9(6): 400-414.

Andrae, J., R. Gallini, et al. (2008). "Role of platelet-derived growth factors in physiology and medicine." Genes & Development 22(10): 1276-1312.

Augoff, K., B. McCue, et al. (2012). "miR-31 and its host gene lncRNA LOC554202 are regulated by promoter hypermethylation in triple-negative breast cancer." Molecular Cancer 11(5): 1-12.

Ballman, K. V., D. E. Grill, et al. (2004). "Faster cyclic loess: normalizing RNA arrays via linear models." Bioinformatics 20(16): 2778-2786.

Baylin, S. B. and J. E. Ohm (2006). "Epigenetic gene silencing in cancer - a mechanism for early oncogenic pathway addiction?" Nature Reviews Cancer 6(2): 107-116.

Bellusci, S., G. Moens, et al. (1994). "Creation of an hepatocyte growth factor/scatter factor autocrine loop in carcinoma cells induces invasive properties associated with increased tumorigenicity." Oncogene 9(4): 1091-1099.

Benjamini, Y. and Y. Hochberg (1995). "Controlling the false discovery rate: a practical and powerful approach to multiple testing." Journal of the Royal Statistical Society. Series B (Methodological) 57(1): 289-300.

Bernardini, S., S. Fauconnet, et al. (2001). "Serum levels of vascular endothelial growth factor as a prognostic factor in bladder cancer." The Journal of Urology 166(4): 1275-1279.

Boffetta, P. (2008). "Tobacco smoking and risk of bladder cancer." Scandinavian Journal of Urology and Nephrology. Supplementum(218): 45-54.

Brabletz, T., A. Jung, et al. (2001). "Variable beta-catenin expression in colorectal cancers indicates tumor progression driven by the tumor environment." Proceedings of the National Academy of Sciences U S A 98(18): 10356-10361.

Caja, L., P. Sancho, et al. (2009). "Overactivation of the MEK/ERK pathway in liver tumor cells confers resistance to TGF-{beta}-induced cell death through impairing up-regulation of the NADPH oxidase NOX4." Cancer Research 69(19): 7595-7602.

Cappellen, D., C. De Oliveira, et al. (1999). "Frequent activating mutations of FGFR3 in human bladder and cervix carcinomas." Nature Genetics 23(1): 18-20.

Chang, A., T. G. Hammond, et al. (1994). "Permeability properties of the mammalian bladder apical membrane." <u>American Journal of Physiology</u> 267(5 Pt 1): C1483-1492.

Chavez, M. G., C. A. Buhr, et al. (2012). "Differential downregulation of e-cadherin and desmoglein by epidermal growth factor." <u>Dermatology Research and Practice</u> 2012(1): 309587.

Cheng, P., C. A. Corzo, et al. (2008). "Inhibition of dendritic cell differentiation and accumulation of myeloid-derived suppressor cells in cancer is regulated by S100A9 protein." <u>The Journal of Experimental Medicine</u> 205(10): 2235-2249.

Chow, J. Y., K. T. Quach, et al. (2007). "RAS/ERK modulates TGFbeta-regulated PTEN expression in human pancreatic adenocarcinoma cells." <u>Carcinogenesis</u> 28(11): 2321-2327.

Chua, K. N., K. L. Poon, et al. (2011). "Target cell movement in tumor and cardiovascular diseases based on the epithelial-mesenchymal transition concept." <u>Advanced Drug Delivery Reviews</u> 63(8): 558-567.

Cittelly, D. M., I. Dimitrova, et al. (2012). "Restoration of miR-200c to ovarian cancer reduces tumor burden and increases sensitivity to paclitaxel." <u>Molecular Cancer Therapeutics</u> 11(12): 2556-2565.

Cochrane, D. R., E. N. Howe, et al. (2010). "Loss of miR-200c: A Marker of Aggressiveness and Chemoresistance in Female Reproductive Cancers." <u>Journal of Oncology</u> 2010(1): 821717.

Coxon, A., K. Rex, et al. (2009). "Soluble c-Met receptors inhibit phosphorylation of c-Met and growth of hepatocyte growth factor: c-Met-dependent tumors in animal models." <u>Molecular Cancer Therapeutics</u> 8(5): 1119-1125.

Crawford, J. M. (2008). "The origins of bladder cancer." <u>Laboratory Investigation</u> 88(7): 686-693.

Degryse, B., J. G. Neels, et al. (2004). "The low density lipoprotein receptor-related protein is a motogenic receptor for plasminogen activator inhibitor-1." <u>The Journal of Biological Chemistry</u> 279(21): 22595-22604.

Dogic, D., P. Rousselle, et al. (1998). "Cell adhesion to laminin 1 or 5 induces isoform-specific clustering of integrins and other focal adhesion components." <u>Journal of Cell Science</u> 111 (Pt 6): 793-802.

Elfiky, A. A. and J. E. Rosenberg (2009). "Targeting angiogenesis in bladder cancer." <u>Current Oncology Reports</u> 11(3): 244-249.

Emaduddin, M., D. C. Bicknell, et al. (2008). "Cell growth, global phosphotyrosine elevation, and c-Met phosphorylation through Src family kinases in colorectal cancer cells." Proceedings of the National Academy of Sciences USA 105(7): 2358-2362.

Feng, B., R. Wang, et al. (2012). "Review of miR-200b and cancer chemosensitivity." Biomedicine & Pharmacotherapy 66(6): 397-402.

Fischer, A. N., E. Fuchs, et al. (2007). "PDGF essentially links TGF-beta signaling to nuclear beta-catenin accumulation in hepatocellular carcinoma progression." Oncogene 26(23): 3395-3405.

Fixman, E. D., T. M. Fournier, et al. (1996). "Pathways downstream of Shc and Grb2 are required for cell transformation by the tpr-Met oncoprotein." The Journal of Biological Chemistry 271(22): 13116-13122.

Freedman, N. D., D. T. Silverman, et al. (2011). "Association between smoking and risk of bladder cancer among men and women." The Journal of the American Medical Association 306(7): 737-745.

Friedl, P., J. Locker, et al. (2012). "Classifying collective cancer cell invasion." Nature Cell Biology 14(8): 777-783.

Gonzalez-Moreno, O., J. Lecanda, et al. (2010). "VEGF elicits epithelial-mesenchymal transition (EMT) in prostate intraepithelial neoplasia (PIN)-like cells via an autocrine loop." Experimental Cell Research 316(4): 554-567.

Graham, T. R., H. E. Zhau, et al. (2008). "Insulin-like growth factor-I-dependent up-regulation of ZEB1 drives epithelial-to-mesenchymal transition in human prostate cancer cells." Cancer Research 68(7): 2479-2488.

Guix, M., A. C. Faber, et al. (2008). "Acquired resistance to EGFR tyrosine kinase inhibitors in cancer cells is mediated by loss of IGF-binding proteins." Journal of Clinical Investigation 118(7): 2609-2619.

Hanahan, D. and R. A. Weinberg (2011). "Hallmarks of cancer: the next generation." Cell 144(5): 646-674.

Harker, W. G., F. J. Meyers, et al. (1985). "Cisplatin, methotrexate, and vinblastine (CMV): an effective chemotherapy regimen for metastatic transitional cell carcinoma of the urinary tract. A Northern California Oncology Group study." Journal of Clinical Oncology 3(11): 1463-1470.

Haslehurst, A. M., M. Koti, et al. (2012). "EMT transcription factors snail and slug directly contribute to cisplatin resistance in ovarian cancer." BMC Cancer 12(1): 91-100.

Hattori, N., S. Mochizuki, et al. (2009). "MMP-13 plays a role in keratinocyte migration, angiogenesis, and contraction in mouse skin wound healing." The American Journal of Pathology 175(2): 533-546.

Heldin, C. H. and A. Moustakas (2012). "Role of Smads in TGFbeta signaling." Cell and Tissue Research 347(1): 21-36.

Heldin, C. H., M. Vanlandewijck, et al. (2012). "Regulation of EMT by TGFbeta in cancer." FEBS Letters 586(14): 1959-1970.

Hernandez, S., E. Lopez-Knowles, et al. (2006). "Prospective study of FGFR3 mutations as a prognostic factor in nonmuscle invasive urothelial bladder carcinomas." Journal of Clinical Oncology 24(22): 3664-3671.

Hiratsuka, S., A. Watanabe, et al. (2006). "Tumour-mediated upregulation of chemoattractants and recruitment of myeloid cells predetermines lung metastasis." Nature Cell Biology 8(12): 1369-1375.

Hochhaus, A., B. Druker, et al. (2008). "Favorable long-term follow-up results over 6 years for response, survival, and safety with imatinib mesylate therapy in chronic-phase chronic myeloid leukemia after failure of interferon-alpha treatment." Blood 111(3): 1039-1043.

Hough, C., M. Radu, et al. (2012). "Tgf-beta induced Erk phosphorylation of smad linker region regulates smad signaling." PLoS One 7(8): e42513.

Hu, X., D. M. Macdonald, et al. (2009). "A miR-200 microRNA cluster as prognostic marker in advanced ovarian cancer." Gynecologic Oncology 114(3): 457-464.

Huang da, W., B. T. Sherman, et al. (2009). "Bioinformatics enrichment tools: paths toward the comprehensive functional analysis of large gene lists." Nucleic Acids Research 37(1): 1-13.

Huang da, W., B. T. Sherman, et al. (2009). "Systematic and integrative analysis of large gene lists using DAVID bioinformatics resources." Nature Protocols 4(1): 44-57.

Hung, T. T., H. Wang, et al. (2008). "Molecular profiling of bladder cancer: involvement of the TGF-beta pathway in bladder cancer progression." Cancer Letters 265(1): 27-38.

Huttenlocher, A. and A. R. Horwitz (2011). "Integrins in cell migration." Cold Spring Harbor Perspectives in Biology 3(9): a005074.

Inglese, J., C. E. Shamu, et al. (2007). "Reporting data from high-throughput screening of small-molecule libraries." Nature Chemical Biology 3(8): 438-441.

Iyer, S., Z. G. Wang, et al. (2005). "Targeting TGFbeta signaling for cancer therapy." Cancer Biology and Therapy 4(3): 261-266.

Kaplan, R. N., R. D. Riba, et al. (2005). "VEGFR1-positive haematopoietic bone marrow progenitors initiate the pre-metastatic niche." Nature 438(7069): 820-827.

Khaled, H. M., A. A. Bahnassy, et al. (2009). "Clinical significance of altered nm23-H1, EGFR, RB and p53 expression in bilharzial bladder cancer." BMC Cancer 9(1): 32-44.

Kim, H. J., B. C. Litzenburger, et al. (2007). "Constitutively active type I insulin-like growth factor receptor causes transformation and xenograft growth of immortalized mammary epithelial cells and is accompanied by an epithelial-to-mesenchymal transition mediated by NF-kappaB and snail." Molecular Cell Biology 27(8): 3165-3175.

Kim, S. H., J. Turnbull, et al. (2011). "Extracellular matrix and cell signalling: the dynamic cooperation of integrin, proteoglycan and growth factor receptor." Journal of Endocrinology 209(2): 139-151.

Kiselyov, V. V., G. Skladchikova, et al. (2003). "Structural basis for a direct interaction between FGFR1 and NCAM and evidence for a regulatory role of ATP." Structure 11(6): 691-701.

Kompier, L. C., I. Lurkin, et al. (2010). "FGFR3, HRAS, KRAS, NRAS and PIK3CA mutations in bladder cancer and their potential as biomarkers for surveillance and therapy." PLoS One 5(11): e13821.

Korman, H. J., J. O. Peabody, et al. (1996). "Autocrine motility factor receptor as a possible urine marker for transitional cell carcinoma of the bladder." The Journal of Urology 155(1): 347-349.

Kutluk Cenik, B., K. T. Ostapoff, et al. (2013). "BIBF 1120 (nintedanib), a triple angiokinase inhibitor, induces hypoxia but not EMT and blocks progression of preclinical models of lung and pancreatic cancer." Molecular Cancer Therapeutics 12(6): 992-1001.

Lai, A. Z., J. V. Abella, et al. (2009). "Crosstalk in Met receptor oncogenesis." Trends Cell Biol 19(10): 542-551.

Lee, J. M., S. Dedhar, et al. (2006). "The epithelial-mesenchymal transition: new insights in signaling, development, and disease." The Journal of Cell Biology 172(7): 973-981.

Lehmann, K., E. Janda, et al. (2000). "Raf induces TGFbeta production while blocking its apoptotic but not invasive responses: a mechanism leading to increased malignancy in epithelial cells." Genes & Development 14(20): 2610-2622.

Lemmon, M. A. and J. Schlessinger (2010). "Cell signaling by receptor tyrosine kinases." Cell 141(7): 1117-1134.

Lewis, S. A., D. C. Eaton, et al. (1976). "The mechanism of Na+ transport by rabbit urinary bladder." The Journal of Membrane Biology 28(1): 41-70.

Li, Q. Q., Z. Q. Chen, et al. (2011). "Involvement of NF-kappaB/miR-448 regulatory feedback loop in chemotherapy-induced epithelial-mesenchymal transition of breast cancer cells." Cell Death & Differentiation 18(1): 16-25.

Li, Y., X. Yang, et al. (2010). "VEGFR and EGFR inhibition increases epithelial cellular characteristics and chemotherapy sensitivity in mesenchymal bladder cancer cells." Oncology Reports 24(4): 1019-1028.

Lightfoot, A. J., B. N. Breyer, et al. (2013). "Multi-institutional analysis of sequential intravesical gemcitabine and mitomycin C chemotherapy for non-muscle invasive bladder cancer." Urologic Oncology 32(1): 35.e15.

Lim, J. and J. P. Thiery (2012). "Epithelial-mesenchymal transitions: insights from development." Development 139(19): 3471-3486.

Lu, Z., S. Ghosh, et al. (2003). "Downregulation of caveolin-1 function by EGF leads to the loss of E-cadherin, increased transcriptional activity of beta-catenin, and enhanced tumor cell invasion." Cancer Cell 4(6): 499-515.

Marchini, S., R. Fruscio, et al. (2013). "Resistance to platinum-based chemotherapy is associated with epithelial to mesenchymal transition in epithelial ovarian cancer." European Journal of Cancer 49(2): 520-530.

Matsuzaki, K., C. Kitano, et al. (2009). "Smad2 and Smad3 phosphorylated at both linker and COOH-terminal regions transmit malignant TGF-beta signal in later stages of human colorectal cancer." Cancer Research 69(13): 5321-5330.

Minowa, T., K. Kawano, et al. (2009). "Increase in tumour permeability following TGF-beta type I receptor-inhibitor treatment observed by dynamic contrast-enhanced MRI." British Journal of Cancer 101(11): 1884-1890.

Mok, T. S., Y. L. Wu, et al. (2009). "Gefitinib or carboplatin-paclitaxel in pulmonary adenocarcinoma." The New England Journal of Medicine 361(10): 947-957.

Morali, O. G., V. Delmas, et al. (2001). "IGF-II induces rapid beta-catenin relocation to the nucleus during epithelium to mesenchyme transition." Oncogene 20(36): 4942-4950.

Moustakas, A. and C. H. Heldin (2007). "Signaling networks guiding epithelial-mesenchymal transitions during embryogenesis and cancer progression." Cancer Science 98(10): 1512-1520.

Neuzillet, Y., X. Paoletti, et al. (2012). "A meta-analysis of the relationship between FGFR3 and TP53 mutations in bladder cancer." <u>PLoS One</u> 7(12): e48993.

Nowell, P. C. (1976). "The clonal evolution of tumor cell populations." <u>Science</u> 194(4260): 23-28.

O'Reilly, K. E., F. Rojo, et al. (2006). "mTOR inhibition induces upstream receptor tyrosine kinase signaling and activates Akt." <u>Cancer Research</u> 66(3): 1500-1508.

Olsson, A. K., A. Dimberg, et al. (2006). "VEGF receptor signalling - in control of vascular function." <u>Nature Reviews Molecular Cell Biology</u> 7(5): 359-371.

Oskarsson, T. and J. Massague (2012). "Extracellular matrix players in metastatic niches." <u>The EMBO Journal</u> 31(2): 254-256.

Pacchiana, G., C. Chiriaco, et al. (2010). "Monovalency unleashes the full therapeutic potential of the DN-30 anti-Met antibody." <u>The Journal of Biological Chemistry</u> 285(46): 36149-36157.

Pao, W., V. A. Miller, et al. (2005). "Acquired resistance of lung adenocarcinomas to gefitinib or erlotinib is associated with a second mutation in the EGFR kinase domain." <u>PLoS Medicine</u> 2(3): e73.

Parsons, C. L., D. Boychuk, et al. (1990). "Bladder surface glycosaminoglycans: an epithelial permeability barrier." <u>The Journal of Urology</u> 143(1): 139-142.

Peinado, H., M. Aleckovic, et al. (2012). "Melanoma exosomes educate bone marrow progenitor cells toward a pro-metastatic phenotype through MET." <u>Nature Medicine</u> 18(6): 883-891.

Petit, V., B. Boyer, et al. (2000). "Phosphorylation of tyrosine residues 31 and 118 on paxillin regulates cell migration through an association with CRK in NBT-II cells." <u>The Journal of Cell Biology</u> 148(5): 957-970.

Plati, J., O. Bucur, et al. (2008). "Dysregulation of apoptotic signaling in cancer: molecular mechanisms and therapeutic opportunities." <u>Journal of Cellular Biochemistry</u> 104(4): 1124-1149.

Powell, A. A., A. H. Talasaz, et al. (2012). "Single cell profiling of circulating tumor cells: transcriptional heterogeneity and diversity from breast cancer cell lines." <u>PLoS One</u> 7(5): e33788.

Psaila, B., R. N. Kaplan, et al. (2006). "Priming the 'soil' for breast cancer metastasis: the pre-metastatic niche." <u>Breast Disease</u> 2006-2007(26): 65-74.

Rafii, S. and D. Lyden (2006). "S100 chemokines mediate bookmarking of premetastatic niches." Nature Cell Biology 8(12): 1321-1323.

Reddy, K. B., S. M. Nabha, et al. (2003). "Role of MAP kinase in tumor progression and invasion." Cancer Metastasis Reviews 22(4): 395-403.

Reese, D. E., T. Mikawa, et al. (2002). "Development of the coronary vessel system." Circulation Research 91(9): 761-768.

Reya, T. and H. Clevers (2005). "Wnt signalling in stem cells and cancer." Nature 434(7035): 843-850.

Schaeper, U., N. H. Gehring, et al. (2000). "Coupling of Gab1 to c-Met, Grb2, and Shp2 mediates biological responses." The Journal of Cell Biology 149(7): 1419-1432.

Schenk, S., E. Hintermann, et al. (2003). "Binding to EGF receptor of a laminin-5 EGF-like fragment liberated during MMP-dependent mammary gland involution." The Journal of Cell Biology 161(1): 197-209.

Schlessinger, J. (2000). "Cell signaling by receptor tyrosine kinases." Cell 103(2): 211-225.

Shariat, S. F., R. F. Youssef, et al. (2010). "Association of angiogenesis related markers with bladder cancer outcomes and other molecular markers." The Journal of urology 183(5): 1744-1750.

Shinomiya, N., C. F. Gao, et al. (2004). "RNA interference reveals that ligand-independent met activity is required for tumor cell signaling and survival." Cancer Research 64(21): 7962-7970.

Shinto, O., M. Yashiro, et al. (2010). "Inhibitory effect of a TGFbeta receptor type-I inhibitor, Ki26894, on invasiveness of scirrhous gastric cancer cells." British Journal of Cancer 102(5): 844-851.

Singh, A. B., T. Tsukada, et al. (2004). "Membrane-associated HB-EGF modulates HGF-induced cellular responses in MDCK cells." Journal of Cell Science 117(Pt 8): 1365-1379.

Smith, K., J. A. Fennelly, et al. (1989). "Characterization and quantitation of the epidermal growth factor receptor in invasive and superficial bladder tumors." Cancer Research 49(21): 5810-5815.

Smolen, G. A., R. Sordella, et al. (2006). "Amplification of MET may identify a subset of cancers with extreme sensitivity to the selective tyrosine kinase inhibitor PHA-665752." Proceedings of the National Academy of Sciences U S A 103(7): 2316-2321.

Sternberg, J. J., R. B. Bracken, et al. (1977). "Combination chemotherapy (CISCA) for advanced urinary tract carcinoma. A preliminary report." The Journal of the American Medical Association 238(21): 2282-2287.

Sun, L., Y. Yao, et al. (2012). "MiR-200b and miR-15b regulate chemotherapy-induced epithelial-mesenchymal transition in human tongue cancer cells by targeting BMI1." Oncogene 31(4): 432-445.

Susuki, D., S. Kimura, et al. (2011). "Regulation of microRNA expression by hepatocyte growth factor in human head and neck squamous cell carcinoma." Cancer Science 102(12): 2164-2171.

Thiery, J. P. (2002). "Epithelial-mesenchymal transitions in tumour progression." Nature Reviews Cancer 2(6): 442-454.

Thiery, J. P. (2009). "Metastasis: alone or together?" Current Biology 19(24): R1121-1123.

Thiery, J. P., H. Acloque, et al. (2009). "Epithelial-mesenchymal transitions in development and disease." Cell 139(5): 871-890.

Thiery, J. P. and C. T. Lim (2013). "Tumor Dissemination: An EMT Affair." Cancer Cell 23(3): 272-273.

Thiery, J. P. and J. P. Sleeman (2006). "Complex networks orchestrate epithelial-mesenchymal transitions." Nature reviews. Molecular cell biology 7(2): 131-142.

Thiery, J. P. and J. P. Sleeman (2006). "Complex networks orchestrate epithelial-mesenchymal transitions." Nature Reviews Molecular Cell Biology 7(2): 131-142.

Thykjaer, T., C. Workman, et al. (2001). "Identification of gene expression patterns in superficial and invasive human bladder cancer." Cancer Research 61(6): 2492-2499.

Toh, B., X. Wang, et al. (2011). "Mesenchymal transition and dissemination of cancer cells is driven by myeloid-derived suppressor cells infiltrating the primary tumor." PLoS Biology 9(9): e1001162.

Toyoshima, K., N. Ito, et al. (1971). "Tissue culture of urinary bladder tumor induced in a rat by N-butyl-N-(-4-hydroxybutyl)nitrosamine: establishment of cell line, Nara Bladder Tumor II." Journal of the National Cancer Institute 47(5): 979-985.

Truschel, S. T., W. G. Ruiz, et al. (1999). "Primary uroepithelial cultures. A model system to analyze umbrella cell barrier function." The Journal of Biological Chemistry 274(21): 15020-15029.

Tucker, G. C., B. Boyer, et al. (1991). "Combined effects of extracellular matrix and growth factors on NBT-II rat bladder carcinoma cell dispersion." Journal of Cell Science 100(Pt 2): 371-380.

Valles, A. M., B. Boyer, et al. (1990). "Acidic fibroblast growth factor is a modulator of epithelial plasticity in a rat bladder carcinoma cell line." Proceedings of the National Academy of Sciences USA 87(3): 1124-1128.

van Rhijn, B. W., T. H. van der Kwast, et al. (2004). "FGFR3 and P53 characterize alternative genetic pathways in the pathogenesis of urothelial cell carcinoma." Cancer Research 64(6): 1911-1914.

Wanami, L. S., H. Y. Chen, et al. (2008). "Vascular endothelial growth factor-A stimulates Snail expression in breast tumor cells: implications for tumor progression." Experimental Cell Research 314(13): 2448-2453.

Wang, Z., Y. Li, et al. (2010). "The role of Notch signaling pathway in epithelial-mesenchymal transition (EMT) during development and tumor aggressiveness." Current Drug Targets 11(6): 745-751.

Wijelath, E. S., S. Rahman, et al. (2006). "Heparin-II domain of fibronectin is a vascular endothelial growth factor-binding domain: enhancement of VEGF biological activity by a singular growth factor/matrix protein synergism." Circulation Research 99(8): 853-860.

Williams, S. V., C. D. Hurst, et al. (2013). "Oncogenic FGFR3 gene fusions in bladder cancer." Human Molecular Genetics 22(4): 795-803.

Witsch, E., M. Sela, et al. (2010). "Roles for growth factors in cancer progression." Physiology 25(2): 85-101.

Wong, V. C., H. Chen, et al. (2012). "Tumor suppressor dual-specificity phosphatase 6 (DUSP6) impairs cell invasion and epithelial-mesenchymal transition (EMT)-associated phenotype." International Journal of Cancer 130(1): 83-95.

Xia, G., S. R. Kumar, et al. (2006). "Expression and significance of vascular endothelial growth factor receptor 2 in bladder cancer." The Journal of Urology 175(4): 1245-1252.

Yang, C. C., K. C. Chu, et al. (2004). "The expression of vascular endothelial growth factor in transitional cell carcinoma of urinary bladder is correlated with cancer progression." Urol Oncol 22(1): 1-6.

Yang, L., C. Lin, et al. (2006). "P68 RNA helicase mediates PDGF-induced epithelial mesenchymal transition by displacing Axin from beta-catenin." Cell 127(1): 139-155.

Yang, Y., Y. H. Ahn, et al. (2011). "The Notch ligand Jagged2 promotes lung adenocarcinoma metastasis through a miR-200-dependent pathway in mice." Journal of Clinical Investigation 121(4): 1373-1385.

Yu, M., A. Bardia, et al. (2013). "Circulating breast tumor cells exhibit dynamic changes in epithelial and mesenchymal composition." Science 339(6119): 580-584.

Zavadil, J. (2009). "New TGF-beta and Ras crosstalk in EMT." Cell Cycle 8(2): 184.

Zeisel, A., A. Amir, et al. (2010). "Intensity dependent estimation of noise in microarrays improves detection of differentially expressed genes." BMC bioinformatics 11(1): 400-414.

Zeisel, A., O. Zuk, et al. (2011). "FDR control with adaptive procedures and FDR monotonicity." The Annals of Applied Statistics 5(1): 943-968.

Zheng, H. X., Y. D. Cai, et al. (2013). "Fas signaling promotes motility and metastasis through epithelial-mesenchymal transition in gastrointestinal cancer." Oncogene 32(9): 1183-1192.

Zhong, J., S. Chen, et al. (2012). "ZIC1 modulates cell-cycle distributions and cell migration through regulation of sonic hedgehog, PI(3)K and MAPK signaling pathways in gastric cancer." BMC Cancer 12(1): 290-299.

Zigrino, P., I. Kuhn, et al. (2009). "Stromal expression of MMP-13 is required for melanoma invasion and metastasis." The Journal of Investigative Dermatology 129(11): 2686-2693.

Appendices

Genes that are differentially expressed in both EGF and HGF treatment.

Upregulated by both EGF and HGF				Down-regulated by EGF and HGF		
Dusp7	Glb1l2	Narf	Ripk3	Zfp36l1	Psme2	Krt16
Efhd1	Glipr2	Ncdn	Rnd1	Zfp36	Ptges	Krt1-5
Tspan5	Gnb4	Nek6	Rock2	Xdh	Ptplb	Krt13
Tspan2	Gnl2	Ngf	Rrp8	Wnt6	Ptprf	Add3
Efhd2	Gpr126	Niacr1	Rrp1b	Wfdc15a	Pvrl1	Aes
Egr1	Gprc5a	Nid67	Rras2	Sh3yl1	Pafah2	Afap1l2
Ttc9	Gpsm1	Nol8	Sema3c	Ucp2	Pcmtd2	Klhl24
Ttc39b	Hbegf	Nrp2	Scmh1	Tspan8	Pdcd4	Krt1
Ubash3b	Hk2	Nrg1	Runx1	Tspan1	Ocln	Klf13
Ehbp1l1	Hlx	Nppb	Sertad2	Serpinb8	P2rx4	Agrn
Ttll4	Hmga1	Nup153	Serpine1	Trim29	Nupr1	Klf3
Vegfa	Hpse	Nuak2	Sfrs2ip	Tob1	Nudt1	Aim1
Ehd3	Hs3st1	Orc1l	Sestd1	Tnks1bp1	Nt5dc2	Aldh3a1
Elf4	Htra1	Odc1	Sgms2	Sepp1	Nrep	Aldh6a1
Vcl	Iffo2	Obfc2a	Abcb1b	Tmem9	Npepo	Alkbh7
Elk3	Ing5	P2ry2	Abcb1a	Selenbp1	Nqo1	Ka11
Usp31	Inpp4b	PVR	Smap2	Scrn1	Notch1	Arid5b
Eml4	Itga2	Pak1ip1	Abl2	Scp2	Nme7	Atf5
Usp24	Itga3	Pard6b	Slc25a30	Rxra	Nme3	Kb15
Emp3	Kank1	Papd5	Abhd2	Tecr	Nisch	Kbtbd4
Enc1	Kcnn4	Pctk2	Abhd10	Tgfbi	Nfix	Bad
Enpp1	Kif13a	Pdpn	Abcg1	Rpain	Ndufa2	Jund
Epha2	Klf6	Pelp1	Smc4	Tle3	Nap1l2	Jup
Ercc1	Klk10	Pex11g	Acap1	Tmco6	Ncor2	Barx2
Ereg	Lama3	Phlda1	Actn1	Spon2	Mylip	Bbs9
Ets1	Lamb1	Phtf2	Adam8	Robld3	Mt1a	Bcam
Etv4	Lamb3	Pik3cb	Snx18	Sqle	Msln	Bcl11b
Errfi1	Lamc2	Pik3cd	Snf1lk2	Rhbdl3	Mpzl2	Id4
Exo1	Lass6	Pim3	Afap1	Srebf2	Moxd1	Igfbp5
Ugcg	Ldlr	Pitpnc1	Adfp	Rhbdl2	Mospd3	Hoxd10
Uck2	Lpcat1	Pip4k2a	Adamts6	Rexo2	Mmp15	Bhlhe40
Extl3	Lrp8	Plk2	Aen	Syde2	Mif4gd	Dsp
F3	Lrrfip1	Plaur	Smtn	Renbp	Mid1	Cdh13
Fads3	Lsm11	Plscr1	St3gal4	Tacstd2	Mgst3	Cdkn1c
Fam129b	Macf1	Plk3	Srgap2	Tcfap2a	Mgst1	Grhl3
Fam132b	Magi3	Plscr2	Akr1b10	Tctex1d2	Metrn	Epcam
Zyx	Mboat1	Pmepa1	Akr1b7	Rcan1	Mettl7a	Fgfr3

A

Zfp36l2	Mesdc1	Ppp1r12a	Src	Rapgefl1	Mgmt	Fzd1
Far1	Mfap3l	Polr1b	Spry2	Ranbp3l	Mal2	Gata3
Fat1	Mlf1ip	Prkca	Akr1b8	Rab3d	Map3k9	
Fez2	Mllt4	Procr	Alkbh	Rab38	Mblac2	
Fhdc1	Mmd	Prr5	Sox9	Rab25	Mcee	
Fhl2	Mmp10	Prrg4	Soat1	RT1-DMb	Lztfl1	
Zeb1	Mprip	Prss22	Ankrd50	RT1-DMa	Ly6d	
Fhl3	Mmp3	Ptgs2	Stard13	Pde7a	Lynx1	
Fignl1	Mmp13	Pthlh	Tgfa	Pdgfa	Lphn1	
Whsc1	Mthfd1l	Ptk2b	Thbs2	Pecr	Lss	
Flrt2	Mtap	Ptpn12	Areg	Phyh	Lass3	
Flrt3	Msn	Ptpre	Cav1	Pias3	Lamb2	
Flt1	Mtr	Ptprm	Cd44	Pir	Lad1	
Fnbp1l	Mtmr10	Ptprz1	Ccnd1	Plb1	Lage3	
Fosl1	Mthfd2l	Rasa1	Tpr	Pld3	Lama5	
Vof16	Mybbp1a	Rapgef2	Cxcl1	Pnrc1	Krt4	
Fst	Myc	Rai14	Dusp6	Pof1b	Krt75	
Fv1	Mybl1	Rbms1		Prkag2	Krt17	
Fxyd5	Myo1b	Rasa3		Prkcdbp	Krt19	
Gch1	Myof	Rhpn2		Prtfdc1	Krt2	
Gdnf	Naa25	Rif1		Psmb9	Krt15	

B

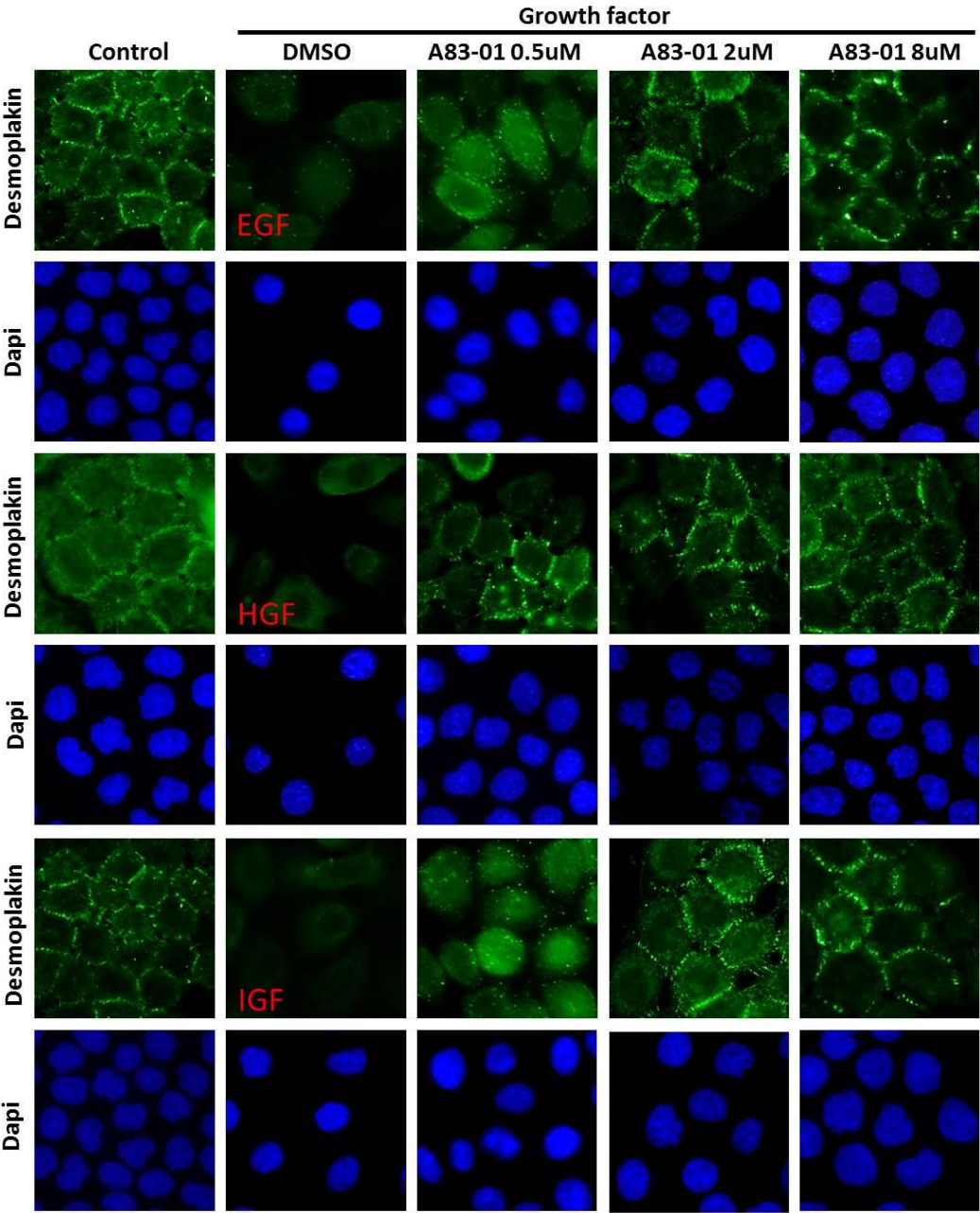**Genes that are differentially expressed in at least 3 time-points (326 genes including 54 probes).**

10701865	10700910	Cpeb2	Fras1	LOC690830	Pgap1	Slc14a1
10705411	10700989	Cpne5	Fxyd5	Lama3	Phf17	Slc20a1
10707620	10701309	Cspg4	Gba2	Lamc2	Phlda1	Slc24a6
10721700	10701605	Csrnp1	Gdnf	Lgr4	Pik3ip1	Slc2a5
10737460	10940508	Cxcl1	Gjb2	Lif	Pitpnc1	Slc30a7
10748440	10940546	Cxcl10	Gjb4	Limk2	Plau	Slc44a2
10758724	Abcg1	Cyp3a9	Glrx1	Lmo1	Plaur	Smad7
10787805	Adam8	Cyp4f39	Gne	Lpar5	Plk1	Smox
10791650	Afap1l2	Cyth1	Gprc5a	Lrrc57	Plk3	Snf1lk2
10793607	Agpat9	Dck	Gpsm1	MGC105649	Plscr1	Sprr1al
10794544	Aim1	Dctd	Gpsm2	Mast4	Ppard	Spry2
10799084	Aloxe3	Ddit4	Hbegf	Mbp	Ppfibp2	Srxn1
10805088	Amac1	Depdc1	Hic1	Megf9	Pragmin	St3gal1
10805597	Ankrd50	Dhcr7	Hlx	Mid1	Prl8a7	St3gal6
10817100	Areg	Dhrs9	Hmmr	Mir483	Procr	St5
10817102	Arl5b	Dlgap5	Hmox1	Mllt3	Prrg4	Stam
10817105	Arsj	Dnajb4	Hpcal1	Mmd	Ptgs2	Stk40
10817111	Aspm	Dsg3	Hpse	Mmp13	Pthlh	Syde2
10817119	Atg9b	Dtl	Hr	Mmp15	Ptpre	Synm
10821105	Atmin	Dtx4	Id1	Mmp3	Ptprm	Synpo
10824719	Atp13a4	Dusp1	Idh1	Mocos	Ptrh1	Tgfa
10824726	Atxn1	Dusp10	Ier2	Mxd1	Pxn	Tgfb1
10839872	Auts2l	Dusp5	Igsf9b	Mxi1	RGD1305254	Tgfbi
10853391	Axin2	Dusp6	Il1a	Myl9	RGD1306556	Tgfbr3
10856998	B3gnt2	Ednra	Il1rn	Ndc80	RGD1311307	Tgm1
10873027	Barx2	Egr1	Il24	Nedd9	RGD1563437	Timp1
10874858	Bbs7	Ehd3	Irs1	Ngf	RGD1564081	Tlcd1
10881468	Bnip3l	Emp3	Itpkc	Niacr1	RGD1564984	Tm4sf1
10884158	Brca2	Enc1	Junb	Nid2	Rab38	Tmc7
10885613	Capn8	Enpp1	Kcnn3	Nid67	Rap2b	Tmem79
10890904	Casc5	Eppk1	Kctd11	Notch1	Rasa1	Tnfrsf26
10891594	Casp7	Ercc1	Kif20a	Nppb	Rasl11b	Trib1
10897037	Ccdc80	Ereg	Kif23	Nrep	Rhbdl3	Trim59
10901713	Ccnb1	Ern1	Kif2c	Nrg1	Ripk4	Trim62
10902762	Ccnb2	Errfi1	Klf6	Oaf	Rnf145	Trpv3
10908670	Ccng2	Extl2	Klk6	Obfc2a	Runx1	Tspan5
10908914	Ccrn4l	Fam107b	Krt15	Odc1	Selm	Ttc9
10920626	Cd34	Fam110c	LOC100125365	P2ry1	Sema4b	Txnrd1
10922779	Cdkn1a	Fam43a	LOC100233213	P2ry2	Sema7a	Ubash3b
10924441	Celsr2	Fat2	LOC100363984	PVR	Serpine1	Uck2
10930342	Cenpf	Fermt1	LOC100365935	Pard6b	Sertad1	Vof16
10933769	Cep57	Fgfr3	LOC290508	Pawr	Sertad4	Wdr19
10722718	Cited2	Fkbp6	LOC305806	Pcdh1	Setd7	Wnt4
10741865	Ckap2	Flt1	LOC363060	Pcyox1l	Sgms2	Xkr6
10817117	Cnot6l	Fn1	LOC679752	Pdgfc	Sgol2	Zswim4
10821067	Cnst	Fosl1	LOC683522	Pdpn	Sh2d5	
10700678		Foxo1	LOC688459	Pex11g	Siah2	

Genes detected in pathway analysis for each time-point

2 hour	Term	PValue	Genes	Benjamini
	rno04010:MAPK signaling pathway	8.16E-06	IL1R2, TNF, MAP2K3, TGFBR2, MAP2K4, NR4A1, HSPA1B, SRF, FLNB, DUSP5, MAP3K6, GADD45G, RAPGEF2, GADD45A,HSPA8, IL1A, NGF	8.32E-04
	rno04520:Adherens junction	0.008157	ACTG1, PVRL4, TGFBR2, ACTN1, CDH1, VCL	0.341433183
	rno04012:ErbB signaling pathway	0.014359	EREG, MAP2K4, HBEGF, AREG, NRG1, PIK3R1	0.388449323
	rno04350:TGF-beta signaling pathway	0.057877	INHBA, TNF, SMAD7, FST, TGFBR2	0.491193822

4 hours	Term	PValue	Genes	Benjamini
	rno04012:ErbB signaling pathway	9.75E-06	ERBB3, ERBB2, PIK3CD, BTC, MAP2K4, RAF1, SRC, NCK2, CDKN1B, EREG, JUN, PAK4, GAB1, HBEGF, AREG, NRG1, PIK3R3, MYC, PIK3R1	5.13E-04
	rno04115:p53 signaling pathway	9.39E-05	BID, ZMAT3, CDK6, CHEK1, SFN, CHEK2, SESN1, ATM, SESN3, CCNB1, CCND1, CCNB2, SERPINE1, GADD45G, GADD45A	0.002470635
	rno04010:MAPK signaling pathway	1.78E-04	IL1R2, IL1R1, MKNK2, NFKB1, HSPA1B, NFKB2, SRF, PRKX, MAP3K6, MAP3K4, MAP3K8, JUND, RAPGEF2, MYC, IL1A, MAP2K5, RASA2, MAP2K3, TGFBR2, MAP2K4, PTPRR, RAF1, NR4A1, FLNB, FLNA, DUSP5, JUN, RRAS2, GADD45G, PLA2G6, GADD45A, PLA2G4E, MAP3K12, DUSP6, NGF	0.003515836
	rno04350:TGF-beta signaling pathway	0.028229	RGD1309707, INHBA, RBL2, ID2, ID1, SMAD7, FST, TGFBR2, ID4, ID3, MYC, BMPR1A	0.165541054
	rno04722:Neurotrophin signaling pathway	0.042526	PIK3CD, RAF1, NFKB1, FOXO3, IRS1, YWHAG, YWHAH, JUN, BCL2, GAB1, RIPK2, PIK3R3, PIK3R1, NGF, MAP2K5	0.217466198
	rno04370:VEGF signaling pathway	0.058643	PTGS2, PIK3CD, RAF1, PLA2G6, PIK3R3, NFATC3, PXN, SRC, PLA2G4E, PIK3R1	0.280539744
	rno04910:Insulin signaling pathway	0.058879	PRKCZ, PHKB, PIK3CD, PHKA1, PRKAB2, MKNK2, HK2, RAF1, IRS1, PRKX, PPP1R3B, PTPN1, PIK3R3, PIK3R1, PYGB	0.273558639
	rno04062:Chemokine signaling pathway	0.066384	ADCY3, PARD3, ADCY2, PIK3CD, RAF1, NFKB1, FOXO3, CXCL12, PXN, PRKX, PTK2B, CXCL16, GRK6, JAK2, GRK4, GRK5, PIK3R3, PIK3R1	0.295378896
	rno04630:Jak-STAT signaling pathway	0.082802	PIK3CD, IL19, IL4RA, IL15, IL24, CISH, LIF, CCND1, IL23A, IL20RB, PIAS3, JAK2, PIK3R3, MYC, PIK3R1	0.338884933

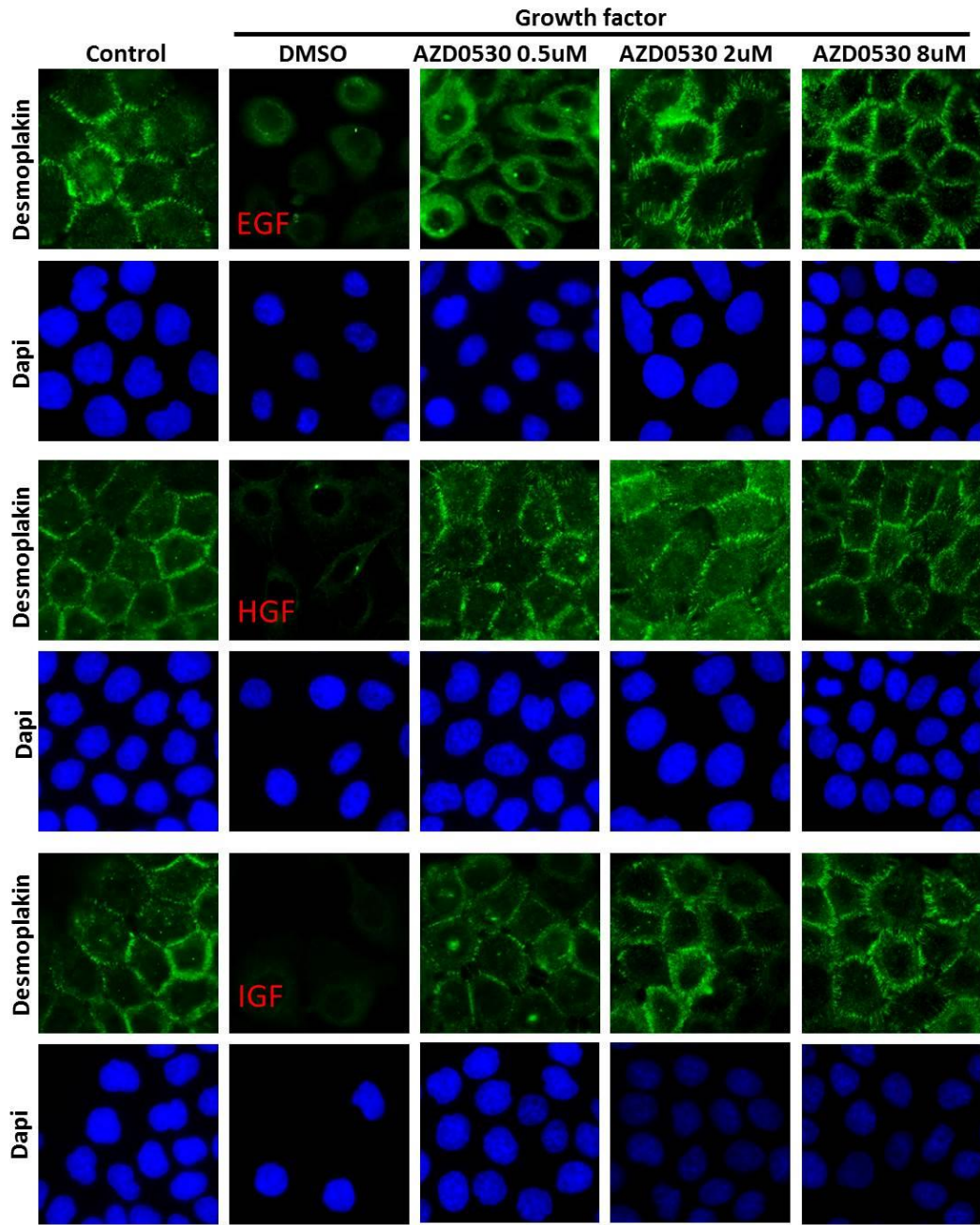| 6 hours	Term	PValue	Genes	Benjamini
	rno04510:Focal adhesion	2.78E-09	CAV1, TLN1, ERBB2, PIP5K1B, ITGB5, ITGB1, PXN, SRC, MYL9, VCL,ACTG1, BCL2, ILK, ITGB6, RGD1309537, SHC1, PDGFC, ZYX, PIK3R3, PIK3R1, PIK3R2, ACTB, FLT1, ACTN4, PIK3CD, ITGA2, RAF1, ACTN1, ITGA3, VAV2, VAV1, FLNB, FLNA, CCND1, LAMA3, LAMA5, RAP1B, LAMC2, PARVB	4.44E-07
	rno04810:Regulation of actin cytoskeleton	6.67E-08	PIP5K3, DIAPH3, IQGAP3, PIP5K1B, ITGB5, ARPC4, ITGB1, PXN, MYL9, VCL, ACTG1, EZR, TIAM1, ITGB6, RGD1309537,RRAS, PDGFC, MSN, PIK3R3, PIK3R1, PIK3R2, ACTB, ARHGEF1, ACTN4, LIMK1, BAIAP2, PIK3CD, ITGA2, RAF1, ACTN1, ITGA3, MYH9, VAV2, VAV1, RRAS2, CFL1, MYH10, SLC9A1	5.34E-06
	rno04070:Phosphatidylinositol signaling system	7.36E-07	PIP5K3, INPP1, RGD1563309, PIK3C2B, PIK3CD, PIP5K1B, ITPKB, CDS1, LOC497978, ITPR2, DGKA, CALML3, PIK3C3, PLCD3, RGD1561955, INPP4B, PIK3R3, PIK3R1, PIK3R2	3.92E-05
	rno04670:Leukocyte transendothelial migration	2.67E-06	ACTB, OCLN, ACTN4, PIK3CD, ACTN1, VAV2, CTNNA1, ITGB1, CXCL12, VAV1, PXN, MYL9, VCL, ACTG1, EZR, PTK2B, RGD1309537, RAP1B, RAPGEF3, MSN, PIK3R3, MLLT4, PIK3R1, PIK3R2	1.07E-04
	rno04012:ErbB signaling pathway	5.47E-05	ERBB3, ERBB2, PIK3CD, MAP2K4, RAF1, SRC, CDKN1B, EREG, GAB1, HBEGF, TGFA, SHC1, AREG, NRG1, PIK3R3, MYC, PIK3R1, PIK3R2	0.001456762
	rno04010:MAPK signaling pathway	0.004976	IL1R2, MKNK2, HSPA1B, NFKB2, SRF, PRKX, MAP3K6, MAP3K1, JUND, MAP3K8, RRAS, PPP3CA, RAPGEF2, MYC, MAP2K6, IL1A, RASA2, MAP2K3, MAP2K4, PTPRR, RAF1, FLNB, FLNA, DUSP5, RPS6KA5, RRAS2, PLA2G6, RAP1B, PLA2G4E,DUSP6, NGF	0.041141522
	rno04115:p53 signaling pathway	0.005122	BID, CCND1, CCNB2, RRM2, SERPINE1, CHEK1, CDK6, SFN, CHEK2, SESN1, ATM, SESN3	0.040245272
	rno04722:Neurotrophin signaling pathway	0.005728	PIK3CD, RAF1, FOXO3, MAGED1, RPS6KA5, YWHAH, CALML3, BCL2, MAP3K1, GAB1, SORT1, SH2B3, RAP1B, SHC1, PIK3R3, PIK3R1, PIK3R2, NGF	0.042825138
	rno04370:VEGF signaling pathway	0.012133	PTGS2, PIK3CD, RAF1, PLA2G6, PPP3CA, PIK3R3, NFATC3, PXN, SRC, PLA2G4E, PIK3R1, PIK3R2	0.081415541

D

9hours	Term	PValue	Genes	Benjamini
	rno04510:Focal adhesion	1.01E-10	TLN1, CAV1, ERBB2, ITGB5, ITGB1, SRC, PXN, MYL9, VCL, ACTG1, BCL2, ITGB6, ILK, PDGFC, SHC1, LAMB1, PIK3R1, ACTN4, PIK3CD, ITGA2, RAF1, ACTN1, ITGA3, VAV2, VAV1, FLNB, FLNA, CCND1, LAMA3, LAMC2, PARVB	1.49E-08
	rno04810:Regulation of actin cytoskeleton	1.12E-08	FGFR3, ITGB5, ARPC4, ITGB1, PXN, MYL9, VCL, ACTG1, EZR, TIAM1, ITGB6, RRAS, PDGFC, MSN, PIK3R1, ARHGEF1, ACTN4, PIK3CD, ITGA2, RAF1, ACTN1, ITGA3, MYH9, VAV2, VAV1, RRAS2, CFL1, MYH10, SLC9A1	8.29E-07
	rno04670:Leukocyte transendothelial migration	4.66E-05	OCLN, ACTN4, PIK3CD, ACTN1, VAV2, VAV1, ITGB1, PXN, VCL, MYL9, ACTG1, EZR, MSN, RAPGEF3, MLLT4, PIK3R1	0.002295619
	rno04012:ErbB signaling pathway	5.21E-04	ERBB3, ERBB2, PIK3CD, GAB1, RAF1, TGFA, HBEGF, SHC1, AREG, NRG1, SRC, PIK3R1	0.015302323
	rno04370:VEGF signaling pathway	0.009048	PTGS2, PIK3CD, RAF1, PPP3CA, NFATC3, PXN, SRC, PLA2G4E, PIK3R1	0.076080242
	rno04115:p53 signaling pathway	0.015767	BID, CCND1, CCNB2, RRM2, CDK6, CHEK2, ATM, SESN3	0.093353235
	rno04360:Axon guidance	0.030465	ABLIM2, PLXNA2, PLXNB2, CFL1, SEMA3C, L1CAM, DPYSL2, PPP3CA, NFATC3, ITGB1, EPHA2	0.146059926
	rno04512:ECM-receptor interaction	0.042695	LAMA3, ITGB6, ITGB5, ITGA2, LAMC2, ITGA3, LAMB1, ITGB1	0.193665382

24hours	Term	PValue	Genes	Benjamini
	rno04012:ErbB signaling pathway	0.002509	ERBB3, JUN, ERBB2, RAF1, HBEGF, SHC1, NRG1, PIK3R1	0.149571651
	rno04070:Phosphatidylinositol signaling system	0.018431	DGKA, CALML3, PIK3C3, CDS1, PIK3R1, ITPR2	0.25915919
	rno04512:ECM-receptor interaction	0.032288	LAMC3, ITGB6, COL3A1, LAMC2, ITGA3, THBS2	0.297298748
	rno04350:TGF-beta signaling pathway	0.040285	ACVR2B, LTBP1, FST, TGFBR2, RHOA, THBS2	0.315371412
	rno04115:p53 signaling pathway	0.056634	BID, CDK6, PERP, ATM, SESN3	0.357510829

E

Desmoplakin relocalized to cell-cell junctions after addition of compounds

F

Growth factor

| | Control | DMSO | PD0325901 0.5uM | PD0325901 2uM | PD0325901 8uM |

G

Growth factor

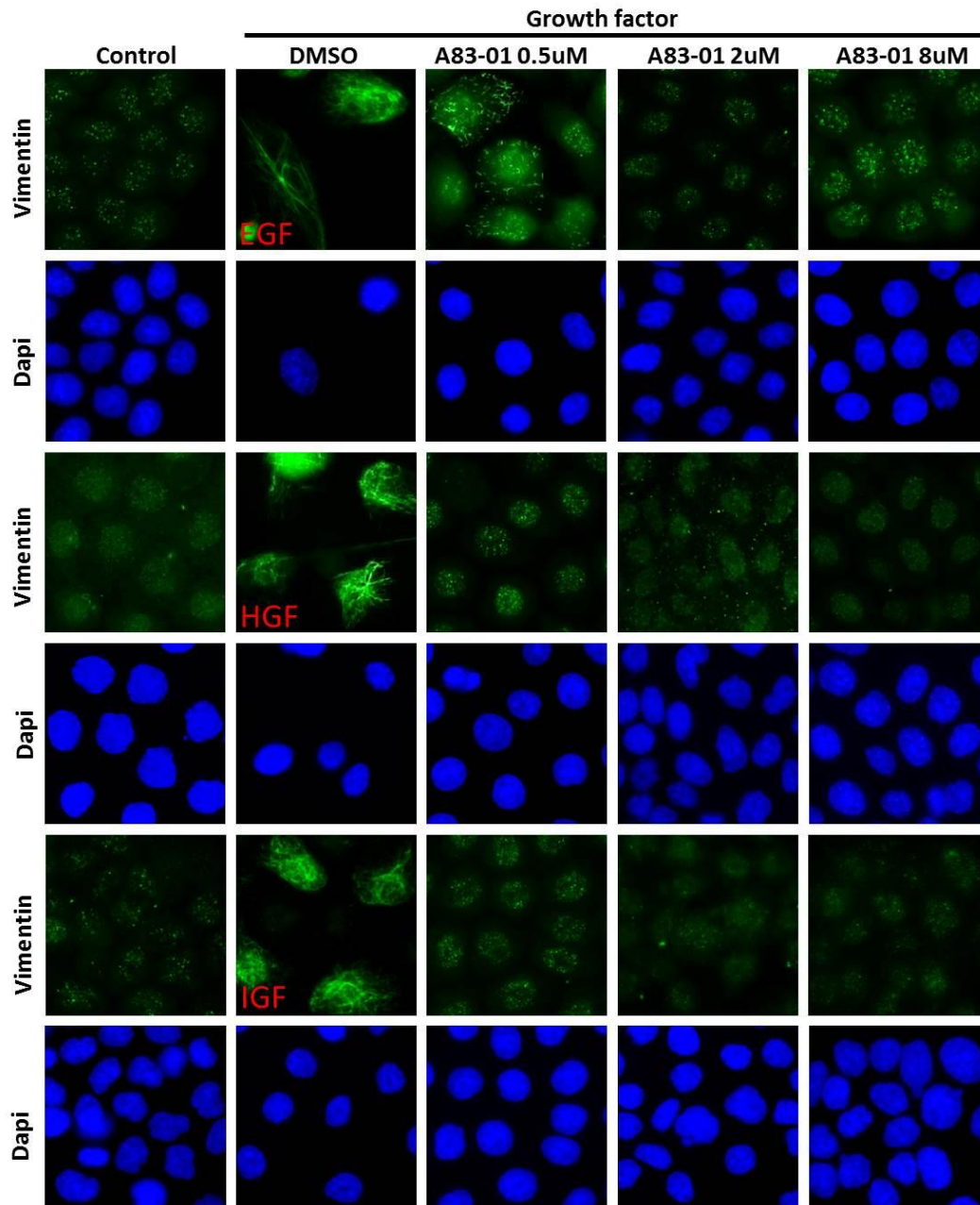|	Control	DMSO	GDC0941 0.5uM	GDC0941 2uM	GDC0941 8uM
Desmoplakin		EGF			
Dapi					
Desmoplakin		HGF			
Dapi					
Desmoplakin		IGF			
Dapi					

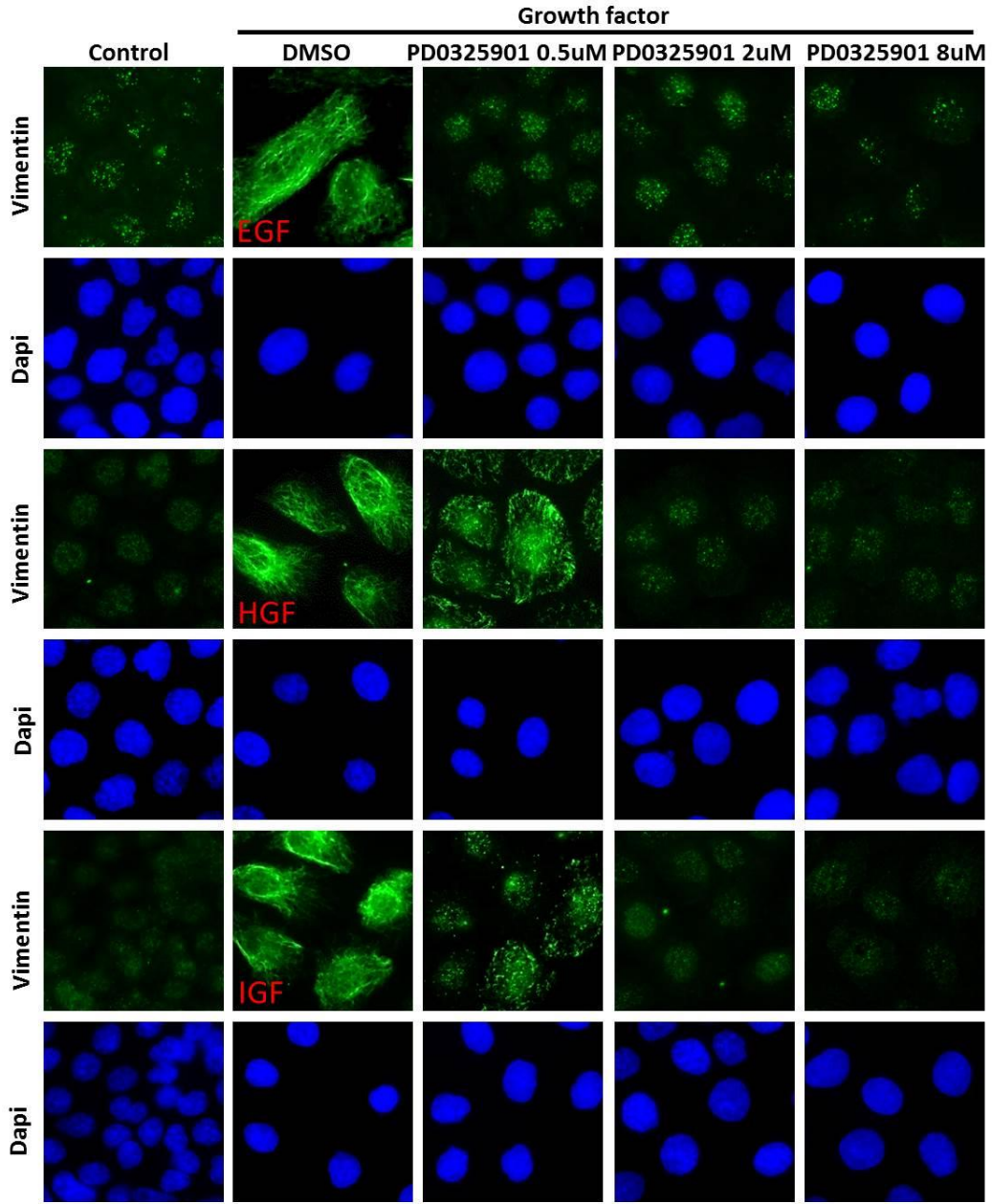H

Growth factor

| | Control | DMSO | AZD0530 0.5uM | AZD0530 2uM | AZD0530 8uM |
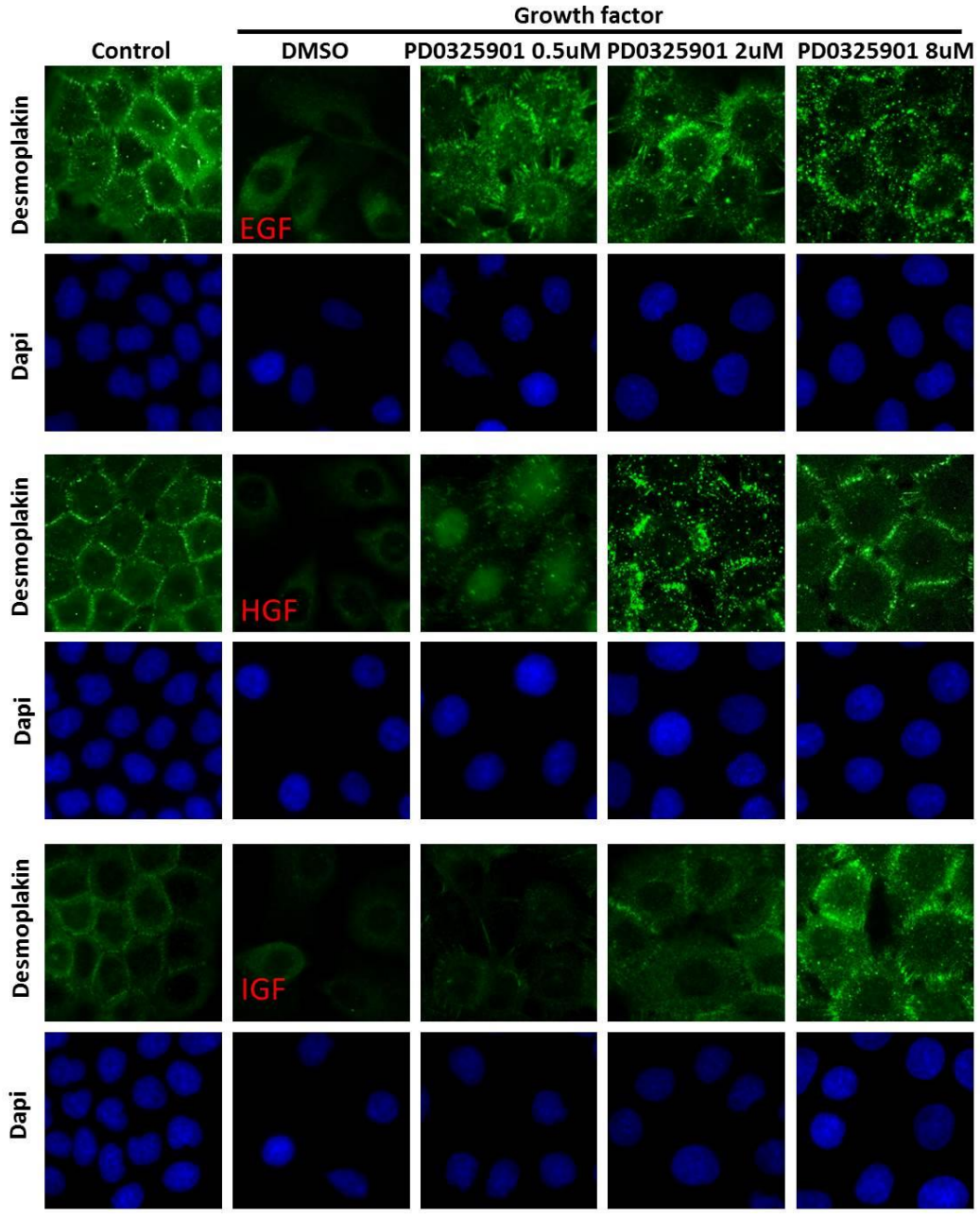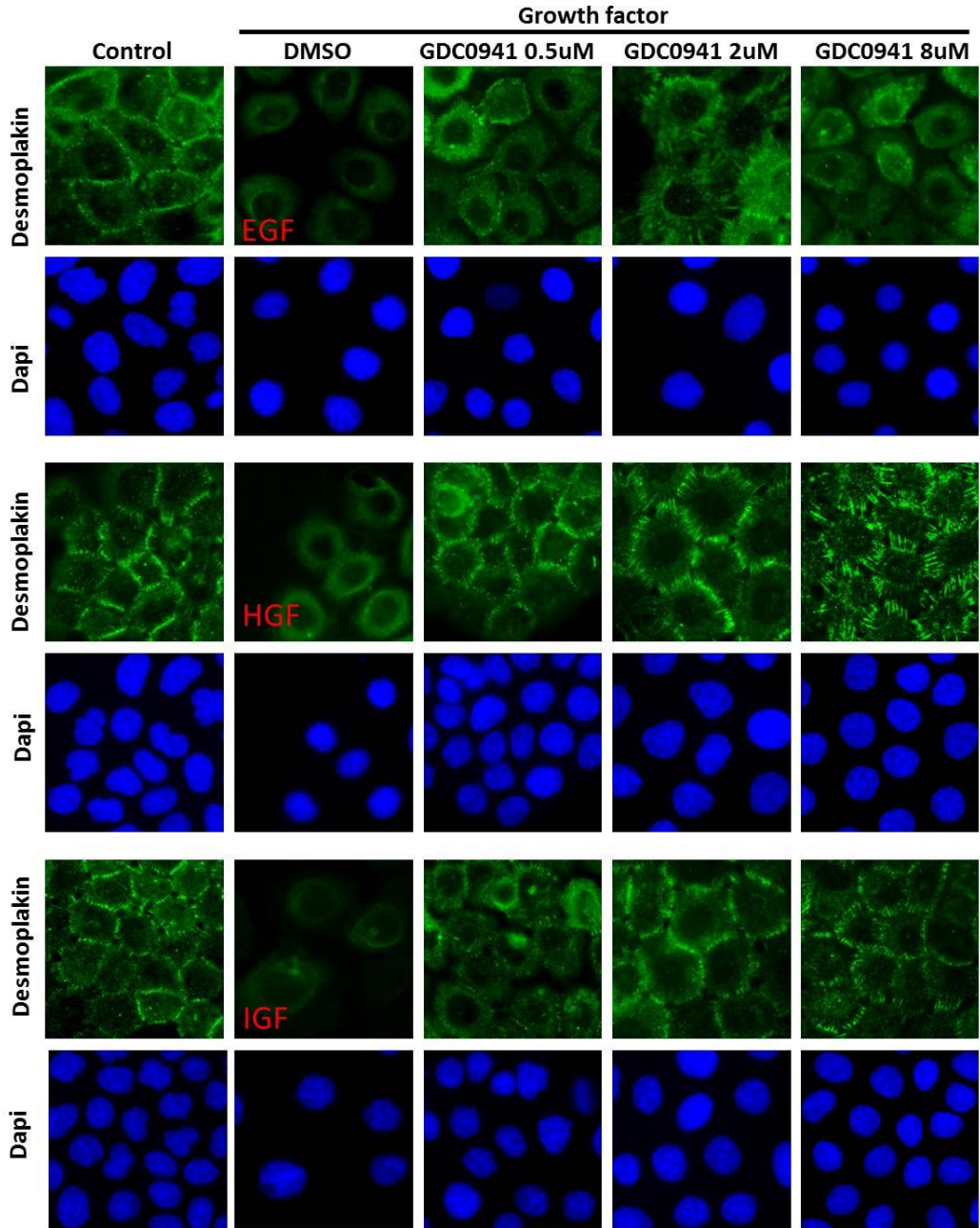
Hit compounds down-regulate Vimentin expression

Growth factor

	Control	DMSO	A83-01 0.5uM	A83-01 2uM	A83-01 8uM

Vimentin

EGF

Dapi

Vimentin

HGF

Dapi

Vimentin

IGF

Dapi

J

K

Growth factor

| | Control | DMSO | GDC0941 0.5uM | GDC0941 2uM | GDC0941 8uM |

Vimentin — EGF
Dapi
Vimentin — HGF
Dapi
Vimentin — IGF
Dapi

L
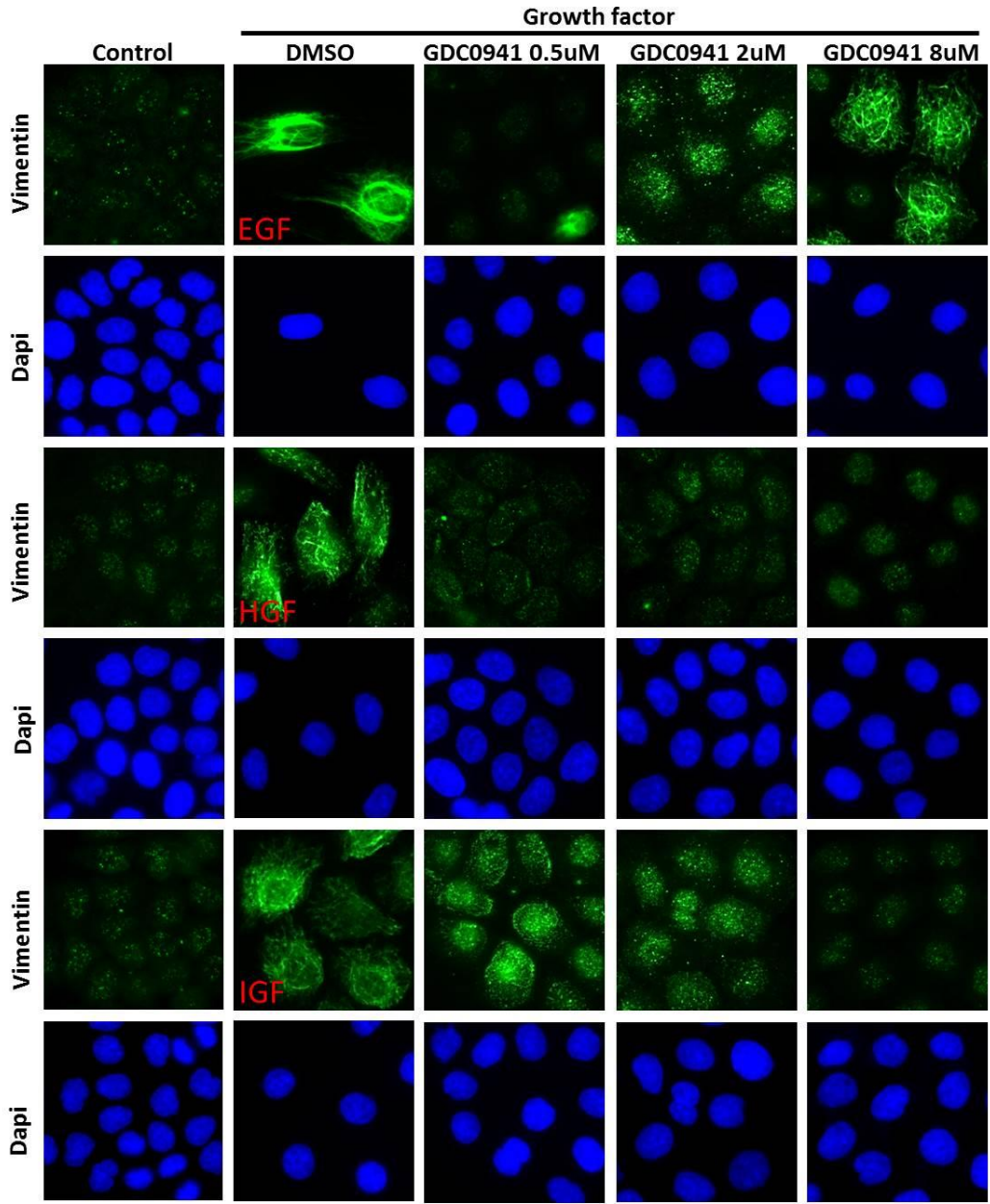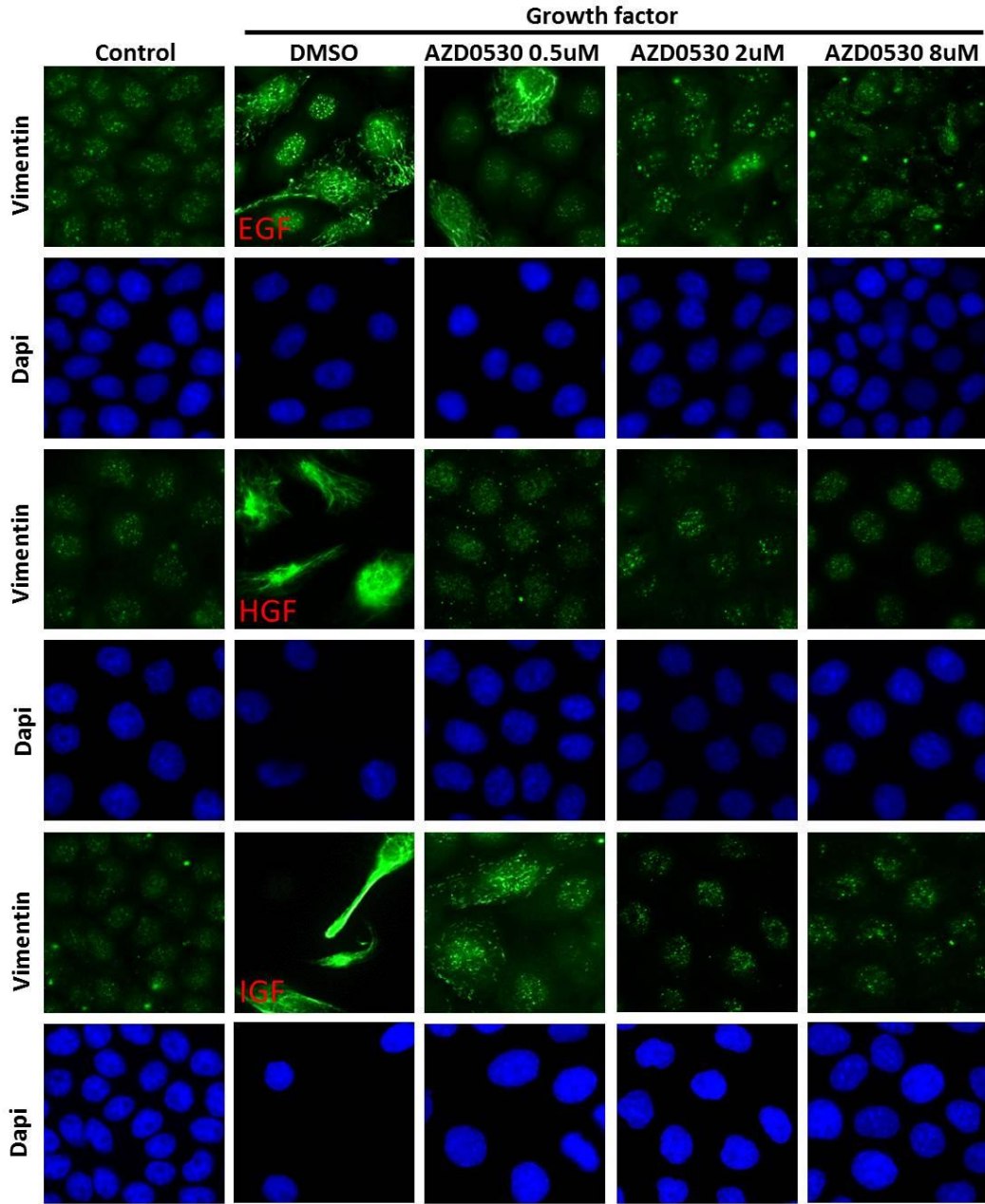
HGF - A83-01 intersection group (280 genes)

|						
10703888	Actn1	Dusp6	Gprc5a	Mmp15	Pmepa1	Sema3c
10705411	Adamts6	Ech1	Gstt2	Mmp3	Pnrc1	Serpine1
10707620	Aen	Efhd2	Gstt3	Mpzl2	Ppp1r12a	Sertad2
10710087	Akr1b10	Egr1	Hbegf	Mt1a	Prkcdbp	Sestd1
10758724	Akr1b7	Ehbp1l1	Hbp1	Mtap	Prr5	Sgms2
10787958	Aldh3a1	Ehd3	Hk2	Mthfd1l	Prrg4	Sh3yl1
10801135	Ankrd50	Elf4	Hlx	Mtmr10	Prss22	Slc1a5
10815869	Areg	Elk3	Hmga1	Mtr	Ptges	Slc20a1
10817119	Arrb1	Emp3	Htra1	Mybl1	Ptgs2	Slc44a2
10856998	Arsj	Enc1	Id2	Myof	Ptk2b	Slc4a7
10867832	Atf5	Epgn	Idh1	Nek6	Ptpn12	Slc6a9
10877684	Axl	Epha2	Iffo2	Ngf	Ptpre	Slc7a6
10884158	Baz1a	Ephx1	Igfbp5	Niacr1	Ptprm	Snf1lk2
10885613	Bcar3	Ercc1	Inpp4b	Nid67	Ptprz1	Snx18
10889657	Bspry	Ereg	Itga2	Nme3	RGD1305347	Soat1
10890904	Calml4	Errfi1	Itga3	Nppb	RGD1310935	Spry2
10908670	Camsap1l1	Ets1	Kcnn4	Nrep	RGD1311307	St3gal4
10912282	Capn8	Etv4	Kctd11	Nrg1	RGD1312026	Stxbp6
10924084	Car12	Extl3	Klf6	Nuak2	RGD1560248	Tacstd2
10930564	Car5b	F3	Krt15	Nup153	RGD1561161	Tead1
10930580	Casp3	Fads3	LOC100125362	Nupr1	RGD1561381	Tgfa
10930598	Cd44	Fahd2a	LOC305633	Obfc2a	RGD1561394	Tgm1
10930614	Cenpe	Fam129b	LOC686933	Odc1	RGD1563508	Thbs2
10930618	Cenpf	Far1	LOC688459	PVR	RGD1565002	Tm4sf1
10938288	Cflar	Fat1	LOC689074	Pard6b	RGD1565007	Tmem131
10821067	Cpa6	Fez2	Lama3	Pctk2	RT1-DMb	Tmem176a
10845605	Cpeb2	Fhdc1	Lamb3	Pdcd4	Rab38	Tmem176b
10901956	Csgalnact2	Fhl2	Lamc2	Pdpn	Rai14	Tnfrsf26
10700054	Cttnbp2nl	Fhl3	Lass3	Pex11g	Rapgef2	Tpr
10940470	Cxcl1	Flrt2	Lrp8	Phlda1	Rasa1	Tsc22d2
10940546	Cyp3a9	Flt1	Lyrm2	Pik3cb	Rasa3	Tsku
10940568	Cyr61	Fnbp1l	Macf1	Pik3cd	Rbms1	Tspan1
10940593	Dapk2	Fosl1	Mblac2	Pim3	Rhbdl3	Tspan8
10940627	Dbp	Fst	Mgmt	Pir	Rif1	Ttc39b
10940628	Ddah2	Fut1	Mgst3	Pitpnc1	Rnd1	Ttll4
10940647	Dhrs9	Gbas	Mki67	Plaur	Rras2	Vcl
10940689	Dock5	Gdnf	Mllt4	Plk2	Runx1	Vegfa
Abcb1b	Dock8	Glb1l2	Mmd	Plk3	Scmh1	Vof16
Abcg1	Dtx4	Glipr2	Mmp10	Plscr1	Scp2	Wnt6
Abhd2	Dusp5	Gnb4	Mmp13	Plscr2	Selenbp1	Zyx

NBT-II cells treated with VEGF ligand did not result in cell dispersion.
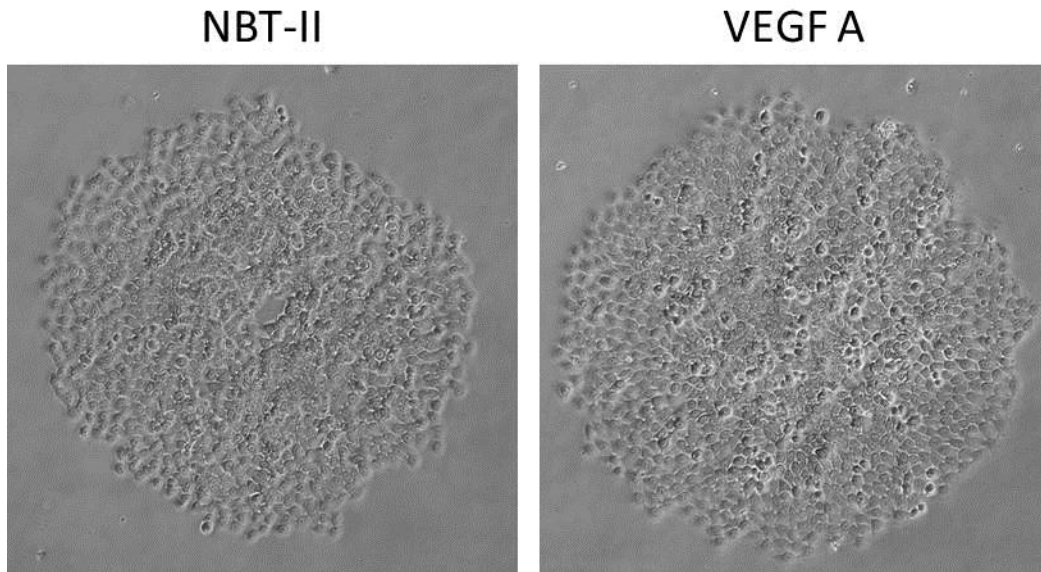
NBT-II cells were treated with 100ng/ml of VEGF-A for 3 days and cell morphology was examined and photographed using a phase-contrast microscope. No dispersion or changes in cell morphology was observed for cells treated with VEGF-A.

UM-UC-3 was exposed to A83-01 for 2 hours per day and resulted in a more epithelial phenotype.
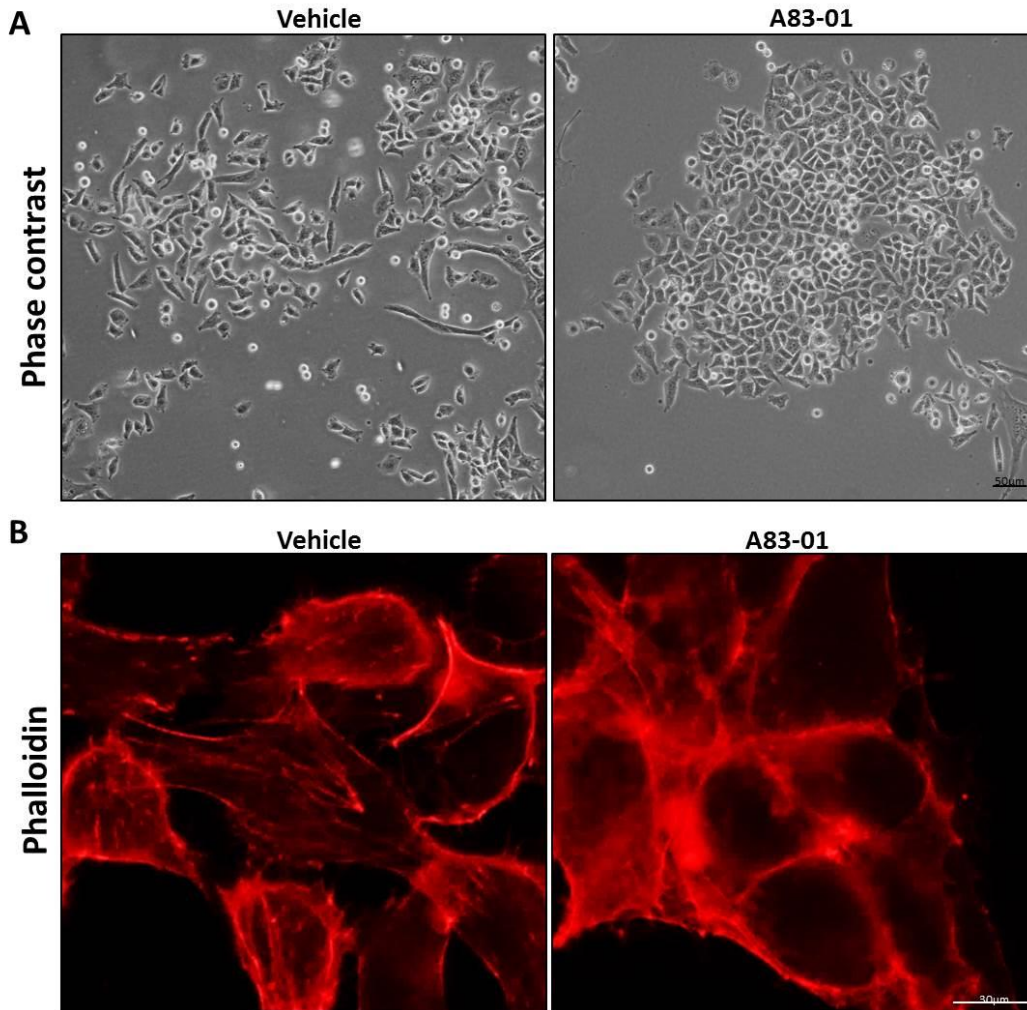
(A) UM-UC-3 was exposed to 10μM A83-01 for 2 hours per day for one week and cell morphology was examined and photographed using a phase-contrast microscope. UM-UC-3 carcinoma cells treated with A83-01 initiated cell-cell contacts and (B) reorganization of the actin cytoskeleton was observed. The stress fibres present in vehicle treated UM-UC-3 carcinoma cells were absent in A83-01 treated UM-UC-3 carcinoma cells. Cortical actin was observed in A83-01 treated cells, suggesting a switch to a more epithelial phenotype.